JAERI-M
9214

ANNUAL REPORT OF THE OSAKA LABORATORY FOR RADIATION CHEMISTRY JAPAN ATOMIC ENERGY RESEARCH INSTITUTE

(No. 13)

April 1, 1979 - March 31, 1980

November 1980

Osaka Laboratory for Radiation Chemistry

日本原子力研究所
Japan Atomic Energy Research Institute

Osaka Laboratory for Radiation Chemistry
Japan Atomic Energy Research Institute
25-1 Mii-minami machi, Neyagawa
Osaka, Japan

JAERI-M 9214

ANNUAL REPORT OF THE OSAKA LABORATORY FOR RADIATION CHEMISTRY JAPAN ATOMIC ENERGY RESEARCH INSTITUTE

(No. 13)

April 1, 1979 - March 31, 1980

(Received November 4, 1980)

This report describes research activities of Osaka Laboratory for Radiation Chemistry, JAERI during one year period from April 1, 1979 through March 31, 1980. The latest report, for 1979, is JAERI-M 8569.

Detailed descriptions of the activities are presented in the following subjects: studies on reactions of carbon monoxide, hydrogen and methane; polymerization under the irradiation of high dose rate electron beams; modification of polymers, degradation, cross-linking, and grafting.

Previous reports in this series are:

Annual Report, JARRP,	Vol. 1	1958/1959*
Annual Report, JARRP,	Vol. 2	1960
Annual Report, JARRP,	Vol. 3	1961
Annual Report, JARRP,	Vol. 4	1962
Annual Report, JARRP,	Vol. 5	1963
Annual Report, JARRP,	Vol. 6	1964
Annual Report, JARRP,	Vol. 7	1965
Annual Report, JARRP,	Vol. 8	1966
Annual Report, No. 1,	JAERI 5018	1967
Annual Report, No. 2,	JAERI 5022	1968
Annual Report, No. 3,	JAERI 5026	1969
Annual Report, No. 4,	JAERI 5027	1970
Annual Report, No. 5,	JAERI 5028	1971
Annual Report, No. 6,	JAERI 5029	1972
Annual Report, No. 7,	JAERI 5030	1973
Annual Report, No. 8,	JAERI-M 6260	1974
Annual Report, No. 9,	JAERI-M 6702	1975
Annual Report, No.10,	JAERI-M 7355	1976
Annual Report, No.11,	JAERI-M 7949	1977
Annual Report, No.12,	JAERI-M 8569	1978

*Year of the activities

Keywords: Electron Beam Irradiation, γ-Irradiation, Carbon Monoxide-Hydrogen Reaction, Methane, Radiation-Induced Reaction, Polymerization, Emulsion Polymerization, Grafting, Polymer Modification, Cross-Linking, Vinyl Monomer, Dienes, Polystyrene, Polyvinyl Chloride Powder, Cellulose Triacetate Film Dosimeter, Radiation Chemistry

JAERI－M 9214

昭和54年度日本原子力研究所　大阪研究所年報

日本原子力研究所　大阪研究所

（1980年11月 4日受理）

本報告は、大阪研究所において昭和54年度に行なわれた研究活動を述べたものである。主な研究題目は、一酸化炭素、水素およびメタンの反応ならびにそれに関連した研究、高線量率電子線照射による重合反応の研究、ポリマーの改質および上記の研究と関連して重合反応、高分子分解、架橋ならびにグラフト重合に関する基礎的研究などである。

日本放射線高分子研究協会年報　Vol. 1			1958／1959
日本放射線高分子研究協会年報　Vol. 2			1960
日本放射線高分子研究協会年報　Vol. 3			1961
日本放射線高分子研究協会年報　Vol. 4			1962
日本放射線高分子研究協会年報　Vol. 5			1963
日本放射線高分子研究協会年報　Vol. 6			1964
日本放射線高分子研究協会年報　Vol. 7			1965
日本放射線高分子研究協会年報　Vol. 8			1966
日本原子力研究所大阪研における放射線化学の基礎研究 No. 1	JAERI	5018	1967
日本原子力研究所大阪研における放射線化学の基礎研究 No. 2	JAERI	5022	1968
日本原子力研究所大阪研における放射線化学の基礎研究 No. 3	JAERI	5026	1969
日本原子力研究所大阪研における放射線化学の基礎研究 No. 4	JAERI	5027	1970
日本原子力研究所大阪研における放射線化学の基礎研究 No. 5	JAERI	5028	1971
日本原子力研究所大阪研における放射線化学の基礎研究 No. 6	JAERI	5029	1972
日本原子力研究所大阪研における放射線化学の基礎研究 No. 7	JAERI	5030	1973
Annual Report, Osaka Lab., JAERI, No. 8	JAERI－M	6260	1974
Annual Report, Osaka Lab., JAERI, No. 9	JAERI－M	6702	1975
Annual Report, Osaka Lab., JAERI, No. 10	JAERI－M	7355	1976
Annual Report, Osaka Lab., JAERI, No. 11	JAERI－M	7949	1977
Annual Report, Osaka Lab., JAERI, No. 12	JAERI－M	8569	1978

This is a blank page.

CONTENTS

目　　次

I. INTRODUCTION

Osaka Laboratory was founded in 1958 as a laboratory of the Japanese Association for Radiation Research on Polymers (JARRP), which was organized and sponsored by some fifty companies interested in radiation chemistry of polymers. The JARRP was merged with Japan Atomic Energy Research Institute (JAERI) on June 1, 1967, and the laboratory changed its name from Osaka Laboratory, JARRP to Osaka Laboratory for Radiation Chemistry, JAERI. The research activities of Osaka Laboratory have been oriented towards the fundamental research on applied radiation chemistry.

The results of the research activities of the Laboratory were published from 1958 until 1966 in the Annual Reports of JARRP which consisted essentially of original papers. During the period between 1967 and 1973, the publication had been continued as JAERI Report which also consisted mainly of original papers. From 1974, the Annual Report has been published as JAERI-M Report which contains no original papers, but presents outlines of the current research activities in some detail. Readers who wish to have more information are advised to contact with individuals whose names appear under subjects.

The present annual report covers the research activities of the Laboratory between April 1, 1979 and March 31, 1980.

Most of the studies carried out in the Laboratory are continuation from the previous year, emphasis being laid on two fields; one is "Effect of radiation on the reaction of carbon monoxide, methane and hydrogen" and the other, "Radiation-induced polymerization by high dose rate electron beams".

Studies in an attempt to elucidate the mechanism of hydrocarbon formation from carbon monoxide and hydrogen over silica gel reveal that (i) hydrocarbons containing two or more carbon atoms are produced by the reaction of hydrogen with carbonaceous solid deposited on silica gel, and (ii) methane

is mainly produced by the reaction of carbon monoxide and hydrogen at transient acidic sites on the silica gel surface, which were also produced by the irradiation.

The studies on radiation chemical reaction of carbon monoxide and hydrogen without the presence of solid catalyst have been continued in order to find optimum reaction condition of acetaldehyde formation. Results of the investigation indicate that the G value of acetaldehyde formation of about 2 was obtained at CO content of 60 ∿ 70 mole%, temperature between 20°C and 40°C, and the reactant pressure of 5,000 Torr. However, since the apparatus has several points to be improved, there still remains possibility that the G value will increase.

Acetic acid and propionic acid are selectively formed with the G values of 1.7 and 1.2, respectively, from the gas mixture of methane and carbon monoxide by electron beam irradiation. In order to elucidate the mechanism of this reaction, spin trapping technique was successfully applied to this system to detect H, $\dot{C}H_3$, $\dot{C}_2H_5$, and $R\dot{C}=O$ radicals.

In order to know concentrations of products and remaining reactant when methane is irradiated with extremely large dose, a batch experiment was carried out up to 3×10^4 Mrad. About 90% of methane was converted to the products containing mainly hydrogen, liquid hydrocarbon, and ethane. The amounts of these products except ethane increase with dose, and seem to approach certain values. The amount of ethane decreased with increasing dose above 3×10^3 Mrad. The fact that the amount of methane decreased is approximately equal to that of hydrogen and to the sum of the amounts of CH_2 units contained in the hydrocarbon products indicates that the irradiation of large dose may produce mainly hydrocarbons and hydrogen and the deposition of carbon may not be important. The G values of the main products obtained by the batch experiment decrease with increasing dose, but they are on smooth curves extended from the points obtained by the flow experiments at lower doses below 1.1×10^3 Mrad.

The investigations have been carried out on the mechanism of energy transfer which reduces the W value of the gas mixture

of argon and ethane, and it is revealed that the energy transfer from Ar_2^* to ethane occurs in addition to that from Ar^*, which has been reported by other authors.

Coloration mechanism of cellulose triacetate (CTA) to be used for film dosimeter has been studied further. The post coloration which proceeds after irradiation is ascribed to the formation of carbonyl groups induced by NO_2 which is produced in air by irradiation.

General aspects of the radiation-induced polymerization of styrene in butylamine in a wide range of dose rate were reported last year. The most prominent effect of butylamine was that it inhibited cationic polymerization of styrene. As the continuation, radical polymerization of styrene in binary mixtures with butylamine is studied. Styrene content is varied from 100 to 200 vol% and it is found that one mole butylamine forms 5.8 times more initiating radicals than styrene. Though in the catalytic solution polymerization chain transfer of growing radicals to solvent molecules is a very important reaction, it is negligibly small in the present case, because chain termination is overwhelming so that the former is masked by the latter.

Radiation-induced polymerization of styrene in benzene is carried out up to a rather high dose rate of 1.2×10^6 rad/sec. It is observed that not only radical but also cationic polymerization occurs simultaneously at higher dose rates as in the case of pure styrene. Tentatively only radical polymerization is investigated and found quantitatively the contribution of the solvent transfer reaction to the polymerization. It should be added that benzene produces much smaller number of initiating radicals than butylamine.

Polymerization of vinyl acetate is carried out in a dose rate range up to 1.6×10^5 rad/sec. No indication of the formation of ionic polymer is observed. The GPC curves of the polymerization products consist essentially of three parts which correspond to oligomer, main radical polymer, and super polymer, respectively. When DPPH is added, all of the three fractions disappear completely. In the absence of inhibitor the rates of formation of the three types of the polymers are

proportional to the square root of the dose rate. These experimental results indicate that all of the polymers are formed by radical mechanism which are similar to one another.

Studies on emulsion polymerization of styrene, vinyl acetate, n-butyl methacrylate were carried out using a flow system. The rate of polymerization of styrene was 5×10^{-5} mole/l/sec, and number average molecular weight was 850. The rate of polymerization of vinyl acetate is about sixty times as fast as that of styrene and the number average molecular weight of the polymer was about 20,000. The solution polymerization of vinyl acetate in carbon tetrachloride proceeds with radical mechanism, while that of butadiene in n-hexane proceeds with cationic mechanism, both to form respective oligomers.

The studies have been carried out on thermal stability of polyethylene filaments grafted with acrylic acid and their salts. Filaments of 30% graft were, after conversion to bivalent or trivalent metal salts, not only thermally more stable but also self-extinguishing. Excellent mechanical properties of the original filaments are not injured by the grafting. The correlation between the distribution of acrylic acid in the filaments and their thermal stability are also studied.

Adsorption behavior of polyvinylchloride (PVC) powder with acrylic acid (AA) to various metal ions has been investigated. In addition to the monomer mixture system containing monomer, water, and ethylenedichloride, which was studied in the previous experiments, acetone and toluene were also employed for the grafting. As was expected, by use of these solvents of various concentrations, the rate of grafting was changed considerably and AA graft PVC powders of different microstructure were obtained, which show different rates and equilibrium values of adsorption.

September 30, 1980

Dr. Yunosuke Oshima , Head
Osaka Laboratory for Radiation Chemistry
Japan Atomic Energy Research Institute

II. RECENT RESEARCH ACTIVITIES

[1] Radiation-Induced Reactions of Carbon Monoxide, Hydrogen, and Methane

1. Irradiation of Circulating Gas Mixtures of Carbon Monoxide and Hydrogen under Elevated Pressure

-- Effect of Dose, CO Content, and Temperature on the Amounts of the Products

As a continuation of the study carried out in the previous year[1] using an apparatus designed for the irradiation of circulating gas under elevated pressure, the studies have been carried out in an attempt to obtain further information on time conversion curves, effects of temperature and composition of the mixture on the G values. A brief description of the irradiation apparatus was given in the previous report[1].

Irradiations were performed by electron beams from the HDRA (0.6 MV and 1 mA) at room temperature. Dose rate measured by N_2O dosimeter was 3.5×10^{-4} eV·N_2O molecule^{-1}·sec^{-1}. The pressure of the gas mixture was about 8000 Torr and two cold traps cooled by dry ice-ethanol mixture to remove condensable products from the circulating gas were used throughout the experiments.

After the irradiation, the reactants and products in the reaction vessel were pumped off through cold traps in which condensable products were collected. The products collected in the cold traps were subjected to gaschromatography and mass spectrometry.

The time-conversion curves are shown for aldehydes and cyclic ethers in Fig. 1, methanol, formic acid and esters in Fig. 2, and hydrocarbons in Fig. 3, which were obtained at room temperature and CO content of 25 mole%. As shown in Fig. 1, the amounts of formaldehyde, acetaldehyde, and tetraoxane increase with irradiation time, but after 400 sec irradiation,

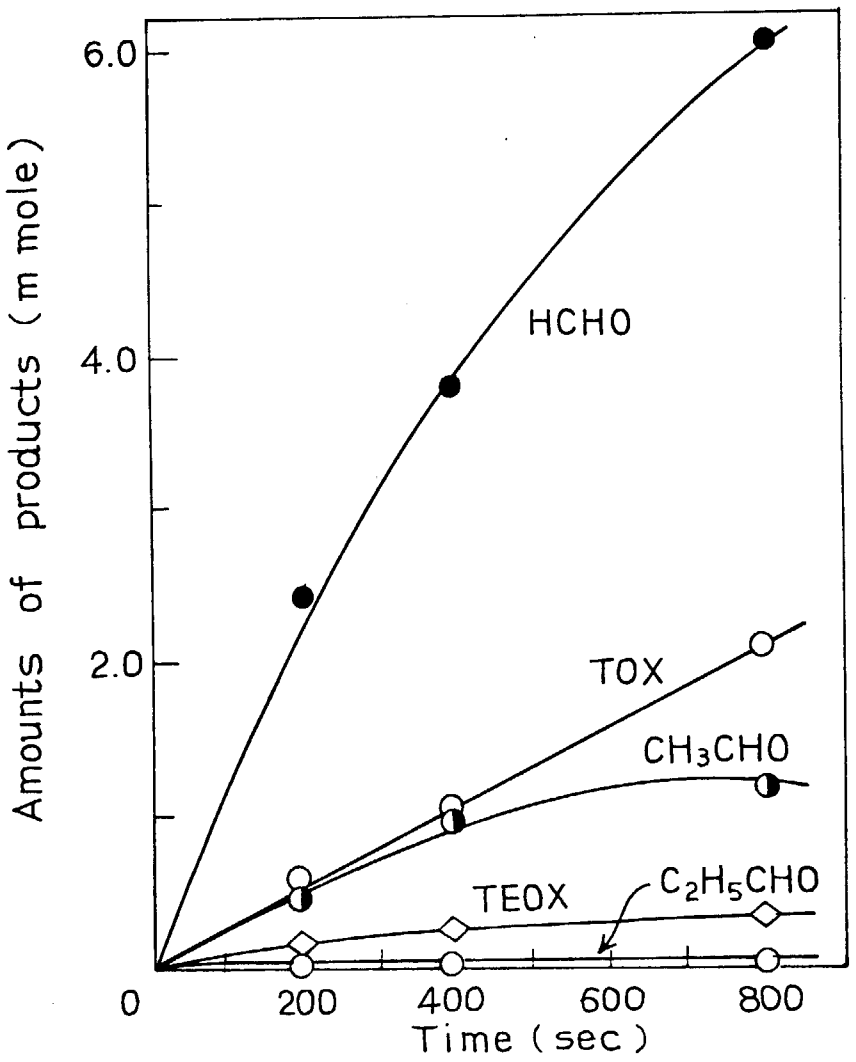

Fig. 1. Amounts of formaldehyde, trioxane, acetaldehyde, tetraoxane, and propionaldehyde as a function of time: CO content, 25 mole%; Pressure, 8000 Torr; Temperature, ca. 20°C; Electron beams, 0.6 MV, 1 mA.

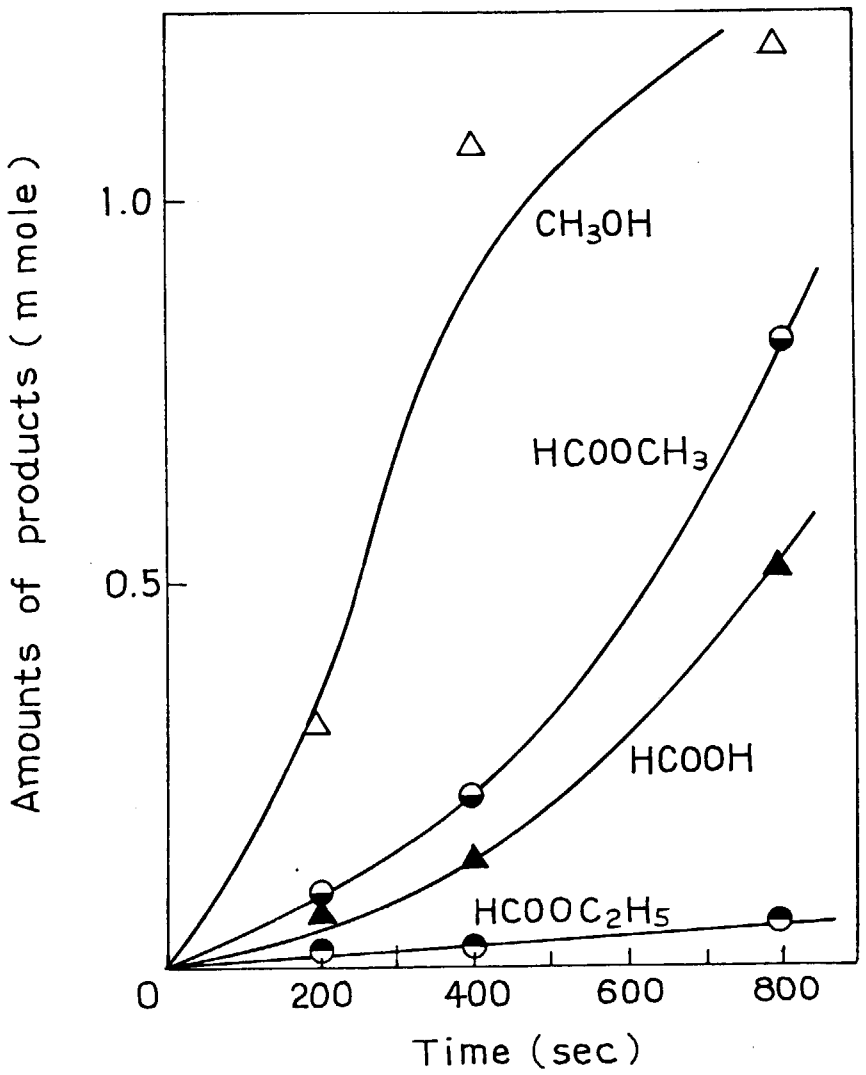

Fig. 2. Amounts of methanol, methyl formate, formic acid, and ethyl formate as a function of time: CO content, 25 mole%; Pressure, 8000 Torr; Temperature, ca. 20°C; Electron beam, 0.6 MV, 1 mA.

the rates of formation become slow. The amounts of trioxane and propionaldehyde increase linearly with time. The amount of methanol increases with dose but seems to deviate downward from a linear line above 400 sec irradiation, while those of methyl formate and formic acid increase with irradiation time showing acceleration from earlier stage of irradiation (Fig. 2). The amount of ethyl formate increases almost linearly with time. The amounts of hydrocarbon products increase linearly with irradiation time as shown in Fig. 3.

The products giving the time conversion curves in which the rate of formation decreases with irradiation time may be

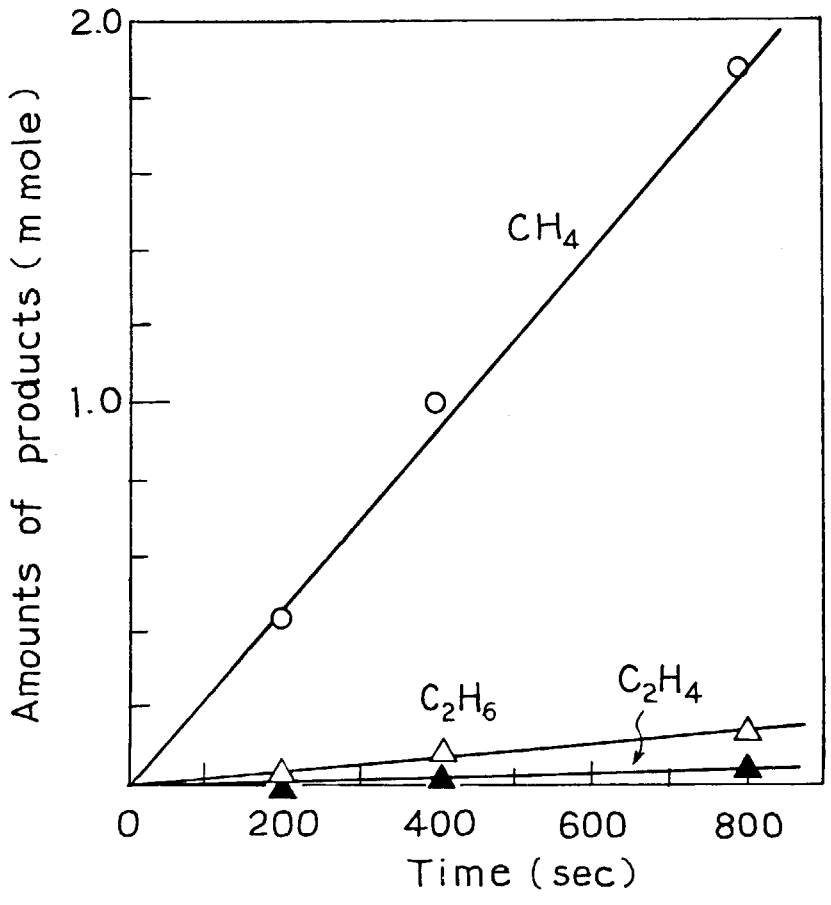

Fig. 3. Amounts of methane, ethane, and ethylene as a function of time: CO content, 25 mole%; Pressure, 8000 Torr; Temperature, ca. 20°C; Electron beam, 0.6 MV, 1 mA.

converted to other compounds as the dose increases. On the other hand, the products showing acceleration may be partly derived from other products which are accumulated in the system as the dose increases.

In Figs. 4 and 5, the G values of the products are plotted as a function of temperature. The G values of the products were calculated from the amounts of products produced from the gas mixture containing 15 mole% of CO by 15.2 Mrad irradiation. As shown in Fig. 4, the G value of acetaldehyde shows maximum value at 40°C, but the G value of formaldehyde is independent of temperature. The G values of trioxane (Fig. 4), propionaldehyde (Fig. 4), and methyl formate (Fig. 5) decrease with increasing temperature, while those of carbon dioxide (Fig. 5), water

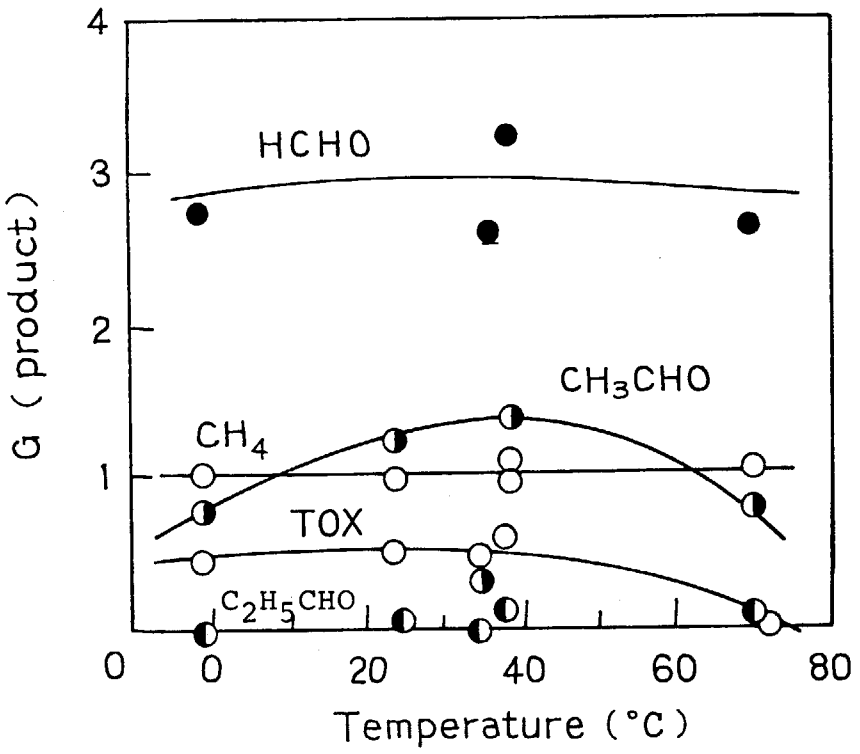

Fig. 4. G values of the formaldehyde, acetaldehyde, methane, and trioxane as a function of temperature: CO content, 15 mole%; Pressure, 8000 Torr; Electron beam, 0.6 MV, 1 mA.

(Fig. 5), and increase with increasing temperature. The G values of methane (Fig. 4) methanol, formic acid are almost independent of temperature.

When compared in the same temperature range (0° ∿ 80°C) the temperature dependences of formaldehyde, methanol, and trioxane are similar to those obtained in the previous work under three different reaction conditions, i.e., (a) without circulation at 760 Torr, 15 CO mole%, 35 Mrad[2], (b) without circulation condition at 5000 Torr, 15 CO mole%, and 22.7 Mrad[2], and (c) with circulation at 1000 Torr, 25 CO mole%, and 55 Mrad[3]. However, the temperature dependence of acetaldehyde obtained in the present study is different from the previous

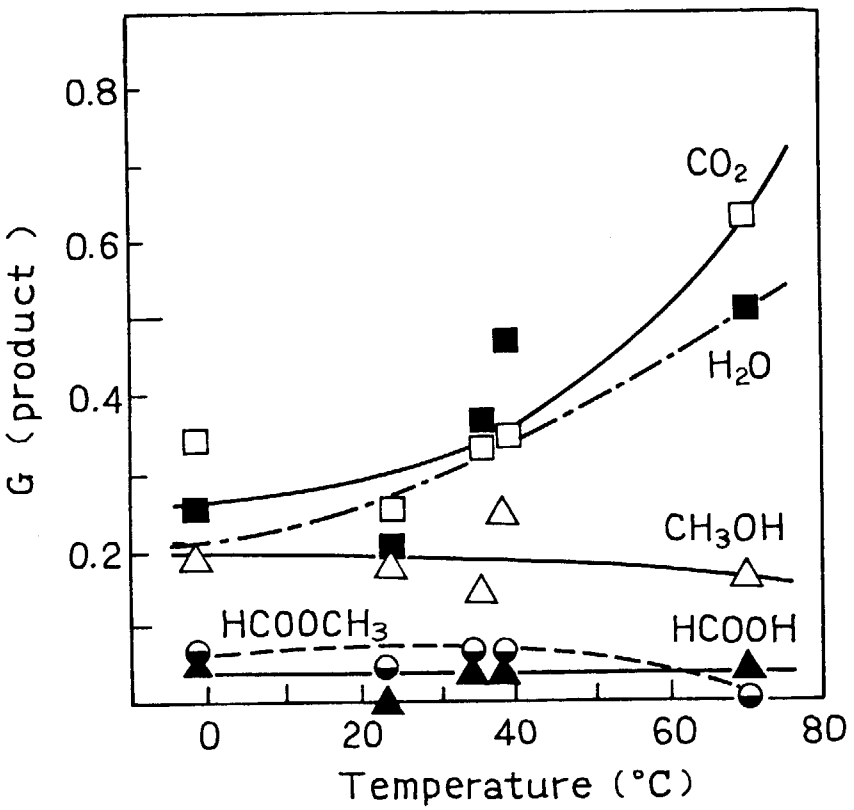

Fig. 5. G values of carbon dioxide, water, methanol, methyl formate, and formic acid as a function of temperature: CO content, 15 mole%; Pressure, 8000 Torr; Electron beam, 0.6 MV, 1 mA.

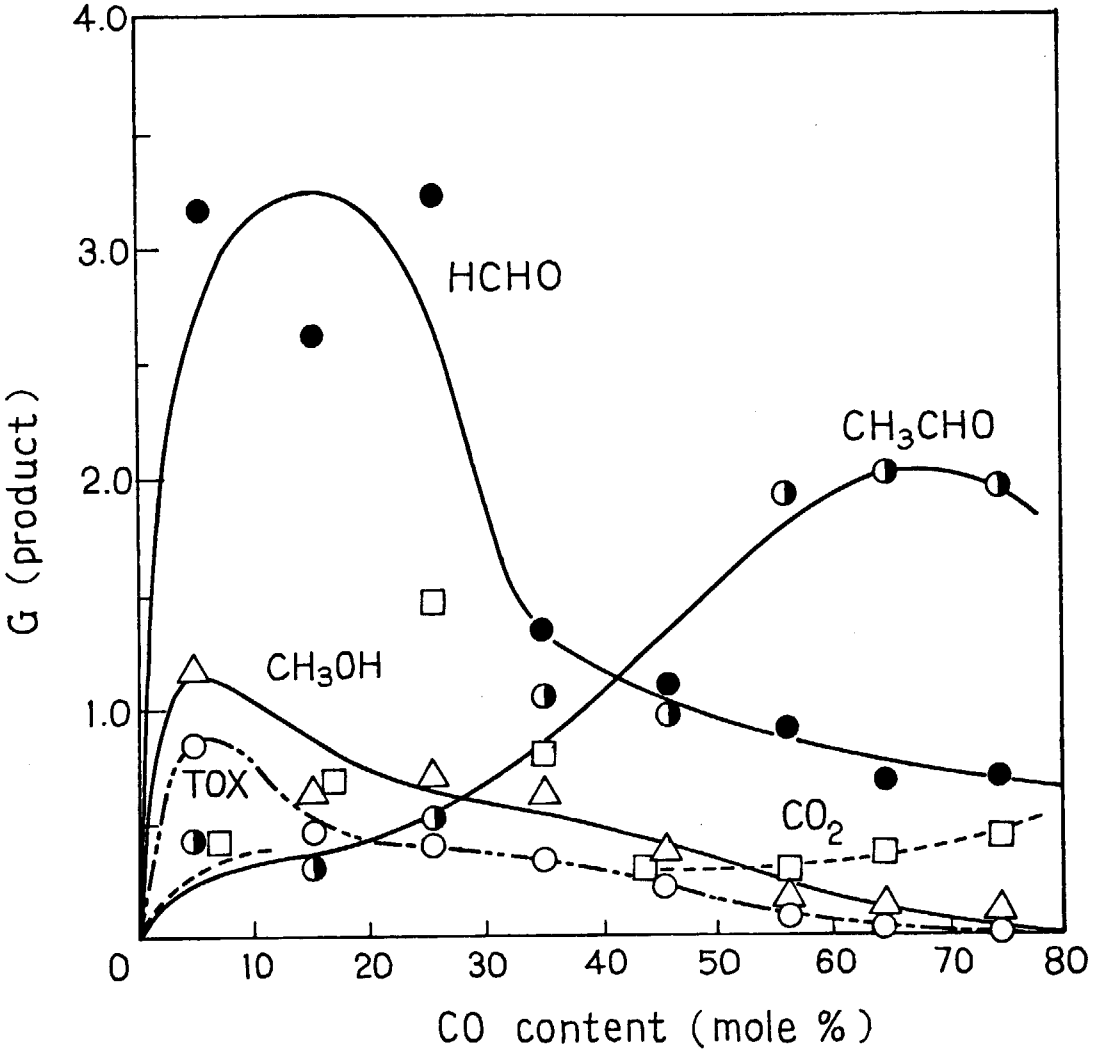

Fig. 6. G values of formaldehyde, acetaldehyde, methanol, trioxane, and carbon dioxide as a function of CO content: Pressure, 8000 Torr; Temperature, ca. 20°C; Electron beam, 0.6 MV, 1 mA; Irradiation time, 100 ∿ 400 sec.

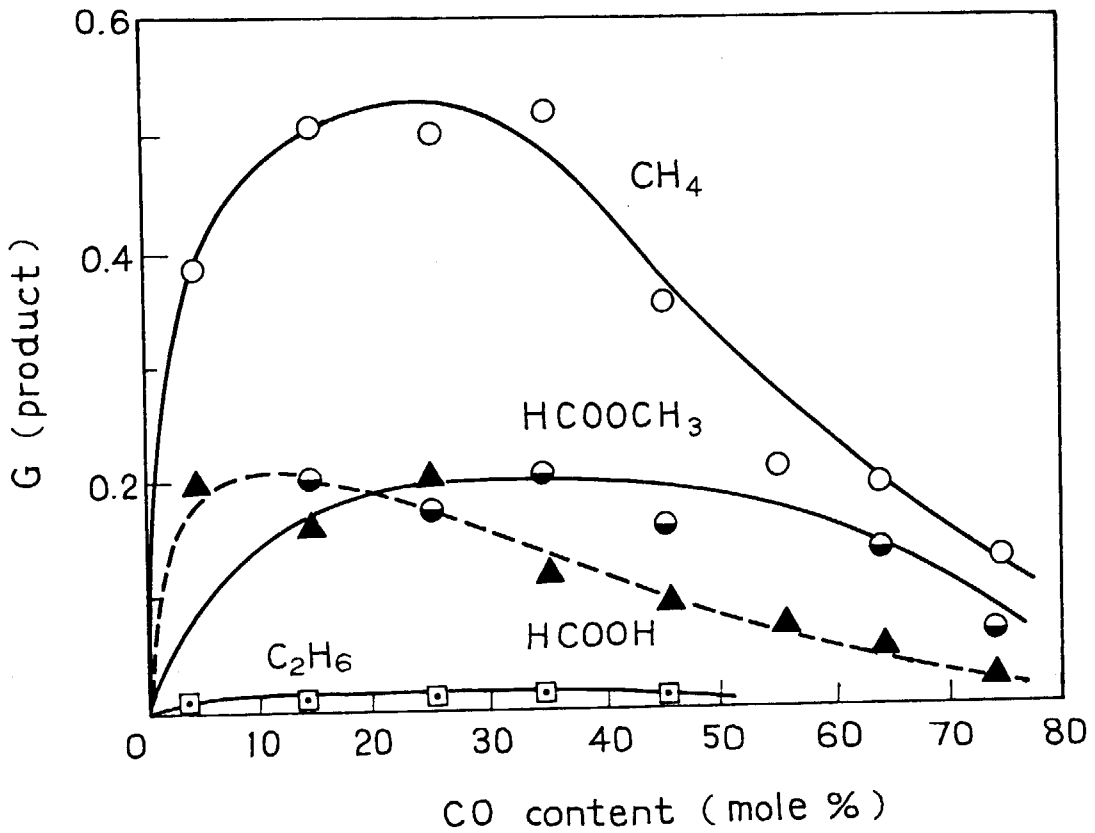

Fig. 7. G values of methane, methyl formate, formic acid, and ethane as a function of CO content: Pressure, 8000 Torr; Temperature, ca. 20°C; Electron beam, 0.6 MeV, 1 mA; Irradiation time, 100 ∿ 400 sec.

studies obtained under different reaction conditions.

The G values of the products are plotted as a function of CO mole% in the gas mixture in Figs. 6 and 7. As shown in Fig. 6, the G value of formaldehyde decreases after maximum of 3.2 at 20 CO mole% with increasing CO mole%, while that of acetaldehyde increases with increasing CO mole% and reaches a maximum value of 2.0 at about 60 CO mole%. The G values of methanol and trioxane have maximum values at about 5 CO mole%,

while that of carbon dioxide increases with increasing CO mole% as shown in Fig. 6. The G values of methane, methyl formate and formic acid have maximum values of 0.52, 0.2, and 0.2, at CO mole% of 25, 35, and 15, respectively. These results

can be regarded qualitatively the same as those obtained at 1000 Torr under gas circulation condition at -30°C, except that the G value of acetaldehyde is about 4 times larger than those obtained at 1000 Torr.

The results obtained in the present study indicate that the G value of acetaldehyde becomes maximum at 60 CO mole% at 8000 Torr and room temperature. Further studies are necessary to obtain data on the effect of dose, dose rate, pressure, and temperature on the G values of acetaldehyde at about 60 mole% in order to find the optimum conditions for acetaldehyde formation. (S. Sugimoto and M. Nishii)

1) S. Sugimoto and M. Nishii, JAERI-M 8569, 16 (1978).
2) S. Sugimoto and M. Nishii, JAERI-M 7899, 19 (1978).
3) S. Sugimoto and M. Nishii, JAERI-M 8569, 6 (1979).

2. Irradiation of Circulating Gas Mixtures of Hydrogen and Carbon Monoxide (55 mole%) at Elevated Pressure

In the previous study[1], it was found that the maximum G value of acetaldehyde formation can be obtained at about 55 ∿ 65 mole% of CO, while dose, dose rate, and temperature were kept constant at 15.2 Mrad, 0.079 Mrad·sec^{-1}, and about 20°C, respectively. In the present study, the G values of acetaldehyde and the other products are studied as a function of irradiation time, temperature, and dose rate at the fixed CO content of 55 mole% in an attempt to find the reaction conditions which give the maximum G value of acetaldehyde.

The irradiation procedure and method of the product analysis were the same as those reported in the previous study.

In Figs. 1, 2, and 3, the amounts of products are plotted as a function of time. The amounts of all products increase with irradiation time, but the rates of formation of most products except methane, methanol and propionaldehyde decrease with irradiation time, suggesting that these compounds are converted to other compounds. The amounts of methane, methanol

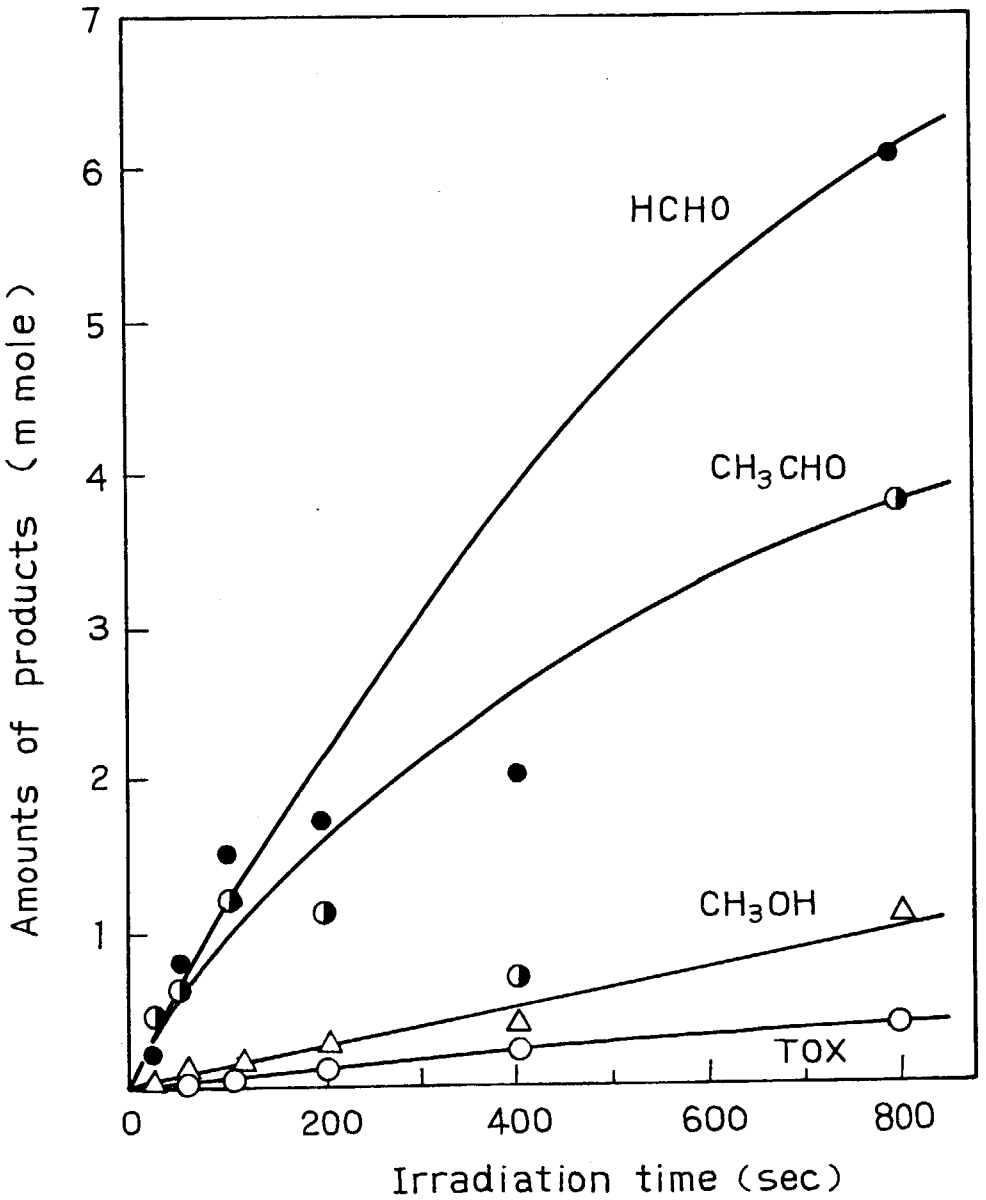

Fig. 1. Amounts of the products as a function of irradiation time: CO content, 55 mole%; Pressure, 8000 Torr; Temperature, 25°C; Dose rate, 7.9×10^4 rad/sec.

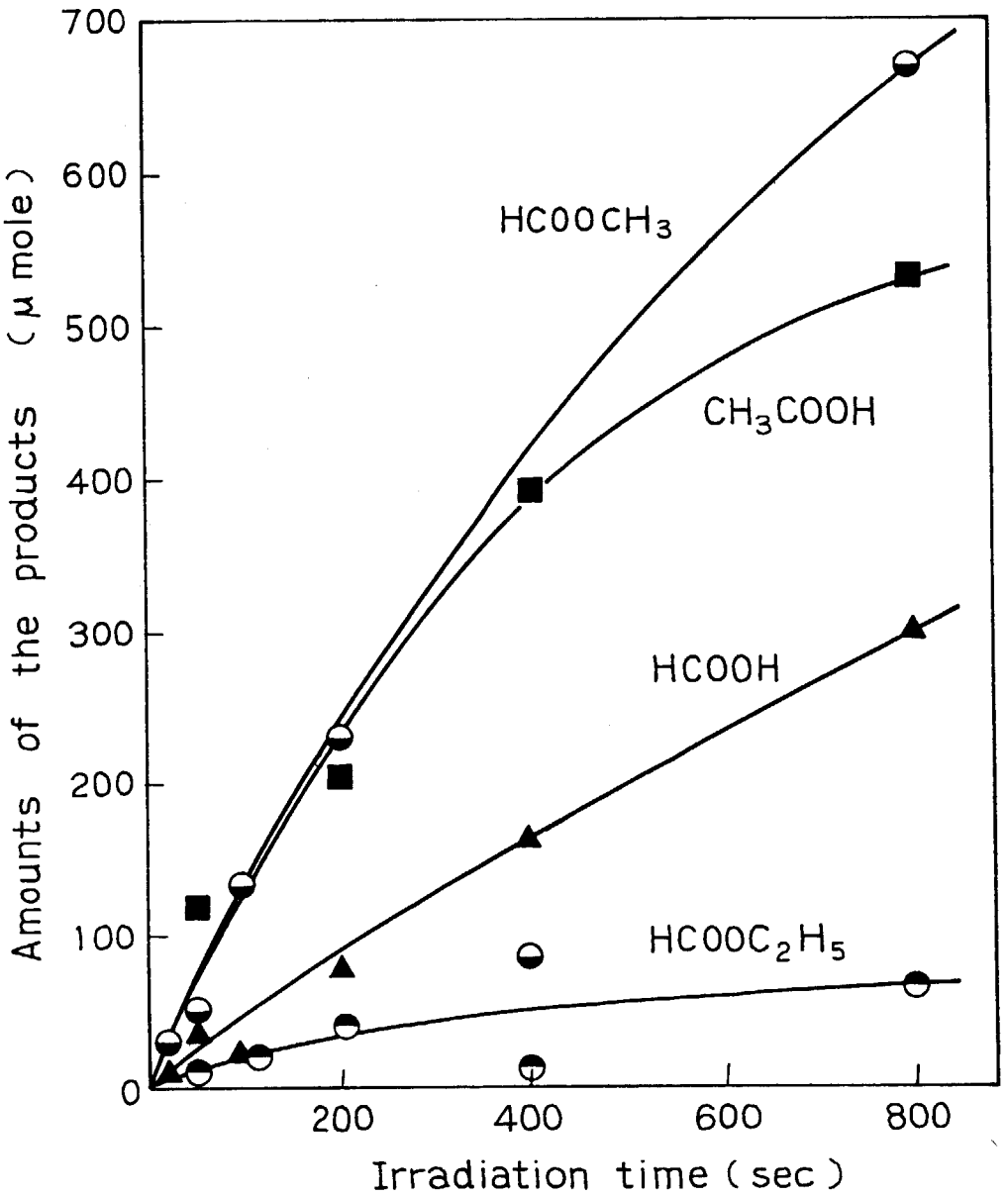

Fig. 2. Amounts of the products as a function of irradiation time: CO content, 55 mole%; Temperature, 25°C; Pressure, 8000 Torr; Dose rate, 7.9×10^4 rad/sec.

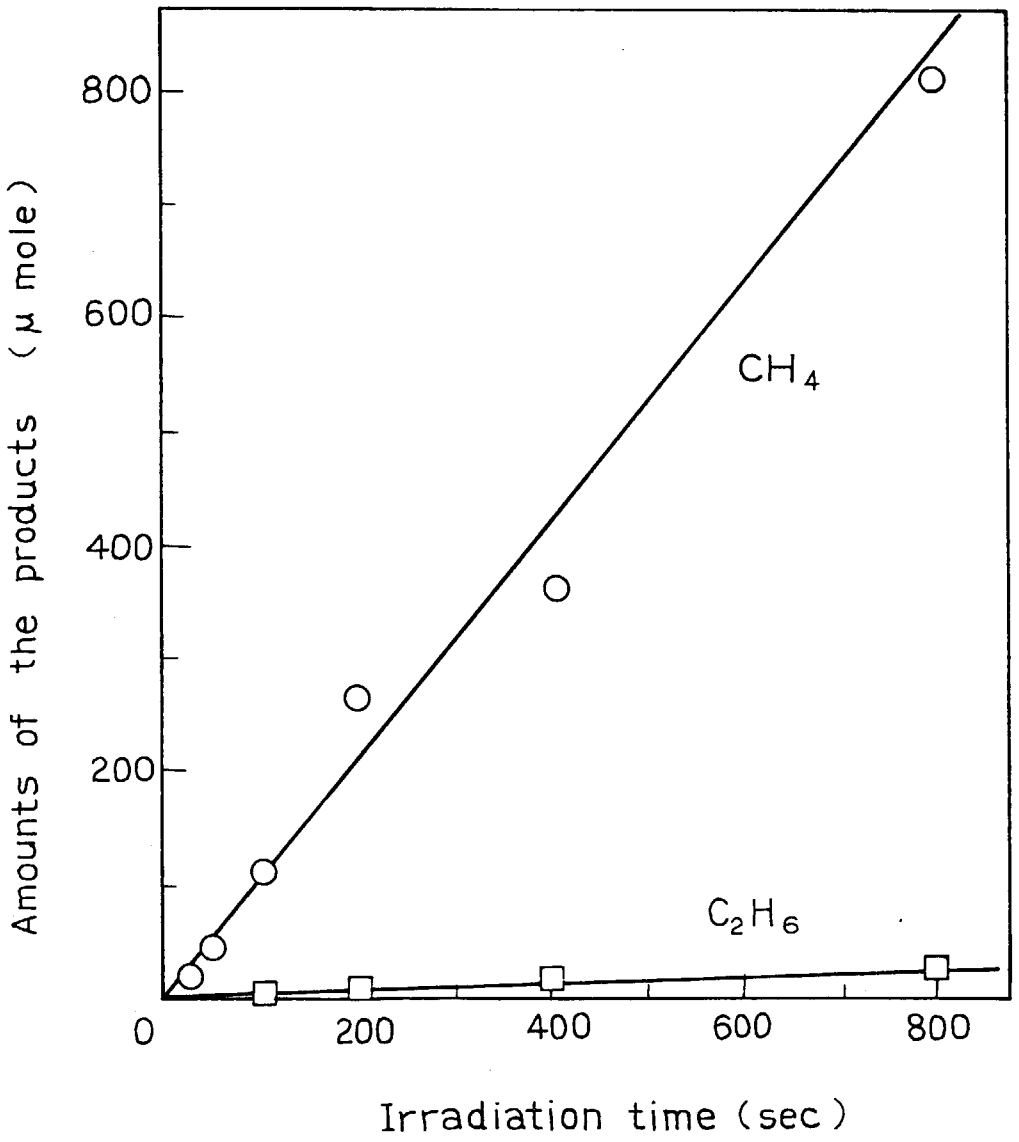

Fig. 3. Amounts of methane and ethane as a function of irradiation time: CO content, 55 mole%; Temperature, 25°C; Pressure, 8000 Torr; Dose rate, 7.9×10^4 rad/sec.

and propionaldehyde increase linearly with irradiation time. The time conversion curves for the products obtained at 55 mole% of CO are similar to those previously obtained at 15 mole% of CO except for methyl formate and formic acid; the rates of formation of these compounds at 55 mole% of CO decrease while those at 25 mole% of CO increased as shown in the previous report.

Preliminary experiment to study the temperature dependence of G values shows that the maximum G values of formaldehyde, acetaldehyde, methanol, and trioxane appear at 50, 25, 50, and 25°C, respectively, but the G value of methane increases slightly with temperature in the temperature range investigated (0 ∿ 85°C) (not shown in Figures). These results except the one for methane are different from the previous results obtained at 15 mole% of CO in that the maximum G value of acetaldehyde appeared at 40°C and no apparent maximum values were recognized for the other products.

In Fig. 4, the G values of the products are plotted as a function of dose rate. The dose, temperature, and CO content were kept constant at 7.8 Mrad, 20°C, and 55 CO mole%, respectively. The G values of acetaldehyde, methanol, methyl formate, trioxane, and carbon dioxide decrease with increasing dose rate, while those of formaldehyde, methane, ethylene, and ethane increase with increasing dose rate.

Table 1 lists the G values of main products obtained with or without traps in a circulation gas loop: (a) no trap, (b) two dry ice-ethanol traps, and (c) one dry ice-ethanol trap and one liquid nitrogen trap. The gas temperature was 20°C for the case (a) and (b), but was -39°C for the case (c), because the gas cooled in the liquid nitrogen trap reduced the temperature in the irradiation vessel when the cooled gas was recirculated, and the decrease of temperature can not be compensated by a heater surrounded the irradiation vessel.

The G values of the most products except methane increased by use of dry ice-ethanol traps suggesting that the products were partly separated from the gas mixture and were not further converted to other compounds by irradiation. The use of the liquid nitrogen trap with the dry ice-ethanol trap decreased

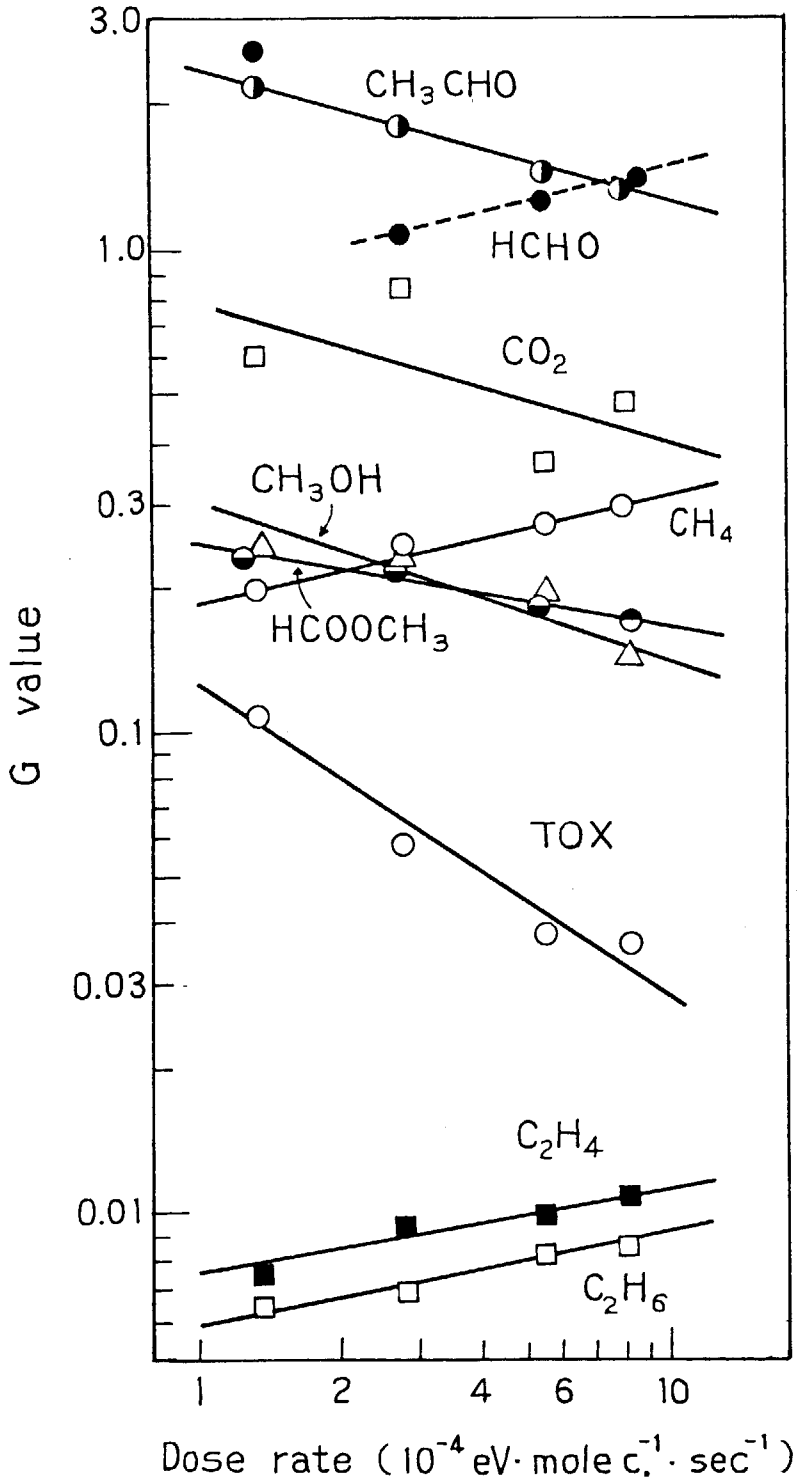

Fig. 4. The G values of the products as a function of dose rate: CO content, 55 mole%; Temperature, 20°C; Pressure, 8000 Torr; Dose, 3.5×10^{22} eV (7.8 Mrad).

Table 1. G values of Main Products with or without Using the Cold Traps

Exp. No.	a*	b	c
Cold Traps	no	two dry ice-ethanol traps	one dry ice-ethanol and one liquid nitrogen traps
Temperature of the reactant gas	20	20	-40
CH_4	0.38	0.23	0.19
CH_3OH	0.13	0.19	0.21
CH_3CHO	0.76	0.99	0.70
C_2H_5CHO	0.034	0.04	0.039
HCHO	1.06	1.50	1.43
$HCOOCH_3$	0.19	0.2	0.083
$HCOOC_2H_5$	0.021	0.034	0.012
HCOOH	0.063	0.068	0.143
CH_3COOH	0.071	0.18	0.165
TDX	0.028	0.095	0.0625
H_2O	0.90	0.83	0.91
CO_2	0.42	0.35	0.63

* Average of two measurements

Table 2. Selectivities of the Products

Product	G value	Selectivity (mole%)
CH_4	0.16	2.9
CH_3OH	0.18	3.2
HCHO	1.35	24.2
CH_3CHO	2.98	53.3
$HCOOCH_3$	0.20	3.6
HCOOH	0.041	0.7
CH_3COOH	0.001	0.01
Trioxane	0.094	1.7
Others	---	10.3
H_2O	3.25	
CO_2	0.38	

55.1 CO mole%, 8060 Torr, 24°C, 0.6 MeV, 1 mA,
25 sec, 8.71×10^{21} eV (1.97 Mrads)

the G values of the products (except for methanol) possibly because of the decrease of irradiation temperature.

The selectivity, S_i, to the product, i, as defined by the following equation was calculated.

$$S_i = \frac{G_i}{G_{total} - (G_{H_2O} + G_{CO_2})} \times 100$$

where G's are the G values of the product denoted by subscript. An example of the results are shown in Table 2 together with the G values. It is possible to obtain high selectivity (50%) of acetaldehyde by selecting the reaction conditions, which are also included in the table. (S. Sugimoto and M. Nishii)

1) S. Sugimoto and M. Nishii, This report.

3. Dependence of the Product Yields on the Reactant Gas Composition in the Radiation-Induced Reaction of $CO-H_2$ Mixture over Silica Gel

As reported already[1], irradiation of 1 : 6 $CO-H_2$ gas mixture in the presence of silica gel efficiently produces hydrocarbons of low-molecular weight together with the by-product, CO_2. The formation of hydrocarbons, at least hydrocarbons higher than methane, in this system has been demonstrated to be due to secondary reactions of H_2 with carbonaceous solid produced from CO.[2] The present report is concerned with the dependence of the product yields on the composition of the feed gas. The principal purpose of this study is to see if there would be any composition favorable to the formation of olefins such as ethylene and organic oxygenates such as acetaldehyde and acetic acid.

Experiments were carried out using the flow reactor described already.[2] Irradiation was carried out with electron beams of 600 keV, 2 mA and scan width of 16 cm. Temperature during irradiation was kept at 300°C. The stainless steel tubing connecting the flow reactor with the gaschromatographs through the gas samplers was heated at about 100°C, to avoid condensation of the products.

Fig. 1 shows the yields of the total hydrocarbon ($C_1 \sim C_5$), CO_2 and H_2O produced in the presence and absence of silica gel as a function of CO content in the reactant. As may be seen from the figure, the yield of the total hydrocarbon produced over silica gel is ca. 20 times greater than that in the absence of silica gel in the whole range of the CO content. The maximum yield of the total hydrocarbon over silica gel is attained at 40 $\sim$ 50% CO, in accordance with the result of the homogeneous radiolysis. On the other hand, over silica gel the yield of H_2O decreases with the CO content in the region above 5 % whereas the yield of CO_2 increases, in marked contrast to the homogeneous radiolysis. This fact suggests that silica gel exhibits catalytic activity for the water-gas shift reaction (1) under electron beam irradiation.

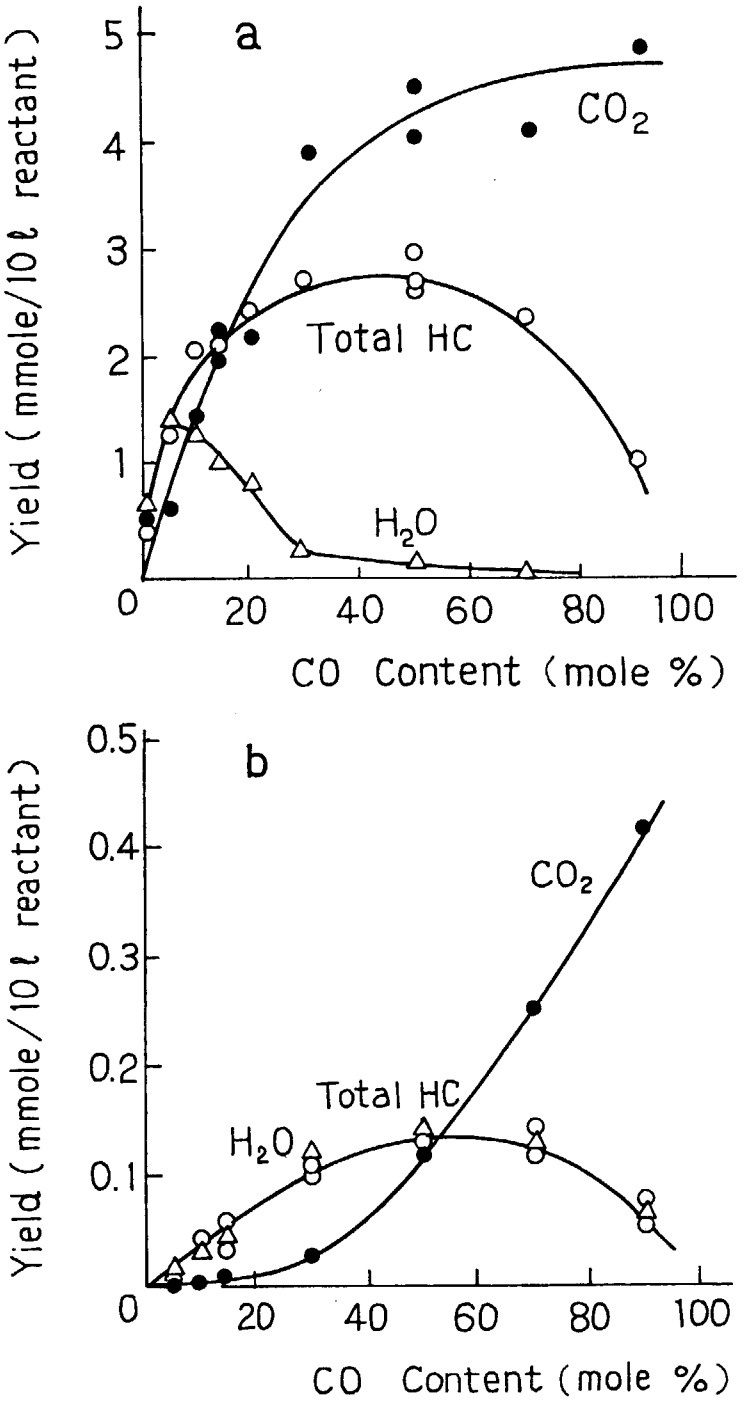

Fig. 1. Yields of total hydrocarbon (○), CO_2 (●) and H_2O (△) by irradiation of CO-H_2 mixtures at 300°C.
(a) over silica gel, (b) homogeneous.

$$CO + H_2O \rightleftharpoons CO_2 + H_2 \qquad (1)$$

The reaction (1) over iron oxide-based catalysts is regarded as a redox reaction over catalyst sites which are oxidized by H_2O and reduced by CO.[3] Since it is known that irradiation of silica gel produces surface sites that are active for both oxidation and reduction[4], it seems reasonable to assume that reaction (1) induced by radiation over silica gel may occur at the transient sites R produced on the surface by irradiation.

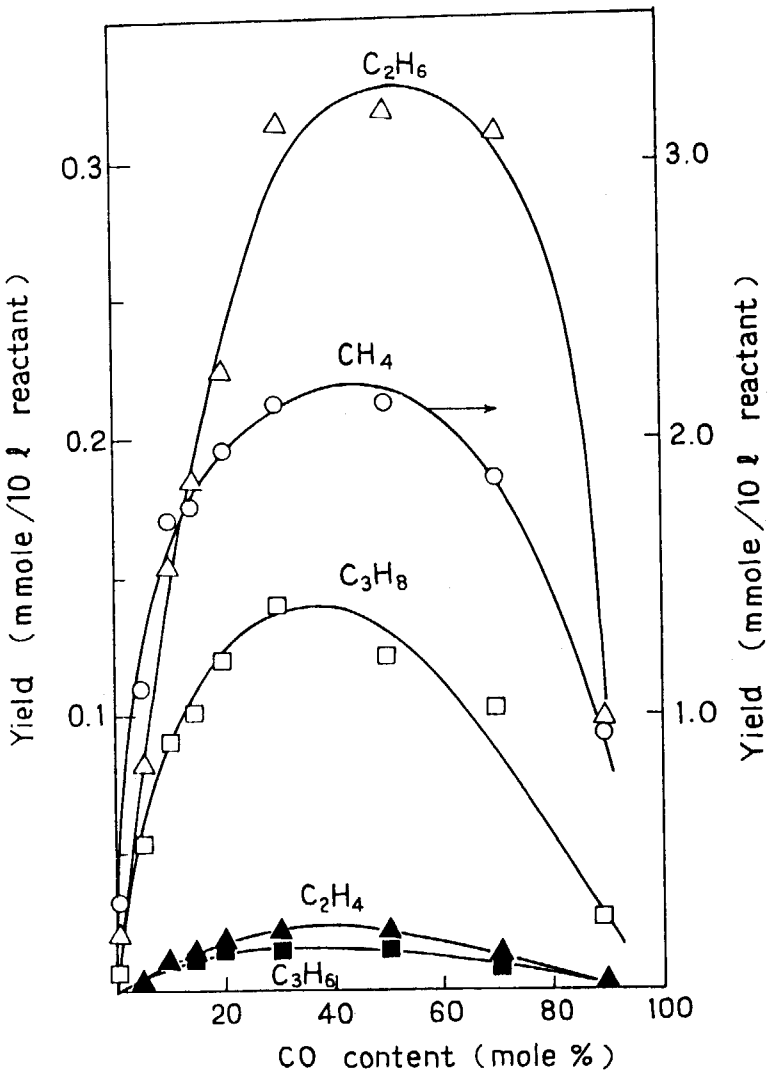

Fig. 2. Yields of $C_1 \sim C_3$ hydrocarbons by irradiation of $CO-H_2$ mixtures over silica gel at 300°C.

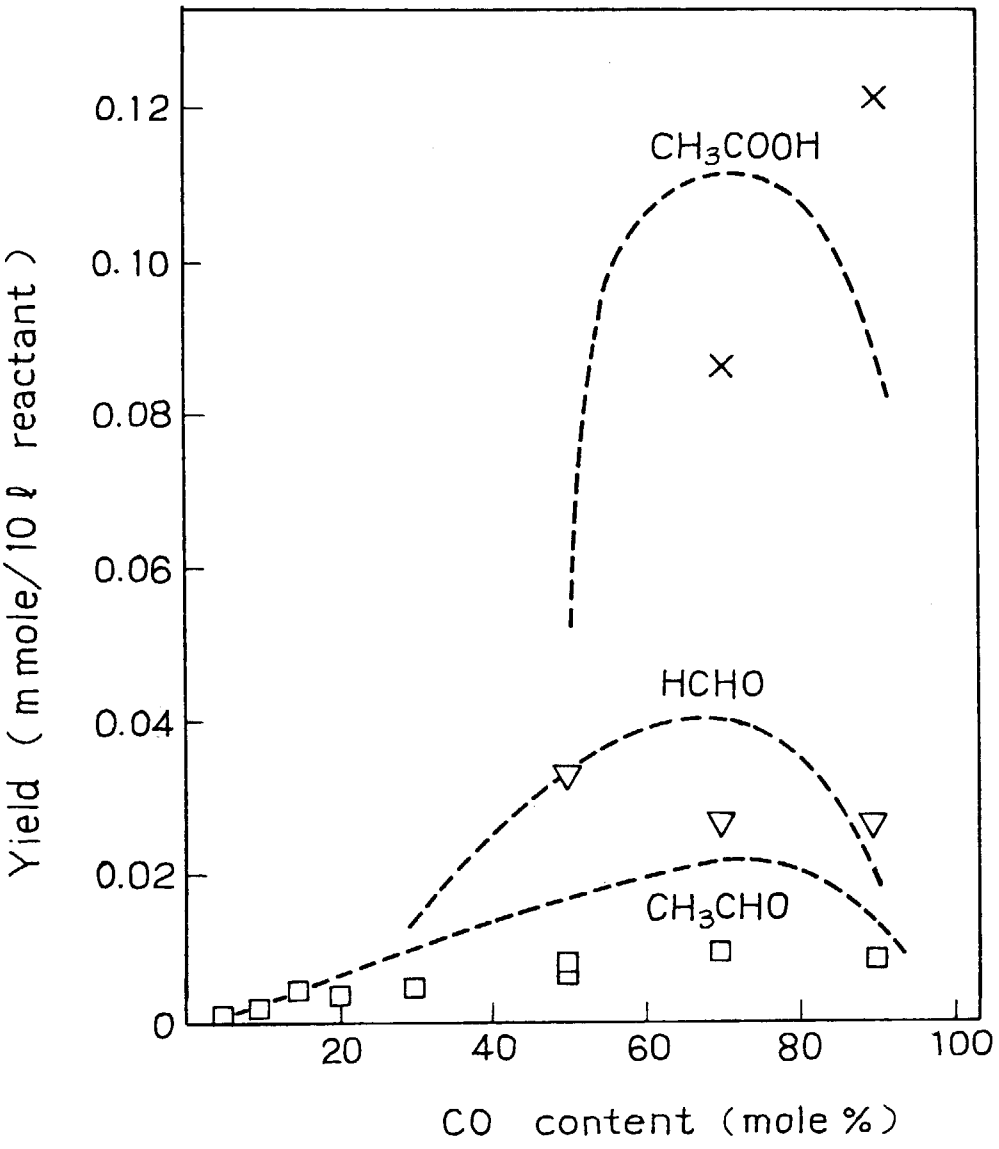

Fig. 3. Yields of acetic acid (×), formaldehyde (▽), and acetaldehyde (□) by irradiation of CO-H_2 mixtures over silica gel at 300°C. Broken lines indicate the yields obtained in the absence of silica gel.

$$H_2O + R \longrightarrow R\cdots O + H_2 \quad (2)$$

$$R\cdots O + CO \longrightarrow R + CO_2 \quad (3)$$

The dominant hydrocarbon produced over silica gel is methane with the yield of more than 75% of the total hydrocarbons over the whole range of the CO content. Fig. 2 shows the dependence of the yields of $C_1 \sim C_3$ hydrocarbons on the composition of the reactant gas. The yields of these hydrocarbons attain the maximum values at 40 ∿ 50 CO content and decrease with the CO content in the region above 50%. The decrease in the CO rich region may be attributed to deposition of the carbonaceous solid on the silica gel surface, which occurs preferably to the reaction producing hydrocarbons. In fact, silica gel after irradiation of CO-H_2 mixtures containing more than 50% CO changed in color to dark brown, due to deposition of the carbonaceous solid. As may be seen from Fig. 2, the yield of ethane is 1/7 of that of methane, and the yield of propane is 1/3 of that of ethane at 50% CO in the feed. The yields of olefins are considerably lower than those of the corresponding paraffins over the whole range; the yield of ethylene is ca. 1/15 of that of ethane and the yield of propylene is ca. 1/10 of that of propane.

Fig. 3 shows the yields of the three principal oxygen-containing products, acetic acid, formaldehyde, and acetaldehyde as a function of CO content in the feed. The yields of these organic oxygenates over silica gel are close to or lower than those produced in the absence of silica gel, indicating that the formation of these oxygenates is not influenced by the presence of silica gel. (S. Nagai, H. Arai, and M. Hatada)

1) JAERI-M 8569, 36 (1979).
2) S. Nagai, H. Arai, and M. Hatada, Radiat. Phys. Chem., 16, 175 (1980)
3) T. van Herwijnen and W. A. de Jong, J. Catal., 63, 83 (1980) and references cited therein.

4) E. H. Taylor, "Advances in Catalysis", 18, 111 (1968).

4. On the Structure of the Carbonaceous Solid Products in the Radiation-Induced Reactions of CO and $CO-H_2$ Mixture over Silica Gel

It has been already shown[1] that the formation of hydrocarbons by irradiation of $CO-H_2$ mixture over silica gel is due to the secondary reactions of H_2 with the carbonaceous solid deposited on the silica gel surface during irradiation. The deposition of the solid has been observed to occur preferably in the irradiation of $CO-H_2$ mixtures containing more than 50% CO. This is true not only in the reaction over silica gel but also in the homogeneous radiolysis. Described below are the preliminary results of our study on the structure of the carbonaceous solids produced from CO-rich $CO-H_2$ mixtures and from CO over silica gel. Regarding the structure of the carbonaceous solid produced in the homogeneous radiolysis of CO, Baird[2] carried out a detailed study using infrared spectroscopy and other techniques and concluded that the solid is a C_3O_2 polymer composed mainly of a linear structure.

Apparatus and procedures for irradiation are the same as in the previous studies. The carbonaceous solid deposited on silica gel was separated from silica gel by dissolving the silica gel into 10% aqueous solution of HF, followed by filtration and drying. The carbonaceous solid thus obtained was inspected by infrared and ESR spectra. For comparison, the carbonaceous solid produced in the homogeneous radiolysis of CO and CO-rich $CO-H_2$ mixture was also studied.

Fig. 1 shows the infrared spectra of the carbonaceous solids produced by irradiation of CO over silica gel and produced in the homogeneous radiolysis of CO and 9 : 1 $CO-H_2$ mixture. Spectrum (b) of the carbonaceous solid from CO in the homogeneous radiolysis agrees well with that reported by Baird[2]. Although the three spectra resemble each other, spectrum (a) and (c) show distinctly the characteristic absorption due to

CH_2 of CH_3 group. Therefore, it may be suggested that the carbonaceous solid produced over silica gel has an analogous structure to that of the solid produced by the homogeneous radiolysis of CO, which is a linear C_3O_2 polymer according to Baird[2], except that the former contains CH_2 or CH_3 group in it.

Fig. 2 shows the ESR spectra of the carbonaceous solids produced over silica gel and produced in the homogeneous radiolysis. Spectrum (a) of the solid produced over silica gel is a structureless single line with the linewidth of 10 G. Exactly the same spectrum was obtained for the carbonaceous solid by irradiation of 9 : 1 CO-H_2 mixture over silica gel. On the other hand, the carbonaceous solid produced by the homogeneous

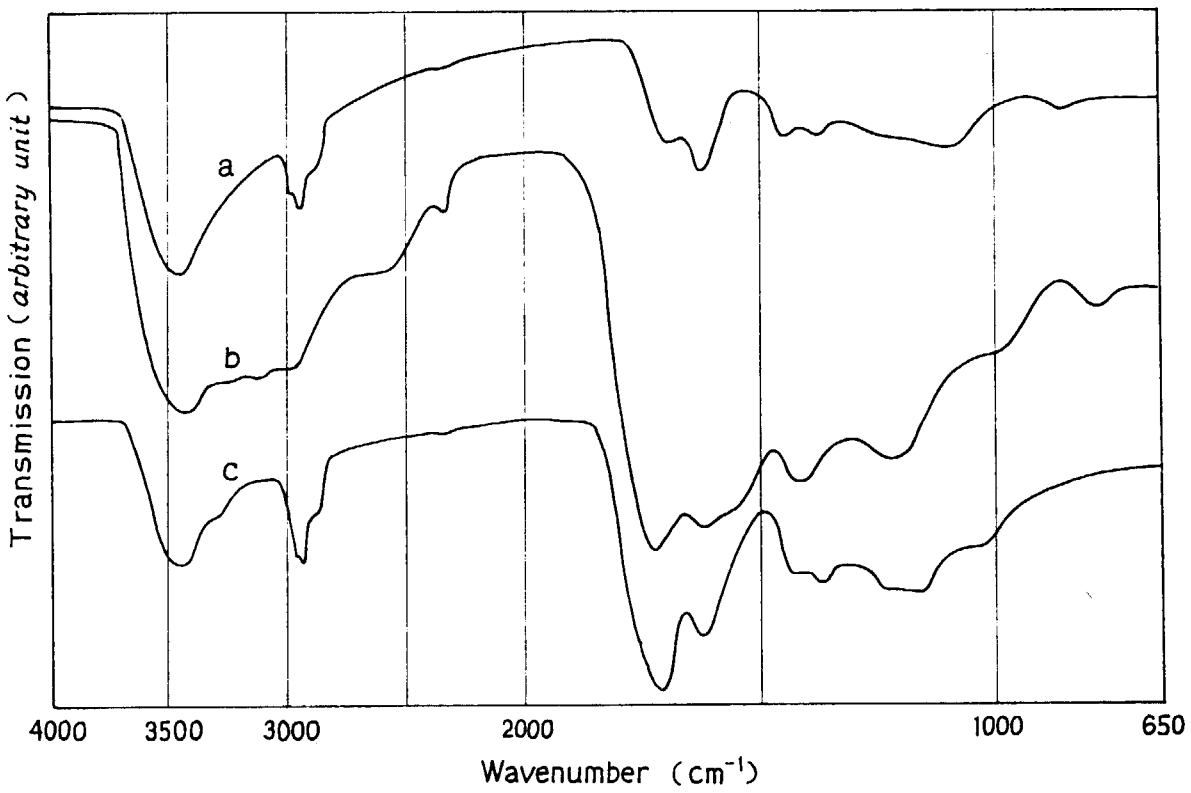

Fig. 1. Infrared spectra of the carbonaceous solids produced by irradiation of CO over silica gel (a), by homogeneous radiolysis of CO (b), and by homogeneous radiolysis of 9 : 1 CO-H_2 mixture (c) at 300°C.

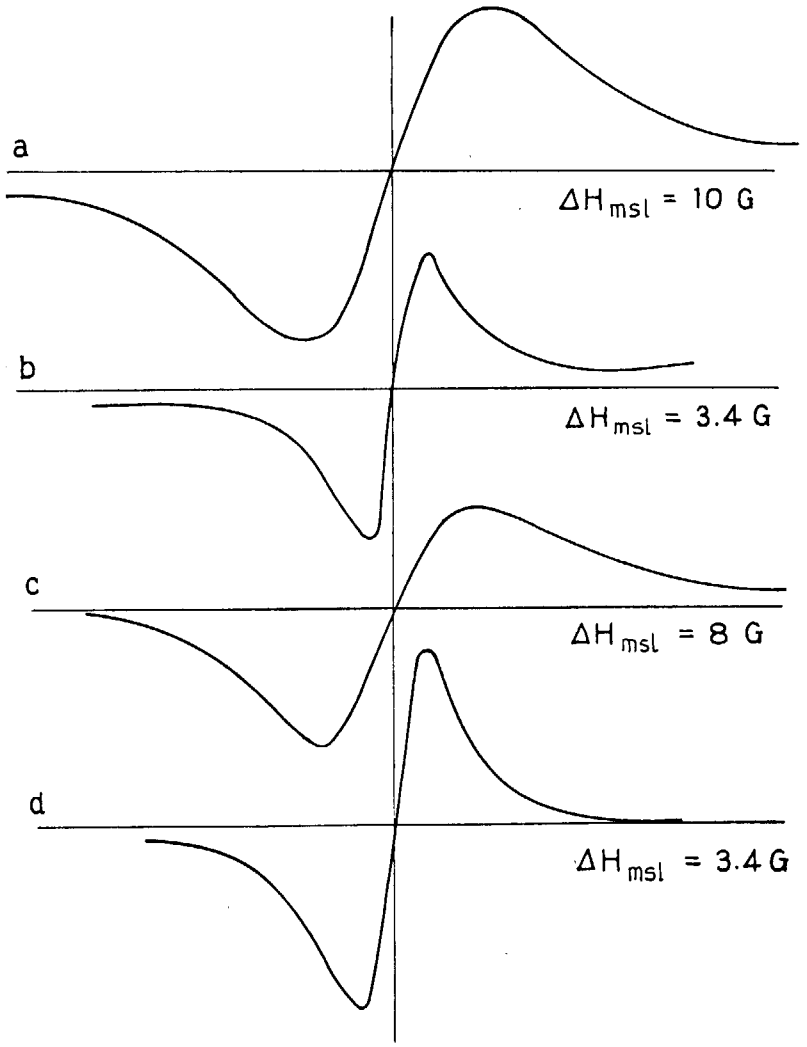

Fig. 2. ESR spectra of the carbonaceous solids produced by irradiation of CO over silica gel (a), by homogeneous radiolysis of CO (b), by homogeneous radiolysis of 9 : 1 $CO-H_2$ mixture (c), and homogeneous radiolysis of 9 : 1 $CO-D_2$ mixture (d) at 300°C.

radiolysis of CO gives spectrum (b) with the linewidth of 3.4 G which agrees well with that reported by Baird[2]. The carbonaceous solid produced by homogeneous radiolysis of 9 : 1 $CO-H_2$ mixture gives spectrum (c) with the linewidth of 8 G, close to that of spectrum (a). In an attempt to see if the difference in linewidth between spectrum (b) and (c) is due to an unresolved hyperfine structure arising from the interaction between the

unpaired electron and proton, 9 : 1 $CO-D_2$ mixture was irradiated in the homogeneous state and the resulting solid was inspected by ESR. The ESR spectrum of this solid is reproduced in Fig. 2 (d), which is apparently identical with spectrum (b) of the solid from CO. From these results, it may be concluded that the carbonaceous solid produced from CO over silica gel contains CH_2 or CH_3 unit in its structure as well as the solid produced from CO-rich $CO-H_2$ mixture, in agreement with the above result of the infrared study.

The incorporation of CH_2 or CH_3 unit in the structure of the carbonaceous solid produced from CO over silica gel suggests that silica gel participates in the formation of the solid, undergoing radiolysis of OH groups or adsorbed water on the surfaces. Further study on the structure and reaction of the carbonaceous solid is continued.

(S. Nagai, H. Arai, and M. Hatada)

1) S. Nagai, H. Arai, and M. Hatada, Radiat. Phys. Chem., 16, 175 (1980).
2) T. Baird, Carbon, 10, 723 (1972).

5. Radiation-Induced Reactions of Carbon Dioxide-Hydrogen Gas Mixture over Silica Gel

It is of interest to see if irradiation of carbon dioxide-hydrogen gas mixtures over silica gel produces hydrocarbon in high yield as found for the reaction of $CO-H_2$ mixtures. Moreover, it is of importance to study the CO_2-H_2 reaction since CO_2 is one of the principal products in the $CO-H_2$ reaction.

The apparatus and procedure employed are the same as in the $CO-H_2$ studies. CO_2 (Osaka Suiso Ind. Co.) was used as received.

Table 1 compares the product yields by irradiation of CO_2-H_2 gas mixtures over silica gel with those obtained by the homogeneous radiolysis. Included in this table are the data for the reaction over Cr_2O_3-ZnO that have been reported in the

Table 1. Product Yields by Irradiation of CO_2-H_2 Mixtures

Flow Rates (ml/min)	H_2	85.7	85.7	75	75	75
	CO_2	14.3	14.3	25	25	25
Solid		—	Silica Gel	—	Silica Gel	$Cr_2O_3 \cdot ZnO$
Beam Current (mA)		2	2	2	2	5
Temp. (°C)		300	300	300	300	275
Product Yields (μmole/10ℓ)						
CH_4		18	655	26	608	51
C_2H_4		0	0.9	0	0.6	0.1
C_2H_6		0.7	46	0.6	41	4.3
C_3H_6		0	1.3	0	0.6	0
C_3H_8		0.7	36	0.7	28	1.8
HCHO		0	0	0	0	3.7
CH_3OH		0	0	0	0	5.6
CH_3CHO		0	0	0	1.3	1.1
iso-C_4H_{10}		0.4	25	0.3	15	0
n-C_4H_{10}		0.5	10	0.5	7.6	0
CO		200	1200	450	1600	1680
H_2O		230	3400	540	3600	(8800)

Table 2. Product Yields by Irradiation of CO_2-H_2 and CO-H_2 Mixtures over Silica Gel

Flow Rates	H_2	85.7	75	50	99	85.7
(ml/min)	CO_2	14.3	25	50	—	—
	CO	—	—	—	1	14.3
Product Yeilds (μmole/10ℓ)						
CH_4		655	608	518	507	1753
C_2H_4		0.9	0.6	0.5	0.3	14
C_2H_6		46	41	24	34	190
C_3H_6		1.3	0.6	0.2	0.1	12
C_3H_8		36	28	14	17	105
CH_3OH		≈0	≈0	≈0	≈0	≈0
CH_3CHO		0.9	1.3	0.7	≈0.2	2.4
iso-C_4H_{10}		25	15	2.3	5.3	46
n-C_4H_{10}		10	7.6	2.7	4.2	24
iso-C_5H_{10}		9.7	6.3	0.9	2.7	20
n-C_5H_{10}		1.6	1.4	0.5	0.6	7.1
CO		1200	1600	2190	—	—
CO_2		—	—	—	37	2200
H_2O		3400	3600	2840	545	1070

Table 3. Product Distribution (%) over Silica Gel at 300°C

Product	H_2/CO_2 ratio			H_2/CO ratio	
	6 : 1	3 : 1	1 : 1	99:1	1 : 9
CH_4	83	86	92	89	87
C_2H_4	0.1	0.1	0.1	0.1	0.2
C_2H_6	6	6	4	6	9
C_3H_6	0.2	0.1	0.04	0.03	0.04
C_3H_8	5	4	3	3	2
iso-C_4H_{10}	3	2	0.4	1	0.2
n-C_4H_{10}	1	1	0.5	1	0.2
iso-C_5H_{12}	1	1	0.2	0.5	0.1
n-C_5H_{12}	0.2	0.6	0.1	0.1	0.04

last annual report[1]. Apparently, the presence of silica gel enhances the yields of paraffins together with those of H_2O and CO. It is noted that the yield of CO is lower than that of H_2O over silica gel, in contrast to the homogeneous radiolysis which produces nearly equal amounts of H_2O and CO. The lower yield of CO compared to H_2O may be accounted for by consumption of a part of CO to produce hydrocarbons, as will be described below.

Table 2 and Table 3 compare the CO_2-H_2 reaction and CO-H_2 reaction over silica gel. As may be seen from Table 2, the yields of hydrocarbons, especially paraffins of low-molecular weight, from CO_2-H_2 are little dependent on the gas composition and close to those in the 1:99 CO-H_2 reaction. The hydrocarbon distribution shown in Table 3 indicates that the CO_2-H_2 reaction is highly selective toward the formation of methane, in accordance with the usual catalytic reactions of CO_2-H_2 over metal catalysts. The good agreement both in the paraffin yields and in the product distribution for the CO_2-H_2 reaction and 1:99 CO-H_2 reaction suggests that hydrocarbons from CO_2-H_2 are produced through the formation of CO. If one takes into account that the yield of H_2O from CO_2-H_2 is much greater than that from 1:99 CO-H_2, one may explain the radiation-induced reaction of CO_2-H_2 mixture by the backward water-gas shift reaction, that is,

$$H_2 + CO_2 \longrightarrow H_2O + CO \qquad (1)$$

followed by the reaction to produce hydrocarbons, predominantly methane, according to

$$CO + 3H_2 \longrightarrow CH_4 + H_2O\ . \qquad (2)$$

If the above explanation is correct, the high yields of hydrocarbons and H_2O by irradiation of CO_2-H_2 over silica gel as observed in this study mean that silica gel would show high catalytic activity not only in the reaction (1) but also the reaction (2) under electron beam irradiation. The activity of silica gel in the reaction (2) may originate from transient

surface sites (R) that is the same as assumed in the $CO-H_2$ reaction in the preceding paper. Then the radiation-induced reaction (1) over silica gel may be represented by the following reaction sequences:

$$CO_2 + R \longrightarrow R\cdots O + CO \qquad (3)$$

$$R\cdots O + H_2 \longrightarrow R + H_2O\ . \qquad (4)$$

(S. Nagai, H. Arai, and M. Hatada)

1) JAERI-M 8569, 44 (1979).

6. The Effects of Dose, Dose Rate, and Temperature on the Radiation Chemical Reaction of Pure Methane

In the annual report of the year before the last year[1], preliminary description was made on the effect of temperature on the amounts of products. Meanwhile it was proved that the correction on absorption dose in the gas flow due to volume expansion resulted by temperature rise can not be ignored. This correction can not be made by simple calculation on the data obtained previously for the products which give non-linear dose-conversion curves. Therefore, we have carried out further experiment this year in order to obtain precise temperature dependence of the amounts of products. In this experiment, the flow rate was adjusted so that the residence time of the reactant molecules in the irradiation zone of the reactor was constant at 6.64 sec regardless of the temperature of the reaction vessel. The flow rate was 100 ml/min at 50°C and 60 ml/min at 270°C. The irradiations were carried out with electron beam (0.6 MV, 0.5 mA; scanning width, 30 cm) from the HDRA. The dose absorbed by methane gas was about 7.8 Mrad. The method of analysis of the products are the same as that described in the previous report[2].

In Table 1, the amounts of products are listed as a

Table 1. Effect of Temperature on the Product Yields: Reactant, CH_4; Electron Beam, 600 keV, 0.5 mA; Scanning Width, 30 cm; FIXCAT-II, 791108

Exp. No.	17:53	17:00	16:10	14:00	13:23	12:45	12:03	11:20
CH_4 Flow Rate (ml/min)	89.4	83.2	76.7	73.1	68.6	65.8	62.7	60.0
Beam Current (mA)	0.5	0.5	0.5	0.5	0.5	0.5	0.5	0.5
Irrad. Temp. (°C)	90	118	150	170	197	220	246	269
1/T (10^{-3} K^{-1})	2.75	2.56	2.36	2.26	2.13	2.03	1.927	1.845
Yield (μmole/10ℓ reactant gas at 25°C, 1 atm), (G-value)								
H_2	336 (6.35)	344 (6.53)	380 (7.18)	414 (7.83)	459 (8.62)	507 (9.59)	565 (10.7)	596 (11.4)
C_2H_2	— }	— }	0.37 (0.0071)	0.43 (0.0081)	0.54 (0.010)	0.64 (0.012)	0.70 (0.013)	0.77 (0.015)
C_2H_4	—	—	7.5 (0.14)	8.6 (0.16)	10.7 (0.200)	12.1 (0.228)	16.1 (0.306)	16.7 (0.318)
C_2H_6	121 (2.29)	130 (2.48)	144 (2.72)	155 (2.92)	177 (3.33)	195 (3.68)	220 (4.17)	243 (4.64)
C_3H_6	0.47 (0.0089)	0.49 (0.0093)	0.61 (0.012)	0.65 (0.012)	1.0 (0.019)	1.3 (0.025)	2.0 (0.038)	2.4 (0.046)
C_3H_8	21.1 (0.400)	23.3 (0.443)	26.8 (0.507)	28.2 (0.533)	32.9 (0.618)	32.3 (0.685)	40.5 (0.769)	43.7 (0.835)
iso-C_4H_{10}	3.1 (0.059)	3.8 (0.071)	4.7 (0.089)	5.2 (0.097)	6.1 (0.12)	6.8 (0.13)	7.7 (0.15)	8.1 (0.16)
1-C_4H_8	0.084 (0.0016)	—	0.10 (0.0020)	0.11 (0.0021)	0.21 (0.0040)	0.23 (0.0044)	0.47 (0.0089)	0.58 (0.011)
n-C_4H_{10}	3.9 (0.074)	3.5 (0.067)	3.6 (0.067)	3.6 (0.067)	3.6 (0.067)	3.9 (0.073)	4.3 (0.081)	4.5 (0.086)
2-C_4H_8	trace	trace	trace	trace	trace	trace	trace	trace
neo-C_5H_{12}	0.63 (0.012)	0.85 (0.016)	1.2 (0.023)	1.4 (0.027)	2.0 (0.037)	2.4 (0.046)	3.0 (0.057)	3.3 (0.062)
iso-C_5H_{12}	3.0 (0.057)	3.3 (0.063)	3.7 (0.069)	3.9 (0.074)	4.2 (0.078)	4.4 (0.082)	4.5 (0.085)	4.6 (0.087)
n-C_5H_{12}	0.25 (0.0047)	0.30 (0.0057)	0.62 (0.012)	0.42 (0.0079)	0.53 (0.0099)	0.88 (0.017)	0.91 (0.017)	1.1 (0.021)
Absorbed Energy (Mrad)	7.81	7.79	7.81	7.83	7.86	7.81	7.79	7.79
(10^{20} ev/g)	4.87	4.86	4.88	4.88	4.91	4.88	4.86	4.86
(10^{21} eV/10ℓ 25°C 1 atm)	3.18	3.18	3.18	3.19	3.20	3.18	3.17	3.18

Note: nd, not detected; nm, not measured.

Table 2. Effect of Temperature on the Product Yields: Reactant, CH_4; Electron Beam, 600 keV, 0.5 mA; Scanning Width, 30 cm; FIXCAT-II, 791107

Exp. No.	15:40	16:35	17:18	17:55	18:40	18:40(791108)
CH_4 Flow Rate (ml/min)	100	85.8	72.8	65.9	63.9	89.7
Beam Current (mA)	0.5	0.5	0.5	0.5	0.5	0.5
Irrad. Temp. (°C)	50	114	174	220	240	56
1/T (10^{-3} K^{-1})	3.10	2.58	2.24	2.03	1.95	3.04
Yield (μmole/10ℓ reactant gas at 25°C, 1 atm), (G-value)						
H_2	287 (5.40)	337 (6.54)	395 (7.47)	492 (9.30)	522 (9.97)	296 (5.59)
C_2H_2	0.51 (0.0098)	0.41 (0.0079)	0.43 (0.0081)	0.66 (0.012)	0.70 (0.013)	—
C_2H_4	4.8 (0.090)	7.1 (0.14)	6.3 (0.12)	10 (0.20)	—	—
C_2H_6	110 (2.07)	136 (2.64)	160 (3.02)	197 (3.72)	206 (3.94)	110 (2.07)
C_3H_6	0.28 (0.0053)	0.31 (0.0061)	0.57 (0.011)	1.0 (0.019)	1.6 (0.030)	0.48 (0.0090)
C_3H_8	19.5 (0.367)	25.7 (0.499)	31.7 (0.598)	38.5 (0.728)	39.9 (0.762)	17.2 (0.325)
iso-C_4H_{10}	2.6 (0.050)	4.1 (0.080)	5.9 (0.11)	7.4 (0.14)	7.8 (0.15)	2.3 (0.043)
1-C_4H_8	0.059 (0.0011)	0.050 (0.00089)	0.11 (0.0020)	0.18 (0.0034)	0.33 (0.0062)	0.097 (0.0018)
n-C_4H_{10}	4.4 (0.083)	3.5 (0.068)	3.3 (0.062)	3.7 (0.070)	4.0 (0.076)	4.6 (0.086)
2-C_4H_8	trace (<0.01)	trace	trace	trace	trace	trace
neo-C_5H_{12}	0.33 (0.0062)	0.81 (0.016)	1.6 (0.029)	2.3 (0.044)	2.7 (0.052)	0.32 (0.0060)
iso-C_5H_{12}	2.3 (0.042)	3.1 (0.060)	3.8 (0.072)	4.4 (0.083)	4.5 (0.085)	2.4 (0.046)
n-C_5H_{12}	0.19 (0.0036)	0.37 (0.0072)	0.53 (0.010)	0.77 (0.015)	0.90 (0.017)	0.19 (0.0036)
Absorbed Energy (Mrad)	7.84	7.63	7.79	7.79	7.79	7.80
(10^{20} eV/g)	4.90	4.76	4.86	4.86	4.86	4.87
(10^{21} ev/10ℓ 25°C 1 atm)	3.20	3.11	3.17	3.17	3.17	3.18

Note: nd, not detected; nm, not measured.

function of temperature, in which the data were obtained at 50°C and then at higher temperature one after the other. The data listed in Table 2 were obtained with reverse order as that done in Table 1. The G values of the products are also listed in the Tables. The plots of the G values of the products are shown in Fig. 1, where a set of data for a product by the two different orders lie on a same line, indicating that a part of the product does not remain in the reaction vessel nor does a part of the products which might have been accumulated in the previous run desorp out to introduce errors to analysis results.

The G values of the most products increase with increasing temperature and the slopes of the plots are higher at higher temperature region above 150°C as shown in Fig. 1. However, there are some exceptions: the G values of n-butane and acetylene decrease and then increase with increasing temperature above 180°C, and the slope of the plot for i-pentane is smaller at higher temperature region than at the lower one. The apparent activation energies as obtained from the slope of the Arrhenius plots in Fig. 1 at 100°C and 200°C are listed in Table 3.

The increase of G value of hydrogen molecule is explained by the reaction (1) which occurs more frequently with increasing temperature:

$$H + CH_4 \longrightarrow H_2 + \dot{C}H_3 \qquad (1)$$

The G value of thermal hydrogen atom formation is reported to be 7.56 by Okazaki, et al.[3] and the thermal hydrogen atoms do not react with methane according to reaction (1) at room temperature and recombine with methyl radical to reform methane. The possibility to form hydrogen molecules by combination of two thermal hydrogen atoms is small unless the third body is present. If we neglect the loss of hydrogen atoms by addition to lefins, the largest $G(H_2)$ value would be 13.26 as a sum of $G(H)$, $G(H')$ and $G^M(H_2)$, where $G(H')$ is hot hydrogen yield and $G^M(H_2)$ is molecularly produced hydrogen yield which are estimated to be 1.07 and 4.63 respectively[3].

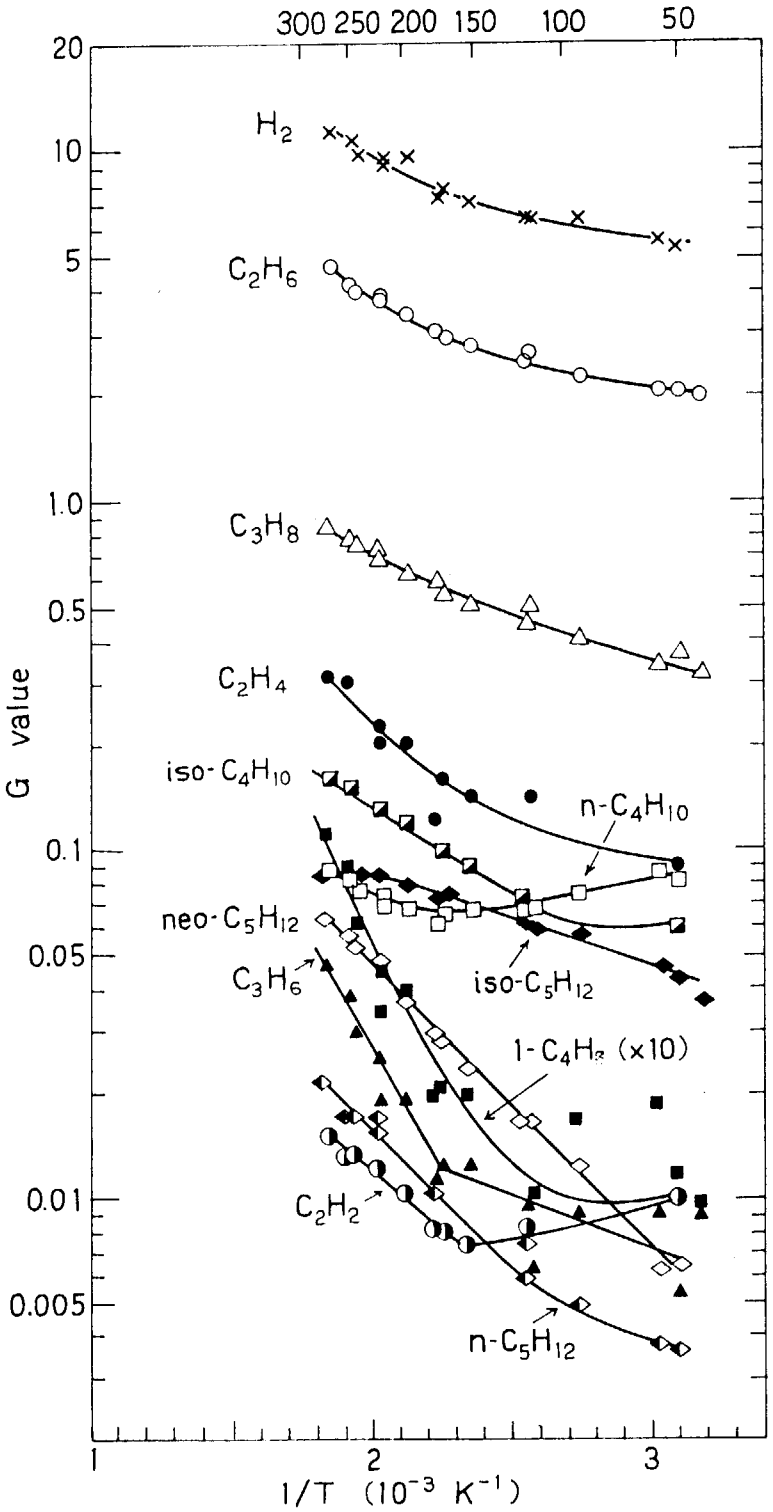

Fig. 1. G value vs. 1/T plots for the products from irradiated methane.

Table 3. Apparent Activation Energy (E_{app}) Estimated from Fig. 1

Product	E_{app} (kcal/mole)	
	75°C	200°C
H_2	0.7 (0.2)	2.0 (3.4)
C_2H_6	0.6	2.8
C_3H_8	1.1	2.0
n-C_4H_{10}	-1.0	1.6
n-C_5H_{12}	1.8	3.7
iso-C_4H_{10}	0	2.3
iso-C_5H_{12}	1.3	0.37
neo-C_5H_{12}	3.7	3.7
C_2H_4	0.69	3.4
C_3H_6	0	6.6
1-C_4H_8	0	7.4
C_2H_2	-0.85	2.9

The values in the parenthses are by Maurin[6].

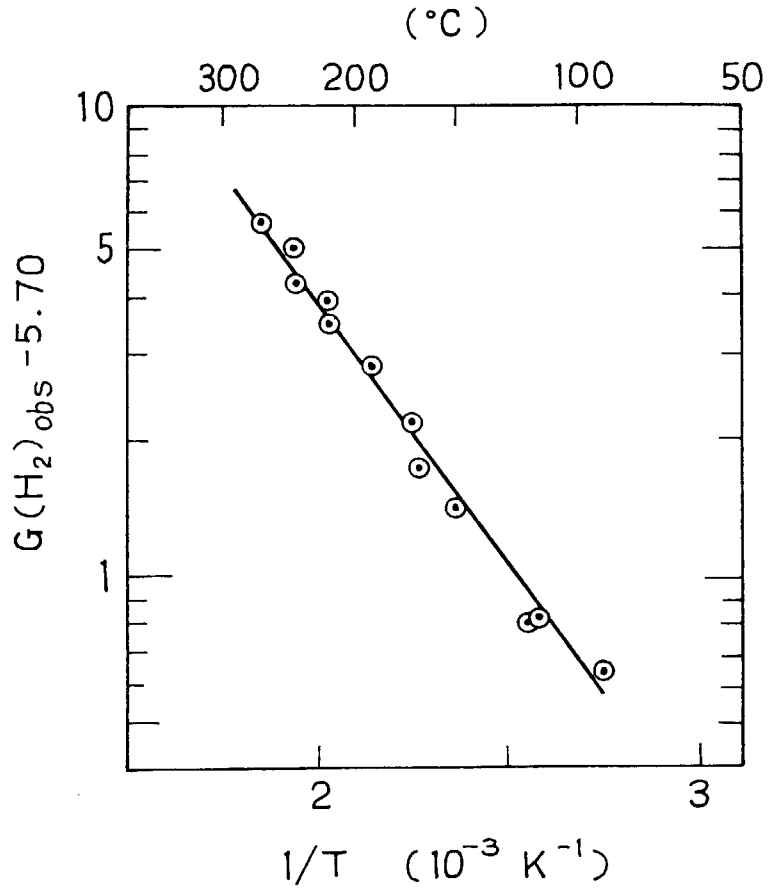

Fig. 2. Plot of $G(H_2)_{obs}$-5.70 as a function of 1/T.

According to the above scheme, $G(H_2)_{obs}$ - 5.70 gives an estimation of hydrogen atoms contributing to hydrogen formation at elevated temperatures, where $G(H_2)_{obs}$ is the observed G values of hydrogen molecule. Fig. 2 shows the plot of $G(H_2)_{obs}$ - 5.70 as a function of 1/T. The activation energy estimated from this figure is about 5.0 kcal/mole, which is close to 4.5 kcal/mole reported for reaction (1)[4].

The increase of G values of most hydrocarbon products may be resulted from the increase of methyl radical concentration according to reaction (1) and subsequent reactions involving methyl radicals.

The temperature dependence of G(n-butane) is more complex. At the lower temperature region, n-butane is considered to be formed mainly via combination of two ethyl radicals (2), which is competed with the disproportionation reaction (3),

$$\dot{C}_2H_5 + \dot{C}_2H_5 \begin{cases} \nearrow n\text{-}C_4H_{10} & (2) \\ \searrow C_2H_6 + C_2H_4 & (3) \end{cases}$$

The ratio of the rate constant of the disproportionation reaction (3), k_d, to that of the combination reaction (2), k_c, is reported to increase with increasing temperature. Moreover, Bevington[5] predicted from, the thermodynamical considerations that disproportionation overcomes combination for aliphatic radicals at higher temperatures. Thus, the decrease of G(n-butane) with temperature in low temperature region can be explained by the above competing reactions. The disproportionation reactions such as reaction (3) may occur more frequently with increasing temperature. The increase of G(n-butane) above 170°C may be explained by the increase of methyl radical concentration with increasing temperature by the reaction scheme (1) resulting in the increase of ethyl radicals by successive reactions of methyl radicals. Thus the number of ethyl radical increased with increasing temperature may be more than that necessary to compensate the loss of ethyl radical by reaction (3), and the net increase of ethyl radical may explain the observed increase of G(n-butane) above 170°C.

The slight decrease of apparent activation energy of i-pentane formation above 100°C may be due to the abstraction reaction of tertiary hydrogen atom of i-pentane by hydrogen atom or methyl radical. The resulting radical may further react to form hexanes which are not determined quantitatively in the present study.

(H. Arai, S. Nagai, K. Matsuda, and M. Hatada)

1) H. Arai, S. Nagai, K. Matsuda, and M. Hatada, JAERI-M 7949, 27 (1978).
2) This annual report.
3) K. Okazaki, S. Sato, and S. Ohno, Bull. Chem. Soc. Japan, 49, 174 (1976).
4) M. R. Berlie and D. J. LeRoy, Can. J. Chem., 32, 650 (1954).

5) J. C. Bevington, Trans. Faraday Soc., 48, 1045 (1952).
6) J. Maurin, J. Chim. Phys., 59, 15 (1962).

7. The Amounts of Products Produced by Electron Beam Irradiation of Large Dose on Methane Gas

In the previous report[1], it was reported that about 90% of methane was consumed by about 3 x 10^4 Mrad irradiation with the formations of hydrogen, ethane, and solid paraffin. However, since the material balance was not good enough to permit further discussion on the fate of the reactant under electron beam irradiation of a large dose, the study has been continued in an attempt to obtain the time conversion curves and quantitative analysis of the products at doses up to 10^4 Mrad.

A cylindrical reactor made of stainless steel of 7.1 ℓ volume (inner diameter, 151 mm; length, 370 mm) was used. An irradiation window (length, 235 mm; width, 86 mm) is equipped on the cylindrical surface so that the longer direction of the window is parallel to the axis of the cylinder. The details of the reactor was the same as those described elsewhere[2] except that an aluminum irradiation window (thickness, 100 μm) was used instead of a titanium window.

The reactor was evacuated to the vacuum above 10^{-6} Torr at 80°C and then cooled down to the room temperature (16°C). Methane was introduced into the reactor up to 760 Torr, and a teflon stop valve was closed. The reactor was disconnected from the vacuum system and carried to the irradiation room for irradiation. The maximum temperatures attained during irradiation (0.6 MV, 1 mA) were estimated by heat labels attached on the wall, at the middle and bottom of the cylinder surface, and at the center of either of the flat surfaces, where the label indicated 104, 127, and 60°C, respectively. The pressure of the gas was monitored by a pressure gauge (Toyoda 2H 2230 with a balance unit, type AA 3011). The mean temperature of the gas calculated from the maximum pressure increase during the irradiation was ca. 80°C, which was in the temperature range

indicated by the heat labels.

After the irradiation, the reaction vessel was cooled down to room temperature, and the pressure was measured. The reactor was connected to a vacuum pump through the gas samplers of the gaschromatographs, and irradiated methane was subjected to gaschromatography on 3 m Porapak Q and 2 m Porapak N columns to determine the amounts of hydrogen, methane, and hydrocarbon products containing carbon atoms less than five. After the gas analysis, the reaction products and unreacted methane in the reactor were transferred through a trap cooled by liquid nitrogen. During this procedure, the reactor was kept at 40°C. The trap was then warmed to room temperature to remove unreacted methane and volatile hydrocarbon products. Remaining liquid in the trap was collected and weighed as condensable products. The irradiation window was removed to collect non-volatile product which is yellowish viscous oil. The condensable and non-volatile products were analyzed by gaschromatography on 3 m OV-1 column. The latter products were further subjected to infrared spectroscopy, GPC and refractive index measurement using a Hitachi 215 type infrared spectrophotometer, a Toyo Soda gel permuation chromatograph (type 801A), and a Shimadzu refractometer (No. 58740), respectively. The GPC curves were obtained on a 2 ft H200 column combined with a 2 ft H4000 column.

Most irradiations were carried out at beam current of 1 mA and electron accelerating voltage of 0.6 MV, except for 3.1×10^4 Mrad irradiation where the beam current was 3.1 mA. Dose rate absorbed by methane estimated from the result of dosimetry carried out by Sugimoto, et al.[2], using nitrous oxide dosimeter was 1.21×10^3 Mrad/h/mA.

The experimental conditions and the amounts of the products are listed in Table 1. The results of gas analysis are listed in Table 2.

It is of interest to know the amounts of products and methane in the system when extremely large dose are absorbed in the system. Suppose that methane is converted to hydrogen and hydrocarbons according to reaction (1)

Table 1. Reaction Condition and the Amounts of Products

Run No.	F-2	SS-1	SS-2	SS-3	SS-4
Beam Current (mA)	1	1	1	1	3.1
Irradiation Time (hr)	0.016	3	6	12	8
Dose Rate (Mrad/s)		1.21	1.21	1.21	3.75
Dose (10^3 Mrad)	0.15	3.6	7.2	14.5	3.0
Average Temperature of Gas (°C)	69	85.3	67.6	95	88
Pressure of CH_4 (Torr)	-	760	760	760	760
Room Temperature	-	15.5	18	16	13
The amounts of Methane (mole)	-	0.300	0.297	0.300	0.303
Pressure after Irradiation (Torr)	-	752	666	756	814
Room Temperature (°C)	-	12.5	11	15	13
The amount of Gas after Reaction(mole)	-	0.300	0.267	0.300	0.324
The amounts of Products (g)					
Gas	0.10	4.00	2.70	2.13	1.35
Condensable Products	-	1.2	0.18	0.55	0
Non-volatile Products	-	0.486	1.05	1.39	1.24
Methane	-	2.77	1.42	0.83	0.67
$\frac{\text{The amount of Methane} \times 100}{\text{The amount of Products and Unreacted Methane}}$	-	95.5	82.6	81.9	64.1

Table 2. The Amounts of Products and Reactant Obtained from Gas Analysis (m mole/10ℓ reactant)

Run No.	F-1	F-2	SS-1	SS-2	SS-3	SS-4
Dcse (10^3 Mrad)	0.049	0.15	3.6	7.2	14.5	25.0
H_2	2.0	5.7	144	225	334.8	395
CH_4	-	-	275.	132.	77.4	41
C_2H_4	0.012	0.016	0.08	0.06	0.08	0.05
C_2H_6	0.691	2.09	34.2	31.6	24.6	10.8
C_3H_6	0.001	0.001	0.010	0	0.016	0.01
C_3H_8	0.11	0.34	6.0	6.3	5.1	1.6
i-C_4H_{10}	0.011	0.038	0.8	0.9	0.9	0.4
n-C_4H_{10}	0.039	0.12	1.5	1.8	1.6	-
neo-C_5H_{12}	0.002	0.009	0.2	0.2	0.2	0.8
i-C_5H_{12}	0.013	0.041	0.6	0.6	0.9	0.7
n-C_5H_{12}	0.001	0.003	0.06	0.07	0.13	0.15

$$n\ CH_4 \xrightarrow{\sim\sim\sim} (CH_2)_n + n\ H_2 \qquad (1)$$

the amount of methane consumed (in mole) should be equal to that of hydrogen formed and to that of CH_2 unit contained in hydrocarbon products. On the other hand, in the case where methane was converted to carbon and hydrogen according to reaction (2),

$$n\ CH_4 \xrightarrow{\sim\sim\sim} n\ C + 2n\ H_2 \qquad (2)$$

the amount of hydrogen would have been twice as much as that of consumed methane.

In Fig. 1, the amounts of products and methane are plotted as a functon of dose. Almost 90% of methane is consumed by 30 Grad irradiation, and the same amount of hydrogen as that of methane consumed are produced. The amounts of the condensable and the non-volatile products increase with dose, while the amount of ethane increases and then decreases with increasing dose after 3000 Mrad irradiation. The amounts of other hydrocarbon products except neo-pentane also increased and then decreased with increasing dose above doses larger than 3000 Mrad. The amount of neo-pentane increases with increasing dose. Sum of CH_2 units contained in hydrocarbon products at 1×10^4 Mrad dose is about 90% of methane consumed. These results suggest that the reaction of type (1) occurs in the system.

In Figs. 2a, 2b and 2c, the G values of hydrocarbons are plotted as a function dose along with those obtained by flow technique at 1 mA beam current[1]. Although the dose rates are not exactly the same for the flow experiment and the batch experiment (2.4 Mrad/sec and 1.12 Mrad/sec, respectively) carried out at the same beam current of 1 mA, we tentatively regarded as approximately the same dose rate for both experiments. The plots lie on a smooth line, indicating the continuity of the two experiments. The decrease in G values of saturated hydrocarbons with increasing dose above 10^3 Mrad may resulted from the fact that most reactant has been consumed.

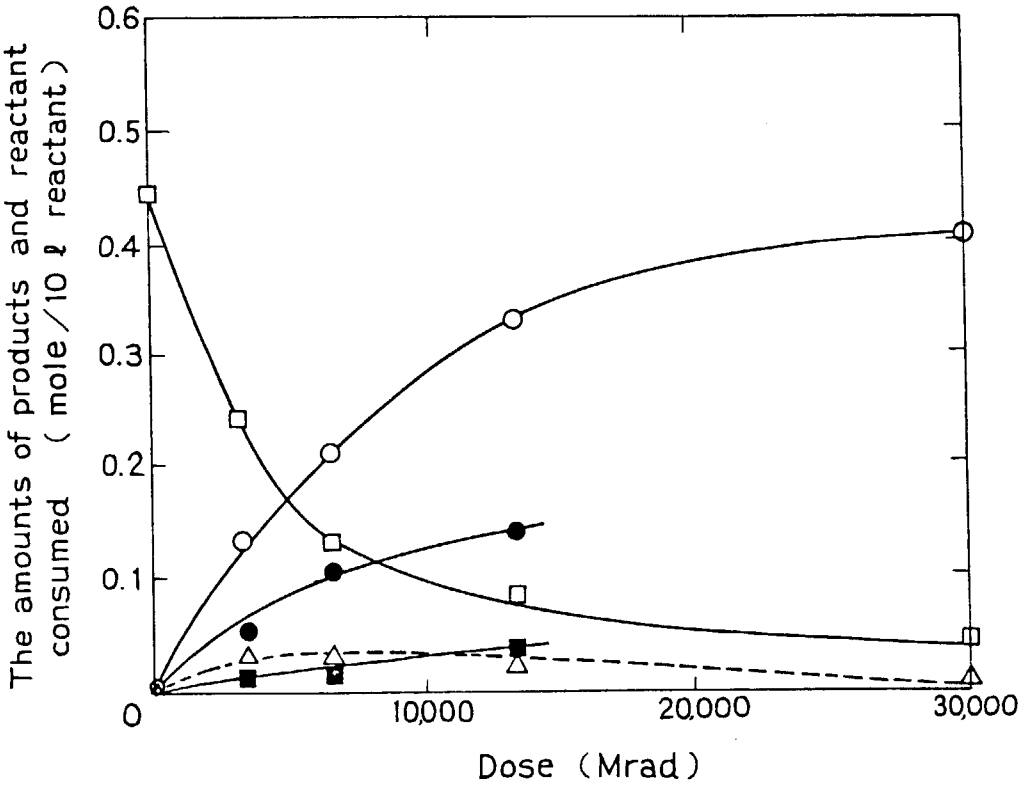

Fig. 1. The amounts of products and remaining methane as a function of dose; (□) remaining methane, (○) hydrogen, (△) ethane, (■) condensable product, (●) non-volatile product; for the latter two, the amounts were calculated on the basis of CH_2 unit. The reactor of the batch type was used. The value plotted at 1050 Mrad were obtained using the flow type reactor.

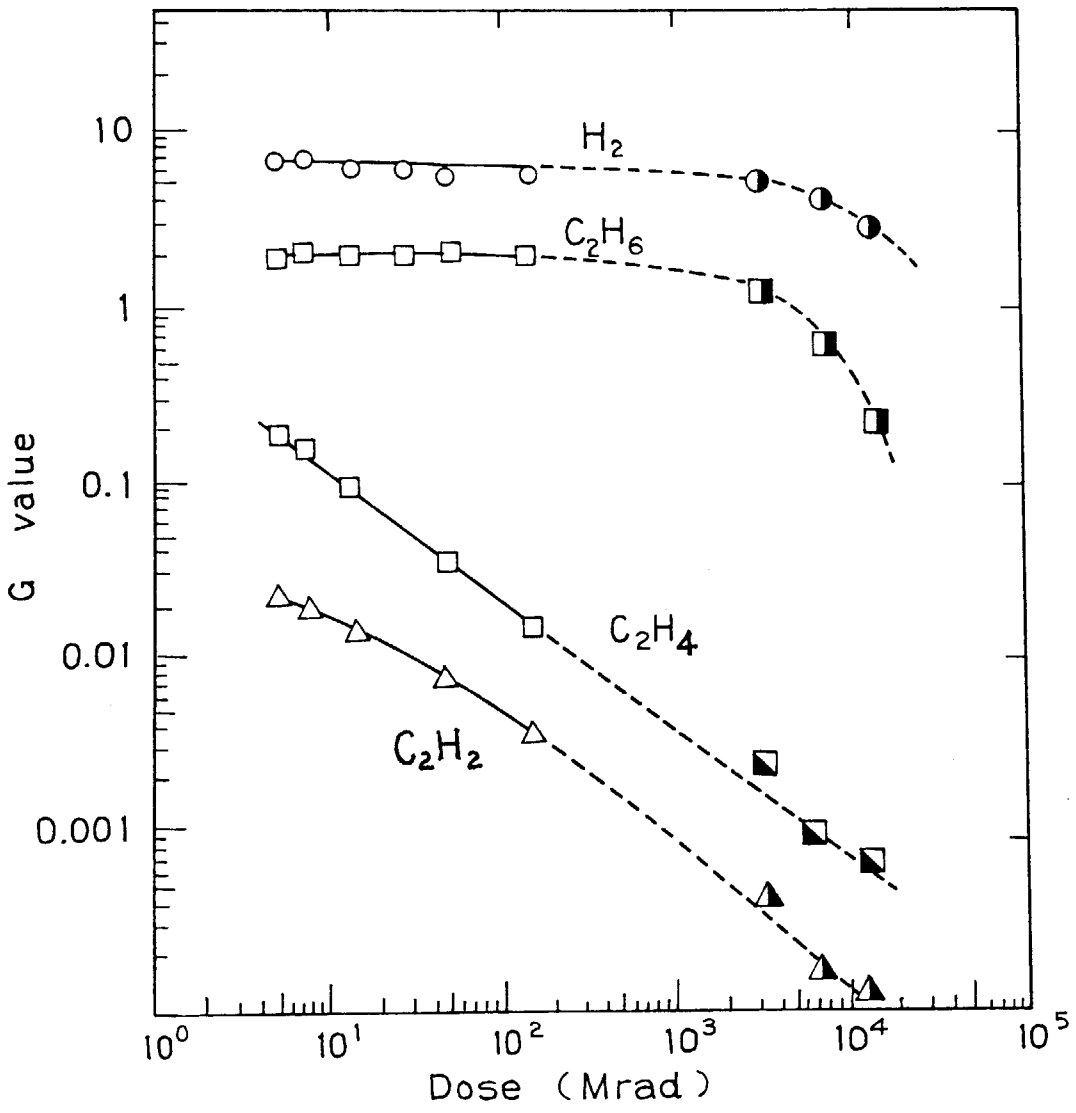

Fig. 2a. G values of hydrogen, ethane, ethylene, and acetylene as a function of dose: Half filled symbols, present work; Blank symbols, ref. 1.

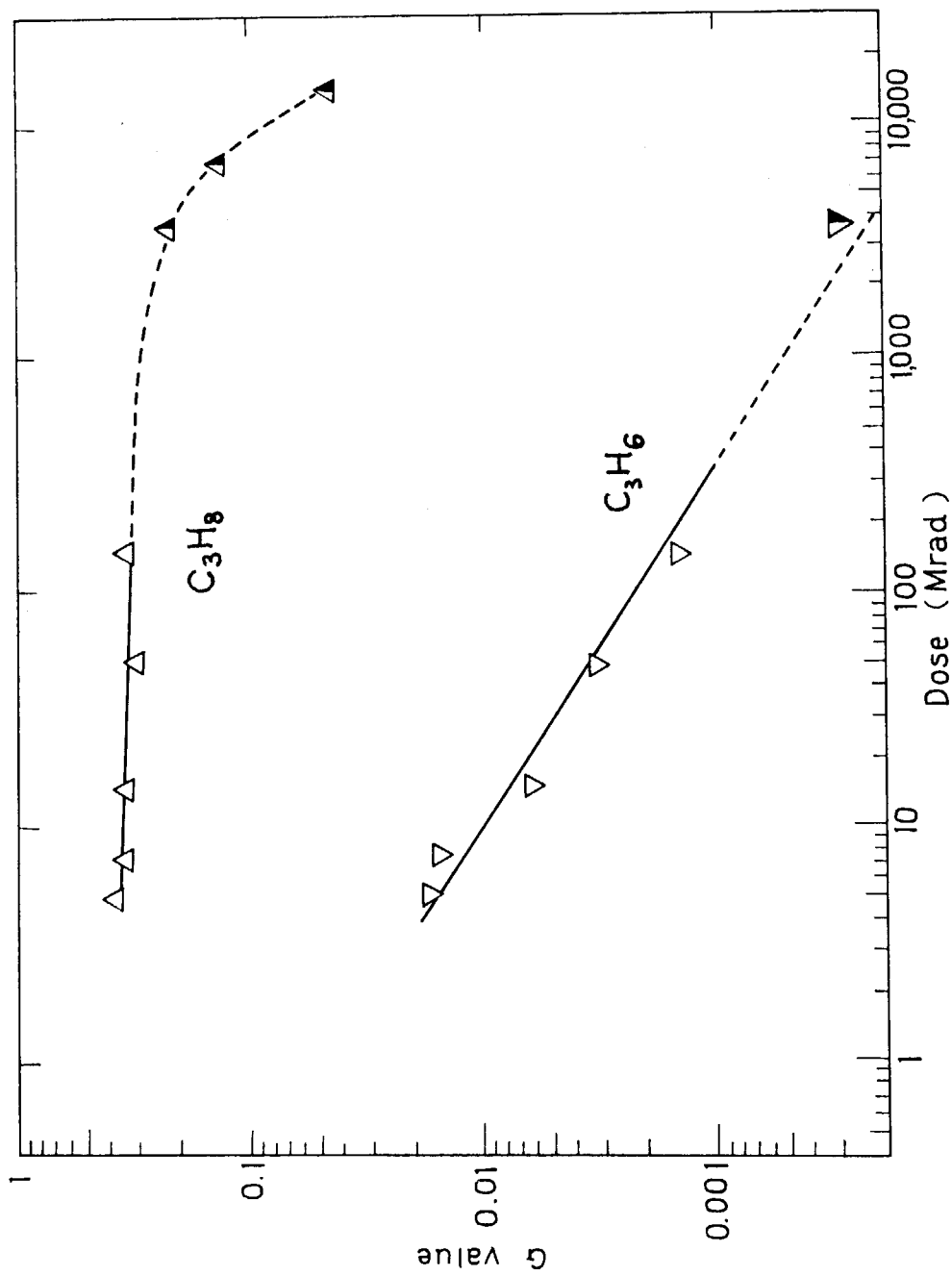

Fig. 2b. G values of propane and propylene as a function of dose: Half filled symbols, this work, Blank symbols, ref. 1.

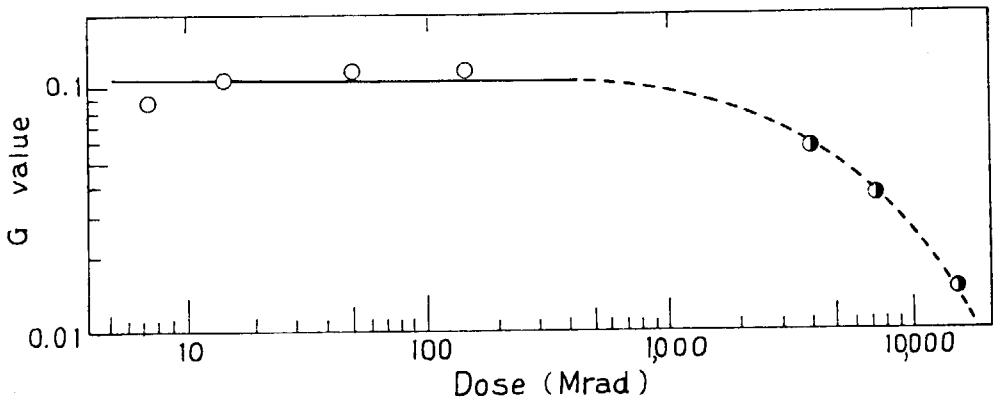

Fig. 2c. G value of n-butane as a function of dose: Half filled symbols, this work; Blank symbols, ref. 1.

The decrease in G values of unsaturated hydrocarbons may be resulted from the addition of hydrogen atom to lefins.

The gaschromatograms of the condensable products are shown in Fig. 3a, 3b, and 3c with an approximate scale of carbon numbers calibrated with retention time of authentic samples. The gaschromatograms indicate that the condensable fractions obtained by different doses give qualitatively the same carbon number-distributions ranging from C_5 to C_{15}.

The gaschromatograms of non-volatile products obtained at different doses (3.4×10^3, 6.7×10^3, and 14.5×10^3 Mrad) in Figs. 4a, 4b, and 4c, respectively, with an approximate carbon number scale obtained from the retention times of authentic samples. It is noted that the maxima appear at the retention time close to that of n-hexadecane for the former two, while for the latter, the maximum appears at the retention time shorter than that for the former two.

The GPC curves for these non-volatile products are shown in Figs. 5a, 5b, and 5c, with a molecular weight scale calibrated by the retention time of polystyrene of known molecular weight. Again it is noted that the maxima appear at the molecular weight of 200, while the maximum for the latter appears at smaller molecular weight than those for the former two.

The infrared spectrum of the non-volatile products

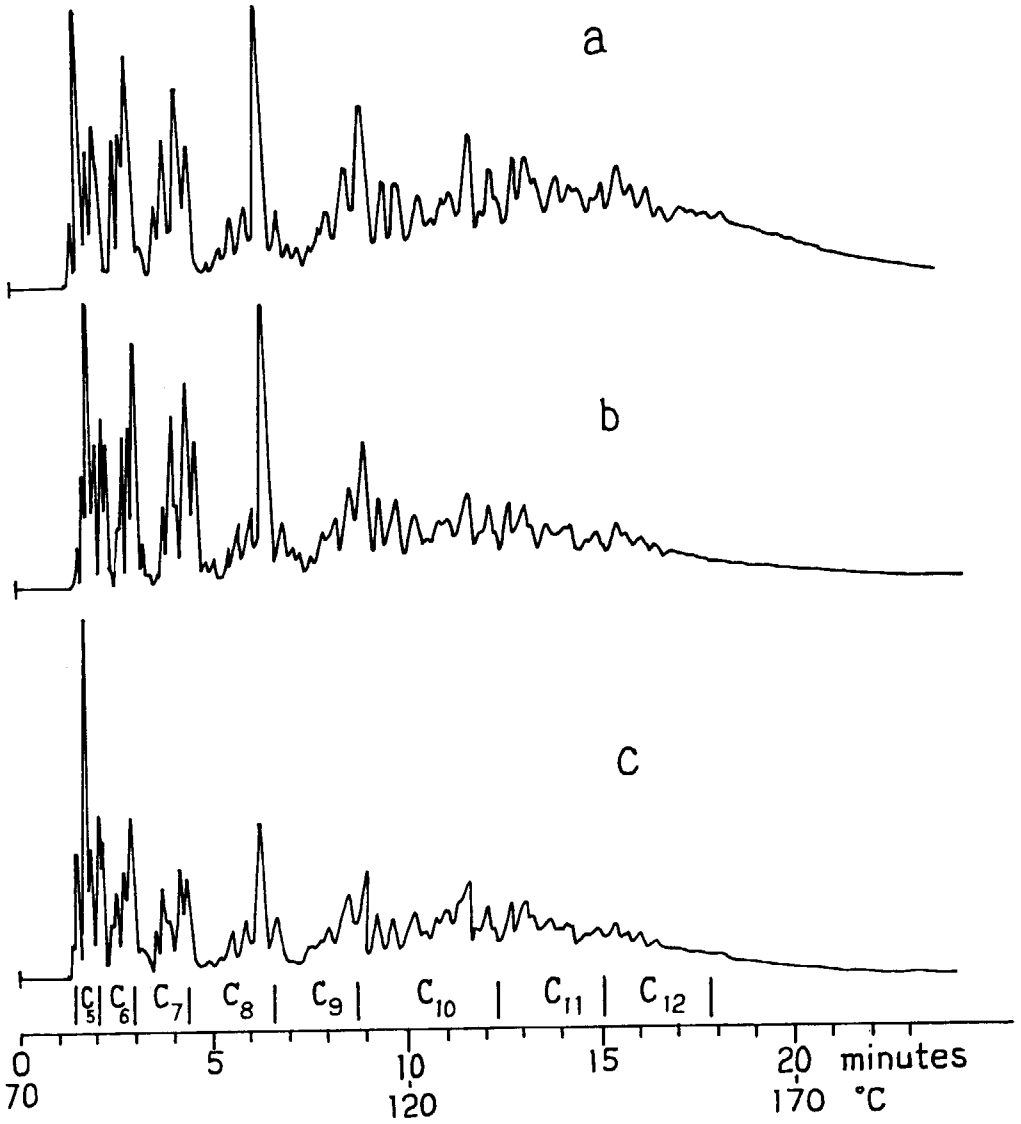

Fig. 3. Gaschromatograms of volatile fraction of the products: Irradiation time, (a) 3.6, (b) 7.2, (c) 14.5 Mrad; Irradiation conditions, 600 kV, 1 mA (1.1×10^3 Mrad/hr); Reactant, CH_4 (760 Torr).

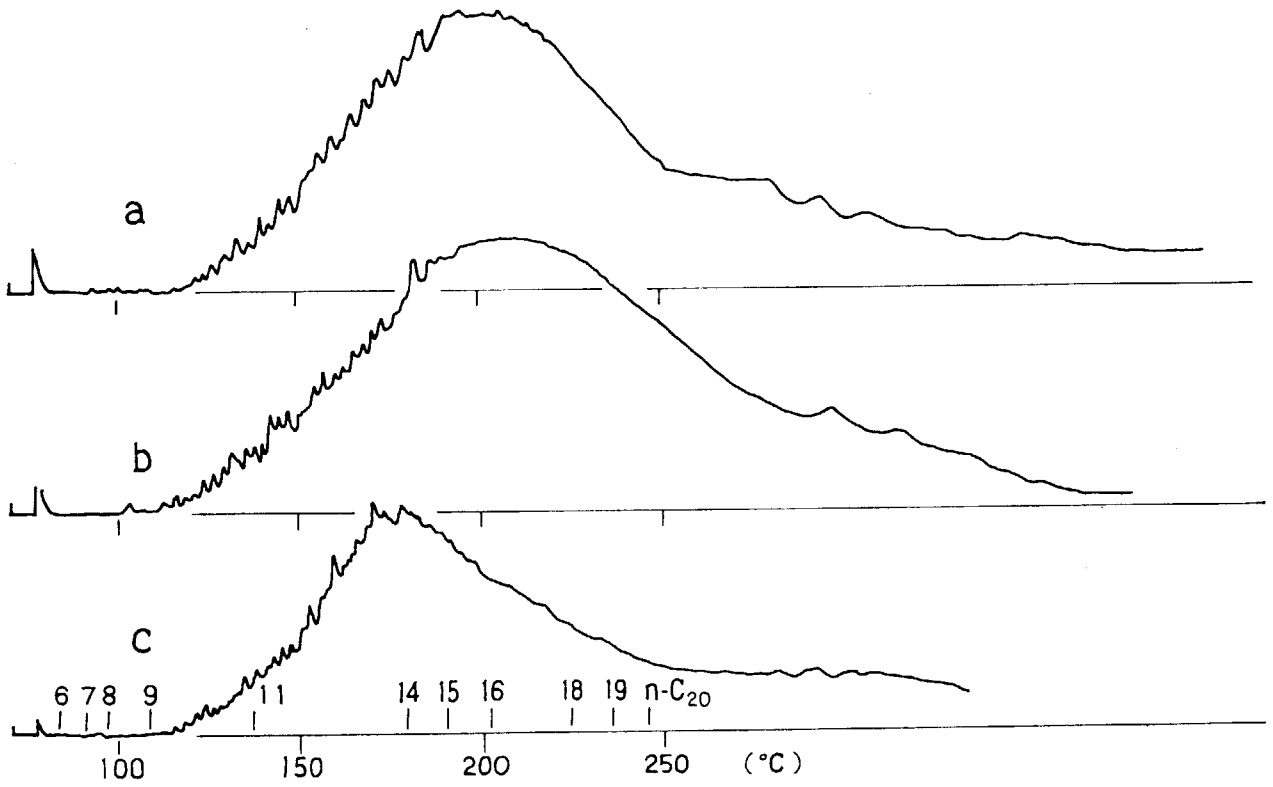

Fig. 4. Gaschromatograms of non-volatile fractions: OV-1 3 m column, 70°C, 5°C/min, 40 ml/min; (a) 3.6 Mrad, (b) 7.2 Mrad, and (c) 14.5 Mrad.

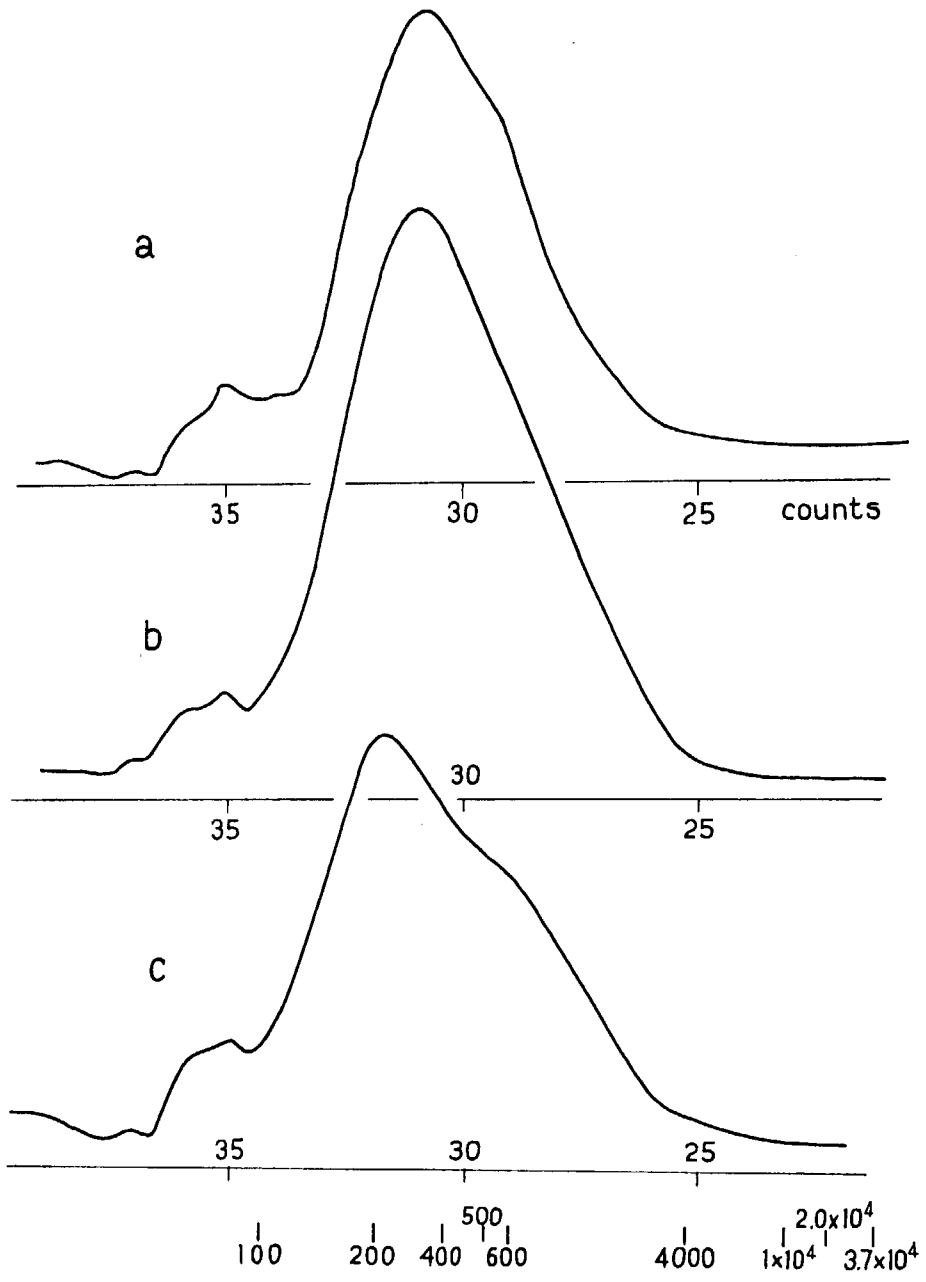

Fig. 5. GPC curves of non-volatile products obtained from methane by (a) 3.6 x 10^4, (b) 7.2 x 10^4, and (c) 14.5 x 10^4 Mrad irradiation.

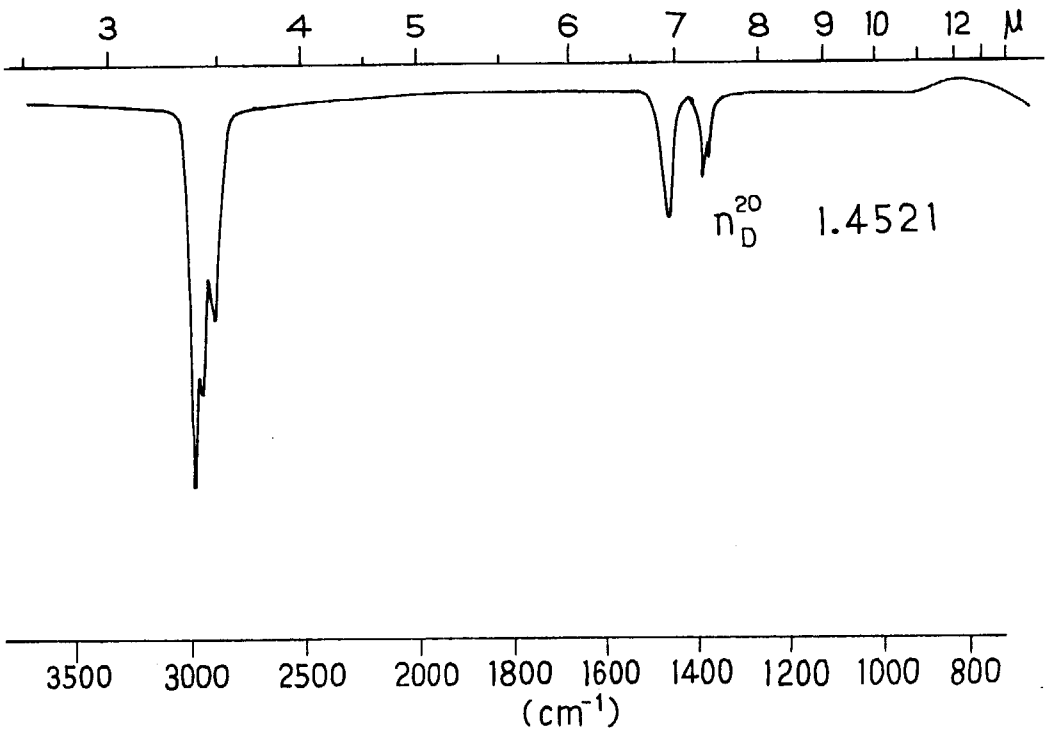

Fig. 6. Infrared spectra of non-volatile fractions of the products: Dose, 7.2 Mrad.

Table 3 Refractive Indices of the Non-volatile Products Obtained from Methane by Electron Beam Irradiation and Those of Related Compounds

Compounds	n_D^{20}
Non-volatile products	
SS-1 3.6 Mrads	1.4496
SS-2 7.2 Mrads	1.4521
SS-3 14.5 Mrads	1.4466
n-Hexane	1.3751*
n-Octane	1.3974*
2, 2'-Dimethyl hexane	1.3949*
2, 2, 3'-Trimethylpentane	1.4030*
n-Tetradecane	1.4290*
1-Tetradecene	1.4351*
Triacontane	1.4352*
Low density polyethylene	1.50 ∿ 1.54*
Medium density polyethylene	1.52 ∿ 1.54*
High density polyethylene	1.54*

* Handbook of Chemistry and Physics, 55th Edition, CRC Press, Inc. (1974)

obtained at 3 x 10^3 Mrad dose is shown in Fig. 6, where no absorption other than those due to CH, CH_2, and CH_3 are observed.

In Table 3, the refractive indices are listed for non-volatile products obtained at three different doses, together with several literature values of known compounds. The results indicate that the average carbon number of the non-volatile products are ranging from 23 to 29.

(M. Hatada, H. Arai, S. Nagai, and K. Matsuda)

1) H. Arai, S. Nagai, K. Matsuda, and M. Hatada, JAERI-M 8569, 47 (1979).
2) S. Sugimoto and M. Nishii, JAERI-M 7899 (1978).

8. The Effect of Gas Composition on the Radiation Chemical Reactions of Gas Mixtures of Methane and Carbon Monoxide

Studies have been carried out on the irradiation of gas mixture containing methane and carbon monoxide at various compositions. The purpose is to know if it is possible to enhance the amount of ethylene by scavenging hydrogen atom formed as a primary product of the methane radiolysis. Another purpose is to synthesize oxygen containing compounds having more than two carbon atoms in a molecule.

The method and technique are the same as those described in the previous report[1]. Takachiho research grade methane (purity, 99.5 mole%) and carbon monoxide "UHP" (99.995%) supplied by Seitetsu Kagaku were used without further purification. Flow without circulation technique was employed throughout the experiment. The flow rates of the reactants were measured separately before mixing using two Ueshima-Brooks thermal mass flow meters (type 5810). In some experiments, extremely small amount of carbon monoxide was fed through an Ueshima-Brooks thermal mass flow controller (type 7907-5187) which permits to maintain flow rate at a constant value between

0.01 and 10 ml/min. The gas mixture was then introduced into a reactor which, as described previously[1], is made of stainless steel with an irradiation window (30 μm thick Ti foil) at the top. The volume of the reactor in the irradiation zone is about 12 cm^3. The irradiations were carried out using electron beams from the HDRA (0.6 MV, 1 mA; scanning width, 30 cm). The dose was determined using N_2O dosimeter followed by correction based on the difference of the stopping power between N_2O and CH_4, and N_2O and CO. The dose absorbed by pure methane was 12.9 Mrad and that for the gas mixture containing 90 mole% CO was 9.52 Mrad. The temperature of the reactor was kept at about 120°C or 170°C.

The irradiated gas was led from the reactor to two gas samplers kept at 120°C in series of gas chromatographs through 20 m stainless steel tubing (1.5 mm inner diameter) which was heated at about 100°C by electric current through the tubing in order to avoid condensation of the condensable products. The irradiated gas from the reactor was simultaneously analyzed with three gaschromatographs (Yanagimoto G 80 equipped with 3 m Porapak Q columns, Shimadzu CG 7A with 2 m Porapak N columns, and Shimadzu 3 BF with 2 m Molecular Sieve 5A columns). In some experiments, the total amount of acids was further determined by titration method, in which the acids contained in the gas were absorbed in alkaline aqueous solution of known concentration of alkali to neutralize the acids, and then the excess alkali was titrated by HCl aqueous solution. The results agreed well with those obtained by gaschromatographic method.

The amounts of the products are shown in Table 1, 2, 3, and 4 for methane and the gas mixture of various compositions containing CO and CH_4 along with the reaction conditions. The G values of the products are calculated on the basis of the amounts of products and are also included in the tables in the parentheses. The G values of main products listed in the tables are plotted in Figs. 1a, 1b, 2, 4, 5, and 7.

The G values of hydrocarbons are shown in Fig. 1a and 1b as a function of CO mole% in the gas mixture. The G values of the saturated hydrocarbons decreased with increasing amount of

Table 1. Electron Beam Irradiation of Gas Mixture of Methane and Carbon Monoxide at 120°C
(Effect of Gas Composition on Product Yields)
Electron Beam, 0.6 MeV, 1 mA; Scanning Width, 30 cm

Exp. No. (19791029)	15:30	16:05	16:37	17:25
Beam Current (mA)	1	1	1	1
Flow-rate (ml/min) CH_4	100	100	100	100
Flow-rate (ml/min) CO	0	0.10	0.10	0.20
Irrad. Temp. (°C)	120	120	120	120
Yield in μmole/10ℓ reactant gas at 25°C, 1 atm, (G-value)				
H_2	560 (6.5)	490 (5.6)	**500 (5.7)**	490 (5.7)
C_2H_2	0.61 (0.0071)	—	**0.71(0.008$_2$)**	0.71 (0.0081)
C_2H_4	6.2 (0.071)	—	**5.9 (0.068)**	6.3 (0.072)
C_2H_6	217 (2.50)	191 (2.20)	**191 (2.20)**	190 (2.18)
C_3H_6	0.77 (0.0088)	0.85 (0.0098)	**0.82(0.009$_4$)**	0.85 (0.0098)
C_3H_8	34.8 (0.400)	30.2 (0.348)	**30.0 (0.345)**	30.0 (0.345)
i-C_4H_{10}	5.8 (0.066)	5.1 (0.059)	**4.9 (0.057)**	5.2 (0.060)
1-C_4H_8	0.15 (0.0017)	0.14 (0.0016)	**0.17(0.001$_9$)**	0.11 (0.0013)
n-C_4H_{10}	6.8 (0.078)	5.8 (0.066)	**5.5 (0.063)**	5.6 (0.064)
neo-C_5H_{10}	**1.4 (0.016)**	1.2 (0.013)	**1.1 (0.013)**	1.2 (0.014)
i-C_5H_{10}	**4.9 (0.056)**	4.1 (0.047)	**4.3 (0.049)**	4.3 (0.049)
n-C_5H_{10}	0.74 (0.0085)	0.71 (0.0081)	**0.46(0.005$_3$)**	0.58 (0.0067)
HCHO	0	0	0	0
CH_3OH	0	0	0	0
CH_3CHO	0	—	0.45 (0.005)	0.65 (0.0075)
C_2H_5OH	0	0	0	0
CH_3COCH_3	0	0	0	0
CH_3COOH	0	0	0	0
C_2H_5COOH	0	0	0	0
CO_2	0	0	0	0
H_2O	0	≈0	≈0	≈0
Absorbed Energy in Mrad	12.9	12.9	12.9	12.9
in eV/g	8.06×10^{20}	8.06×10^{20}	8.06×10^{20}	8.06×10^{20}
in eV/10ℓ gas	5.26×10^{21}	5.26×10^{21}	5.26×10^{21}	5.26×10^{21}
Time after Initiating Irradiation (min)	30	33	65	45

Table 2. Electron Beam Irradiation of Gas Mixture of Methane and Carbon Monoxide at 120°C
(Effect of Gas Composition on Product Yields)
Electron Beam, 0.6 MeV, 1 mA; Scanning Width, 30 cm

Exp. No. (19791029)	18:08	18:55	19:50	10:50
Beam Current (mA)	1	1	1	1
Flow-rate (ml/min) CH_4	100	100	100	100
Flow-rate (ml/min) CO	0.40	0.60	1.0	1.0
Irrad. Temp. (°C)	121	121	121	121
Yield in μmole/10ℓ reactant gas at 25°C, 1 atm, (G-value)				
H_2	470 (5.4)	460 (5.2)	440 (5.1)	450 (5.3)
C_2H_2	0.81 (0.0093)	0.91 (0.011)	1.0 (0.012)	1.2 (0.014)
C_2H_4	6.2 (0.071)	6.3 (0.072)	6.2 (0.072)	6.9 (0.080)
C_2H_6	177 (2.04)	174 (2.01)	166 (1.92)	167 (1.94)
C_3H_6	0.85 (0.0098)	0.87 (0.010)	0.94 (0.011)	0.90 (0.010)
C_3H_8	31.0 (0.357)	32.0 (0.368)	31.6 (0.366)	32.5 (0.377)
$i\text{-}C_4H_{10}$	5.5 (0.064)	5.5 (0.063)	5.3 (0.062)	5.3 (0.061)
$1\text{-}C_4H_8$	0.13 (0.0015)	0.11 (0.0012)	0.11 (0.001)	0.08 (0.0009)
$n\text{-}C_4H_{10}$	5.3 (0.060)	5.4 (0.062)	5.1 (0.059)	5.5 (0.063)
$neo\text{-}C_5H_{10}$	1.5 (0.017)	1.4 (0.016)	1.3 (0.015)	1.4 (0.016)
$i\text{-}C_5H_{10}$	3.8 (0.044)	3.6 (0.042)	3.4 (0.039)	3.6 (0.041)
$n\text{-}C_5H_{10}$	0.59 (0.0068)	0.59 (0.0068)	0.67 (0.0078)	0.69 (0.0080)
HCHO	0	0	0	trace
CH_3OH	trace	trace	trace	trace
CH_3CHO	2.6 (0.030)	4.0 (0.046)	5.3 (0.062)	5.3 (0.062)
C_2H_5OH	trace	trace	trace	trace
CH_3COCH_3	trace	trace	trace	trace
CH_3COOH	30 (0.35)	41 (0.47)	44 (0.51)	43 (0.50)
C_2H_5COOH	73 (0.84)	78 (0.89)	93 (1.0)	90 (1.0)
CO_2	0	0	0	trace
H_2O	≈0	≈0	≈0	≈0
Absorbed Energy in Mrad	12.9	12.9	12.7	12.7
in eV/g	8.06×10^{20}	8.06×10^{20}	7.92×10^{20}	7.92×10^{20}
in eV/10ℓ gas	5.26×10^{21}	5.26×10^{21}	5.21×10^{21}	5.21×10^{21}
Time after Initiating Irradiation (min)	40	47	53	51

Table 3. Electron Beam Irradiation of Gas Mixture of Methane and Carbon Monoxide at 120°C
(Effect of Gas Composition on Product Yields)
Electron Beam, 0.6 MeV, 1 mA; Scanning Width, 30 cm

Exp. No. (19791030)		11:40	12:30	13:35	15:23
Beam Current (mA)		1	1	1	1
Flow-rate (ml/min)	CH_4	100	100	90	80
	CO	2.0	5.0	10	20
Irrad. Temp. (°C)		120	120	122	120
Yield in μmole/10ℓ reactant gas at 25°C, 1 atm, (G-Value)					
H_2		440 (5.2)	410 (4.9)	380 (4.2)	380 (4.1)
C_2H_2		1.3 (0.015)	2.1 (0.025)	3.4 (0.037)	5.4 (0.058)
C_2H_4		7.0 (0.081)	7.8 (0.093)	9.7 (0.11)	12 (0.13)
C_2H_6		153 (1.77)	137 (1.63)	129 (1.45)	118 (1.27)
C_3H_6		0.91 (0.011)	0.84 (0.010)	0.93 (0.010)	0.91 (0.0089)
C_3H_8		30.7 (0.356)	28.4 (0.338)	26.6 (0.297)	27.7 (0.299)
$i\text{-}C_4H_{10}$		5.0 (0.058)	4.1 (0.049)	3.6 (0.040)	2.8 (0.031)
$1\text{-}C_4H_8$		0.1 (0.001)	0.08 (<0.001)	0.11 (0.001)	0.1 (0.001)
$n\text{-}C_4H_{10}$		5.0 (0.058)	4.1 (0.049)	3.4 (0.038)	2.7 (0.029)
$neo\text{-}C_5H_{10}$		1.2 (0.014)	1.1 (0.013)	1.2 (0.013)	1.3 (0.014)
$i\text{-}C_5H_{10}$		3.0 (0.035)	2.4 (0.029)	2.0 (0.022)	1.5 (0.016)
$n\text{-}C_5H_{10}$		0.61 (0.007)	0.68 (0.008)	0.49 (0.0055)	0.45 (0.005)
HCHO		trace	7.0 (0.084)	14 (0.16)	23 (0.25)
CH_3OH		trace	trace	trace	trace
CH_3CHO		8.1 (0.094)	15 (0.182)	25 (0.28)	37 (0.40)
C_2H_5OH		trace	trace	trace	trace
CH_3COCH_3		1.9 (0.021)	3.0 (0.035)	5.2 (0.058)	6.4 (0.069)
CH_3COOH		47 (0.55)	66 (0.79)	78 (0.87)	96 (1.0)
C_2H_5COOH		100 (1.1)	100 (1.1)	110 (1.2)	110 (1.2)
CO_2		trace	9.9 (0.12)	16 (0.17)	28 (0.30)
H_2O		≈0	≈0	≈0	≈0
Absorbed Energy in Mrad		12.5	12.0	12.3	11.9
in eV/g		7.83×10^{20}	7.51×10^{20}	7.68×10^{20}	7.43×10^{20}
in eV/10 gas		5.19×10^{21}	5.08×10^{21}	5.39×10^{21}	5.58×10^{21}
Time after Initiating Irradiation (min)		50	50	50	50

Table 4. Electron Beam Irradiation of Gas Mixture of Methane and Carbon Monoxide at 120°C
(Effect of Gas Composition on Product Yields)
Electron Beam, 0.6 MeV, 1 mA; Scanning Width, 30 xm

Exp. No. (19791031)		16:30	12:15	13:15	14:10
Beam Current (mA)		1	1	1	1
Flow-rate (ml/min)	CH_4	70	50	30	10
	CO	30	50	70	90
Irrad. Temp. (°C)		122	132	129	132
Yield in μmole/10ℓ reactant gas at 25°C, 1 atm, (G-value)					
H_2		370 (3.9)	320 (3.3)	250 (2.4)	130 (1.3)
C_2H_2		7.7 (0.081)	12 (0.12)	15 (0.15)	14 (0.13)
C_2H_4		14 (0.14)	14 (0.14)	11 (0.11)	5.5 (0.051)
C_2H_6		109 (1.15)	95.6 (0.976)	75.6 (0.730)	51.0 (0.472)
C_3H_6		1.1 (0.011)	1.1 (0.011)	0.89 (0.009)	0.55 (0.005)
C_3H_8		21.6 (0.227)	16.4 (0.168)	10.1 (0.098)	4.59 (0.043)
$i\text{-}C_4H_{10}$		2.3 (0.024)	1.7 (0.018)	1.1 (0.011)	0.55 (0.0051)
$1\text{-}C_4H_8$		0.08 (<0.001)	0.11 (0.001)	0.06 (<0.001)	0.04 (<0.001)
$n\text{-}C_4H_{10}$		2.0 (0.021)	1.3 (0.013)	0.67 (0.007)	0.25 (0.0023)
$neo\text{-}C_5H_{10}$		1.0 (0.011)	0.58 (0.006)	trace	trace
$i\text{-}C_5H_{10}$		1.1 (0.011)	0.74 (0.008)	0.33 (0.003)	0.50 (0.0046)
$n\text{-}C_5H_{10}$		0.28 (0.003)	0.18 (0.002)	0.12 (0.001)	≈0
HCHO		32 (0.33)	42 (0.43)	40 (0.38)	30 (0.28)
CH_3OH		trace	trace	trace	trace
CH_3CHO		45 (0.47)	51 (0.52)	50 (0.48)	35 (0.32)
C_2H_5OH		trace	trace	trace	trace
CH_3COCH_3		5.4 (0.057)	11 (0.11)	10 (0.099)	7.5 (0.069)
CH_3COOH		100 (1.0)	120 (1.2)	140 (1.3)	180 (1.6)
C_2H_5COOH		100 (1.0)	100 (1.0)	97 (0.94)	21 (0.19)
CO_2		48 (0.50)	78 (0.80)	130 (1.3)	190 (1.8)
H_2O		≈0	≈0	≈0	≈0
Absorbed Energy in Mrad		11.4	10.8	10.0	9.52
in eV/g		7.14×10^{20}	6.71×10^{20}	6.26×10^{20}	5.94×10^{20}
in eV/10ℓ gas		5.71×10^{21}	6.03×10^{21}	6.24×10^{21}	6.50×10^{21}
Time after Initiating Irradiation (min)		50	44	44	55

CO in the gas mixture, while the G values of the unsaturated hydrocarbons were increased with increasing amount of CO and then decreased by further addition of CO. These results may be qualitatively explained by the loss of hydrogen atom formed as a primary radiolysis product of methane due to a reaction with CO,

$$CH_4 \longrightarrow H + \dot{C}H_3 \qquad (1)$$

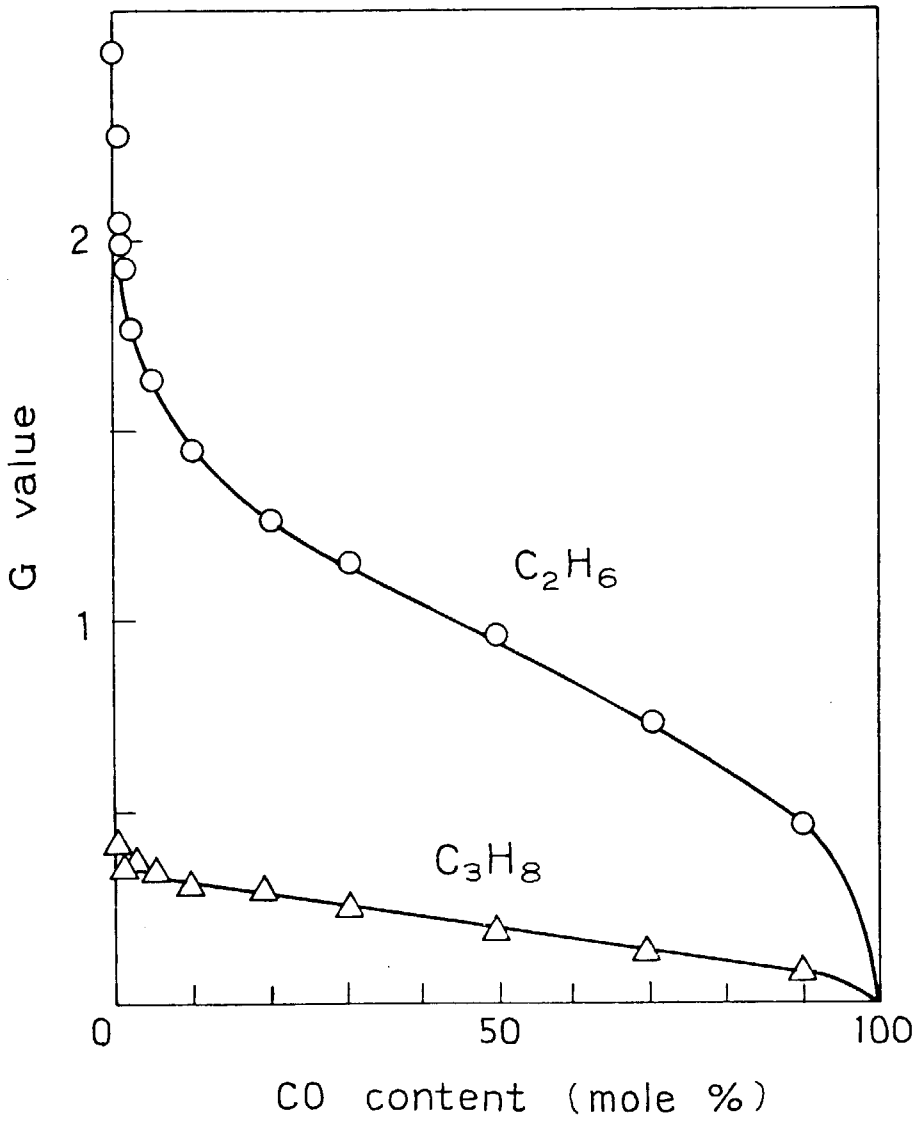

Fig. 1a. G values of ethane and propane as a function of CO content in the feed gas: Temperature, 120°C; Dose, 10 ∿ 13 Mrad; Residence time, 7 sec.

$$H + CO \longrightarrow \dot{H}CO \quad , \qquad (2)$$

and are consistent with the result obtained for hydrogen shown in Fig. 2, where the G value of hydrogen formation decreases by 25% by addition of a small amount of CO (5%), and then decreased gradually with increasing amount of CO.

Thus, the decrease in $G(H_2)$ observed by a small amount of addition of carbon monoxide as shown in Fig. 2 can be assumed to be due to reaction (2) in which hydrogen atom reacts with CO resulting in loss of hydrogen atom which otherwise forms hydrogen molecule via reaction (3).

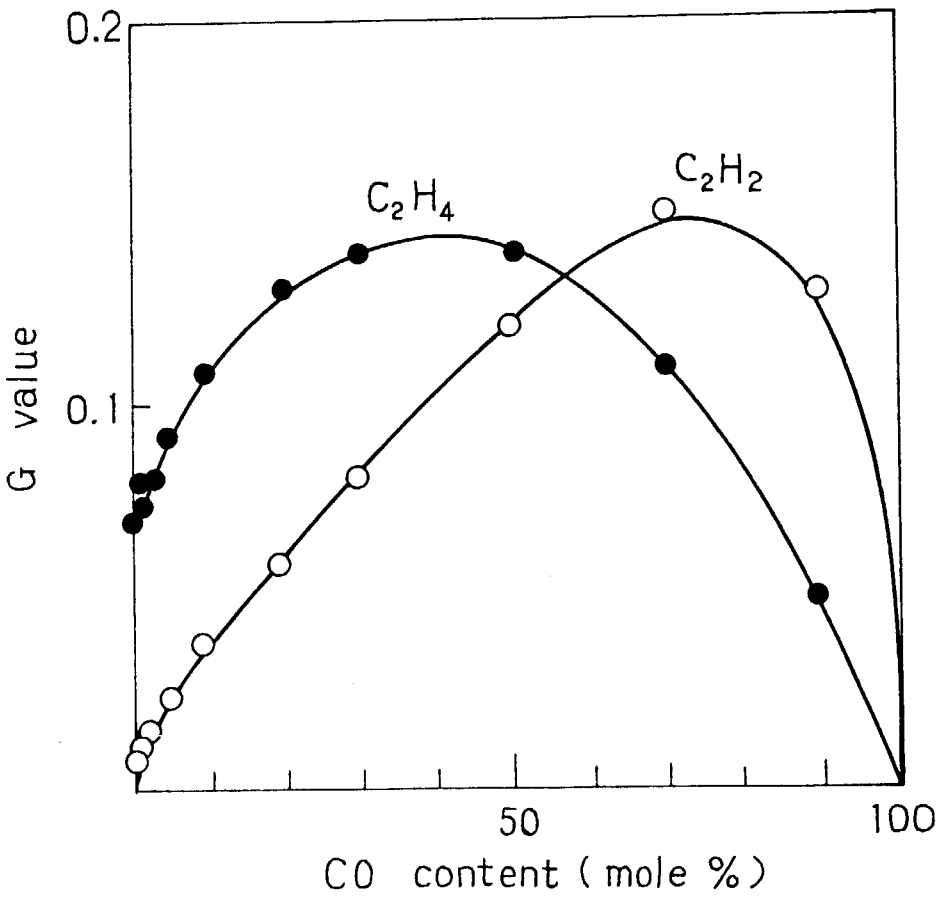

Fig. 1b. G values of ethylene and acetylene as a function of CO content: Temperature, 120°C; Dose, 10 ∿ 13 Mrad; Residence time, 7 sec.

$$H + CH_4 \longrightarrow H_2 + \dot{C}H_3 \qquad (3)$$

As the amount of added CO increases, the $G(H_2)$ value seems to approach apparently to a stationary value at 10 mole% CO content, which corresponds to the hydrogen production by the reaction which do not involve hydrogen atoms. An example of such reactions may be molecular detachment of hydrogen molecule via reaction (4),

$$CH_3^+ + CH_4 \longrightarrow C_2H_5^+ + H_2 \quad k_4 \ . \qquad (4)$$

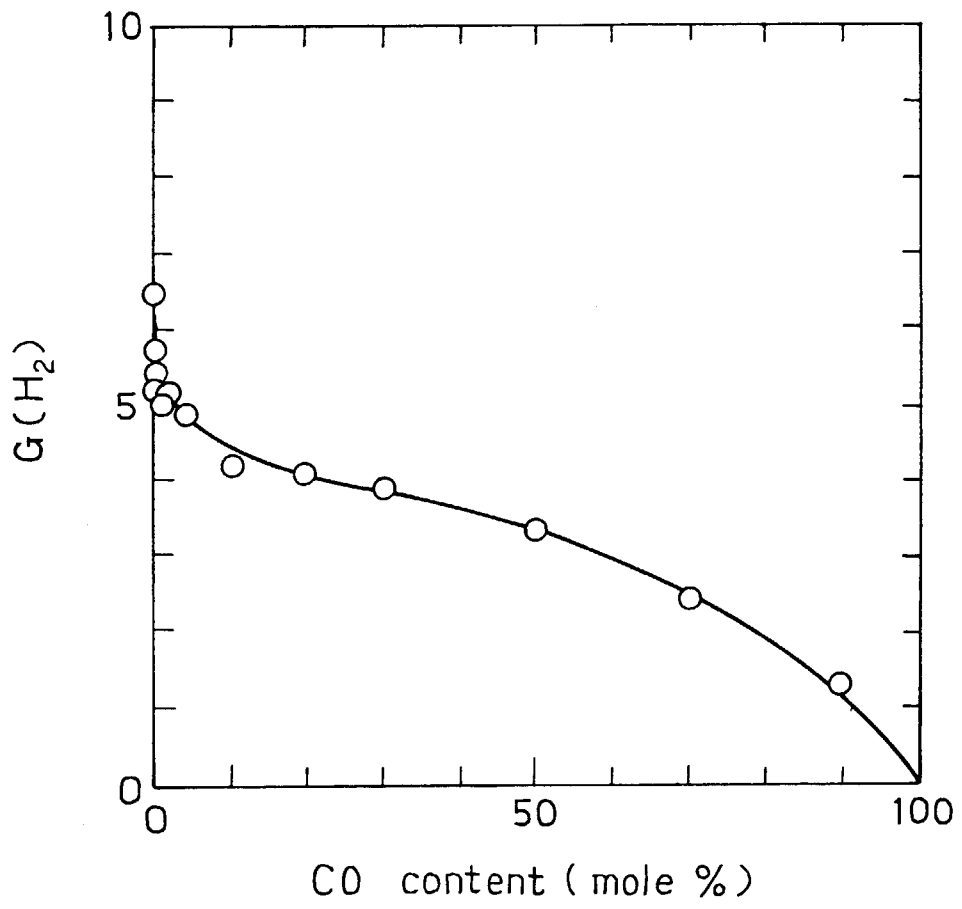

Fig. 2. G value of H_2 as a function of CO content: Temperature, 120°C; Dose, 10 ∿ 13 Mrad; Residence time, 7 sec.

Although a part of CH_3^+ is lost by addition to CO to produce acetic acid as described later, the loss is small at small $[CO]/[CH_4]$ as seen in Fig. 1. Moreover, reaction (4) produces only one-third of hydrogen molecule yield via reactions which do not involve hydrogen atoms. Thus, the production rate of hydrogen molecule, $R^M(H_2)$, by the above scheme can be assumed to be constant at small $[CO]/[CH_4]$.

If we assume the steady state concentration of hydrogen atom,

$$\frac{d[H]}{dt} = k_1 I[CH_4] - k_2[H][CO] - k_3[H][CH_4] = 0 ,$$

$$[H] = \frac{k_1 I[CH_4]}{k_2[CO] + k_2[CH_4]}$$

where I is the dose rate. The rate of hydrogen molecule formation is given by,

$$\frac{d[H_2]}{dt} = R^M(H_2) + k_3[H][CH_4]$$

$$= R^M(H_2) + \frac{k_1 k_3 I[CH_4]^2}{k_2[CO] + k_3[CH_4]} \qquad [1]$$

where k_1, k_2, k_3, and k_4 are the rate constants of respective reactions.

Rearrangement of equation [1] gives the following equation [2],

$$\{\frac{d[H_2]}{dt} - R^M(H_2)\}^{-1} = \frac{1}{k_1 I[CH_4]}\{1 + \frac{k_2}{k_3}\cdot\frac{[CO]}{[CH_4]}\}. \qquad [2]$$

Since the amount of hydrogen formed in known time and at known dose rate is proportional to G value of the reaction, equation [2] can be rewritten as equation [3],

$$\{G(H_2) - G^M(H_2)\}^{-1} = G(H)^{-1}\{1 + \frac{k_2}{k_3}\cdot\frac{[CO]}{[CH_4]}\} , \qquad [3]$$

where $G^M(H_2)$ is the G value of hydrogen formation corresponding to $R^M(H_2)$, and G(H) the G value of hydrogen atom formation according to reaction (1) contributing to produce hydrogen

molecule at that temperature. As shown in Fig. 3, the plot of equation [3] gives a straight line when $G^M(H_2)$ is assumed to be 4.63 which is reported by Okazaki et al.[2)]

From the slope of the curve in Fig. 3, the value of k_2 was calculated using the known value of k_3[3)]. The calculated values are listed in Table 5 together with k_3.

In Fig. 4, the G values of aldehydes and acetone are plotted as a function of CO content. It is apparent that the maximum G values of these compounds appear at 50 mole% CO.

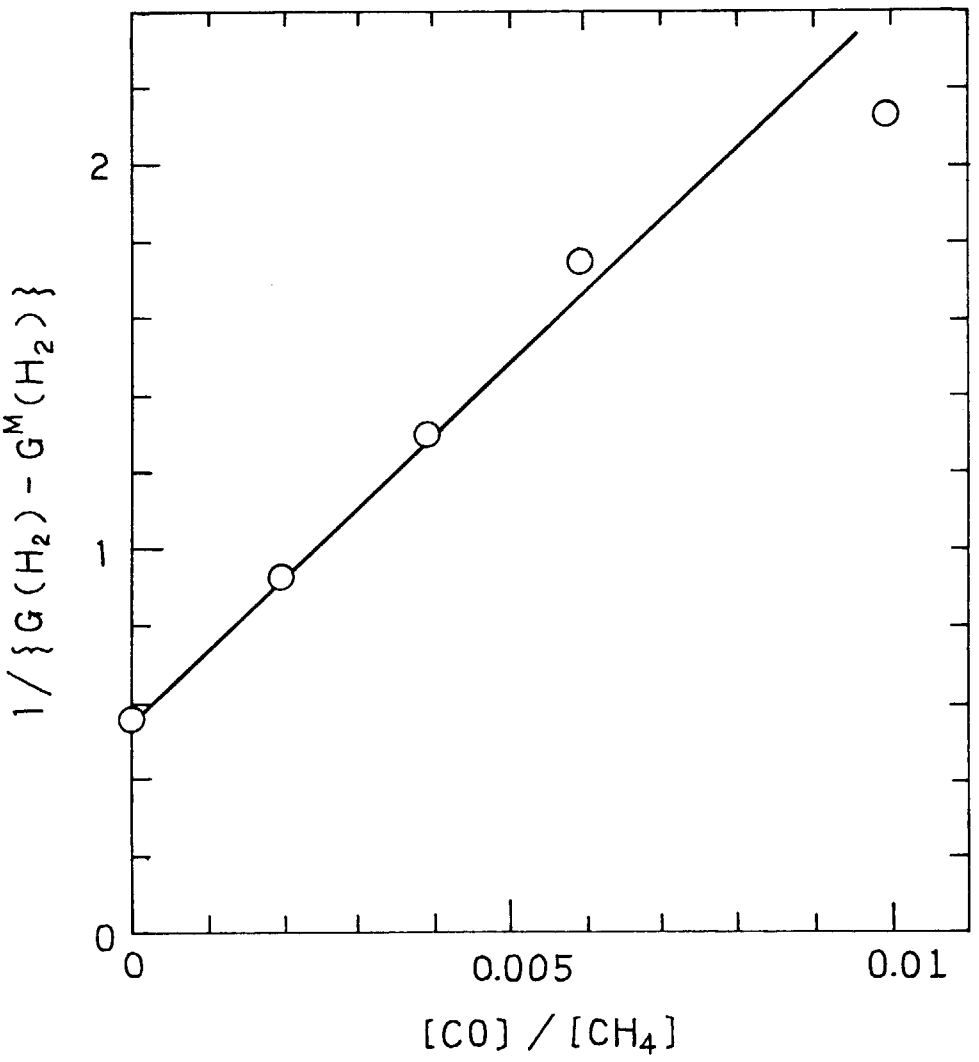

Fig. 3. Plot of $1/\{G(H_2) - G^M(H_2)\}^{-1}$ as a function of $[CO]/[CH_4]$.

Table 5. Estimated Values of k_2 and the Reference Value of k_3 Used for the Estimation of k_2

Temperature (°C)	k_2 (cm^3/s)	k_3[a] (cm^3/s)
72	3.9×10^{-15}	1.52×10^{-18}
120	5.6×10^{-15}	1.51×10^{-17}
176	9.8×10^{-15}	1.23×10^{-16}

a) Sepehrad et al.[3]

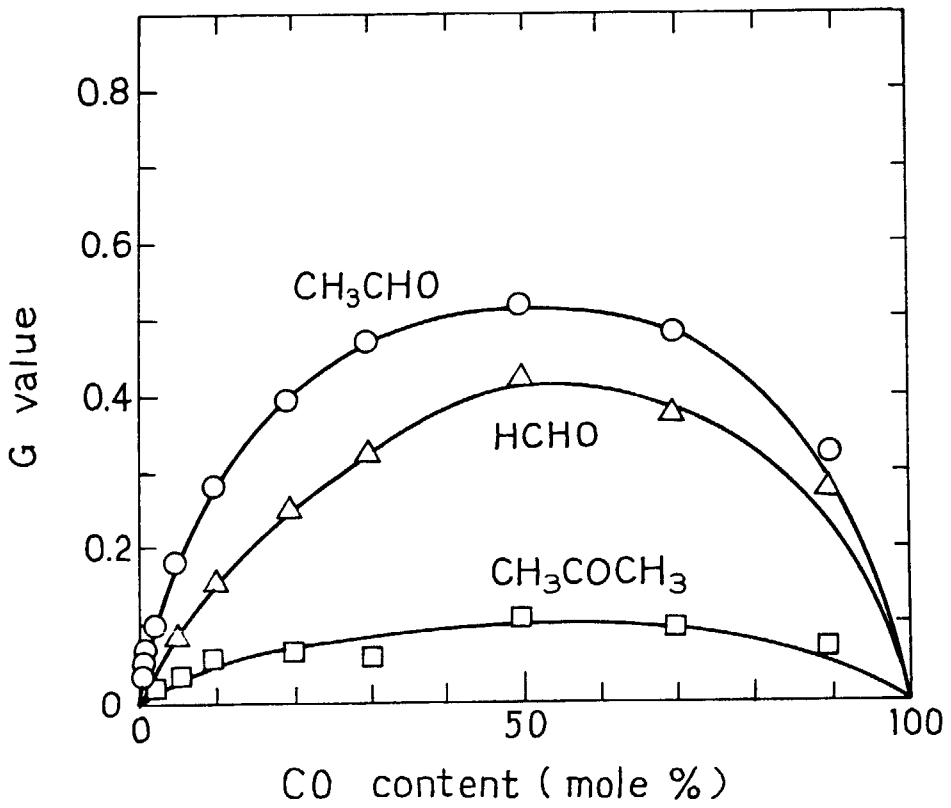

Fig. 4. G values of aldehydes and acetone as a function of CO content: Temperature, 120°C; Dose, 10 ∿ 13 Mrad; Residence time, 7 sec.

In Fig. 5, the G values of acetic acid and propionic acid are plotted as a function of CO content. The G values of these acids increase with increasing amount of CO. The maximum G value of acetic acid appears at 90 mole% of CO, while that of propionic acid appears at 10 mole% of CO. The G value of acetic acid is higher than that of propionic acid below 40 mole% of CO, but above this CO content, the G values of propionic acid is larger than that of acetic acid.

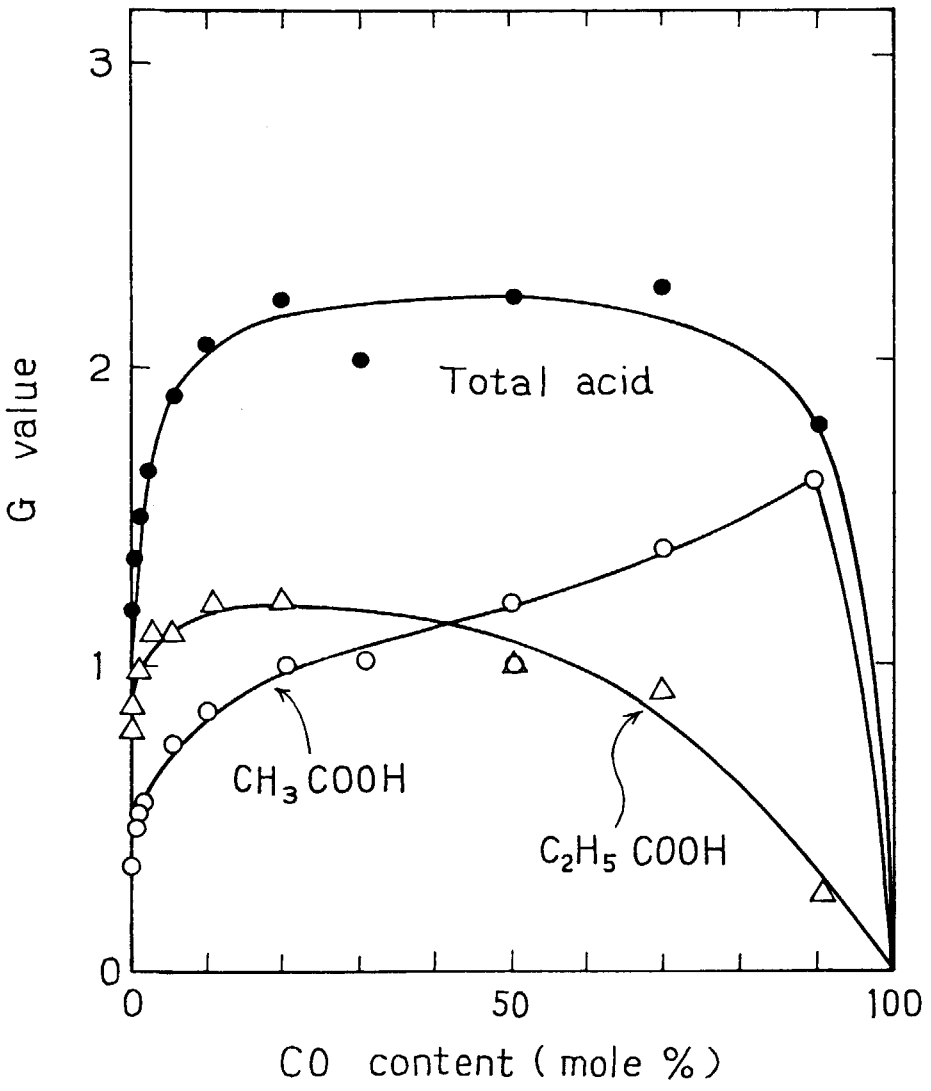

Fig. 5. G values of acetic acid and propionic acid as a function of CO content: Temperature, 120°C; Dose, 10 ∿ 13 Mrad, Residence time, 7 sec.

The dependence of G values of these acids on CO content in the low CO content region below 10 mole% of CO can be understood quantitatively by a series of the following reactions:

$$CH_4 \longrightarrow\!\!\!\!\!\!\sim\!\!\!\!\!\!\rightarrow CH_3^+ + H \qquad (5)$$

$$CH_3^+ + CO \longrightarrow CH_3CO^+ \qquad (6)$$

$$CH_3^+ + CH_4 \longrightarrow C_2H_5^+ + H_2 \qquad (4)$$

$$C_2H_5^+ + CO \longrightarrow C_2H_5CO^+ \qquad (7)$$

$$C_2H_5^+ + CH_4 \longrightarrow C_3H_7^+ + H_2 \qquad (8)$$

Assuming the steady state concentration of CH_3^+ and $C_2H_5^+$:

$$\frac{d[CH_3^+]}{dt} = k_9 \cdot I \cdot [CH_4] - k_{10}[CH_3^+][CO]$$

$$- k_4[CH_3^+][CH_4] = 0$$

$$\frac{d[C_2H_5^+]}{dt} = k_4[CH_3^+][CH_4] - k_{11}[C_2H_5^+][CO]$$

$$- k_{12}[C_2H_5^+][CH_4] = 0$$

The following equations can be derived for the rate of formation of CH_3CO^+ and $C_2H_5CO^+$ ions:

$$\frac{d[CH_3CO^+]}{dt} = \frac{k_9 k_{10} I \cdot [CH_4] \cdot [CO]}{k_4[CH_4] + k_{10}[CO]} \qquad [4]$$

$$\frac{d[C_2H_5CO^+]}{dt} = \frac{k_9 I \cdot k_4 k_{11}[CH_4]^2[CO]}{\{k_{11}[CO] + k_{12}[CH_4]\}\{k_{10}[CO] + k_4[CH_4]\}} \qquad [5]$$

If we divide equation [4] by equation [5] and assume that CH_3CO^+ and $C_2H_5CO^+$ ions will react to form acetic acid and propionic acid, respectively, the following simple relation is

obtained:

$$\frac{G(CH_3COOH)}{G(C_2H_5COOH)} = \frac{k_{10}\cdot k_{12}}{k_4\cdot k_{11}}\{1 + \frac{k_{11}}{k_{12}}\cdot\frac{[CO]}{[CH_4]}\} \qquad [6]$$

The plot of equation [6] is shown in Fig. 6. Since k_4 and k_{12} are known to be 1×10^{-9} $cm^3\cdot sec^{-1}$ [4] and 2×10^{-14} $cm^3\cdot sec^{-1}$ [4], respectively, k_{10} and k_{11} are determined to be 6×10^{-9} and 3×10^{-13} $cm^3\cdot sec^{-1}$, respectively, from the slope and intercept of the plot shown in Fig. 6. Replacing the rate constants in equation [7] with the numerical values thus estimated, we obtain the following relation:

$$\frac{G(CH_3COOH)}{G(C_2H_5COOH)} = 0.4 + 0.6\,\frac{[CO]}{[CH_4]} \qquad [7]$$

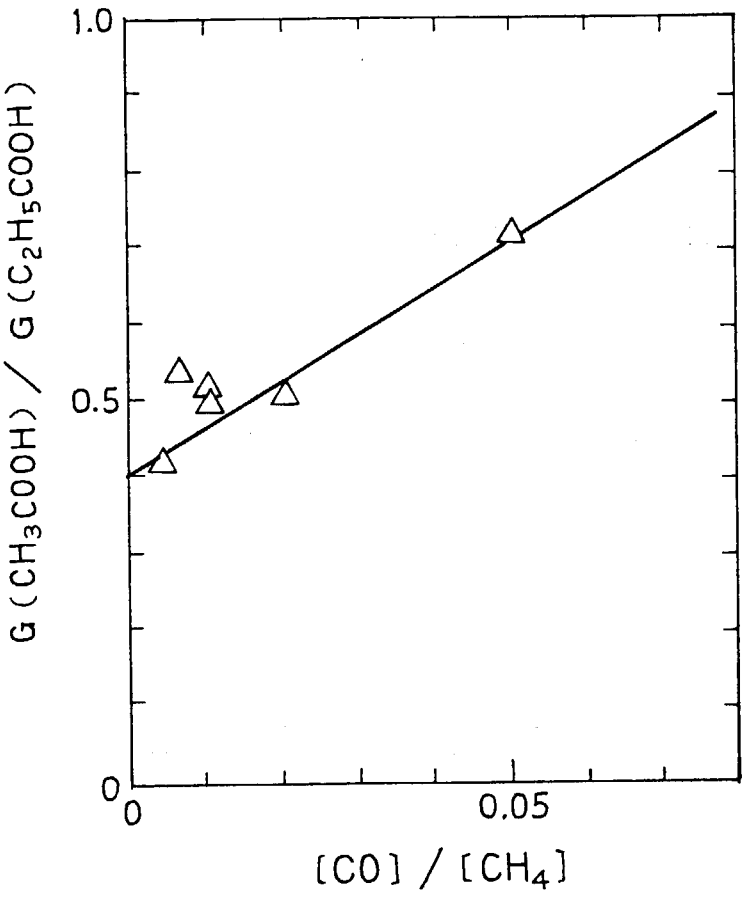

Fig. 6. Plot of G(acetic acid)/G(propionic acid) as a function of $[CO]/[CH_4]$.

According to the above mechanism, the sum of the G values of the acids does not exceed the G value of CH_3^+ ion formation which is estimated to be 1.5 in the radiolysis of pure methane[5]. The fact that the sum of the G values of the acids (2.0) is close to this value, although the former value is a little higher than the latter, supports the proposed mechanism. The analysis on the dependences of G values of the acids on CO content above 10 mole% of CO will be carried out in the future studies.

The G value of carbon dioxide increases with increasing CO content and the extension of the curve toward 100% CO content

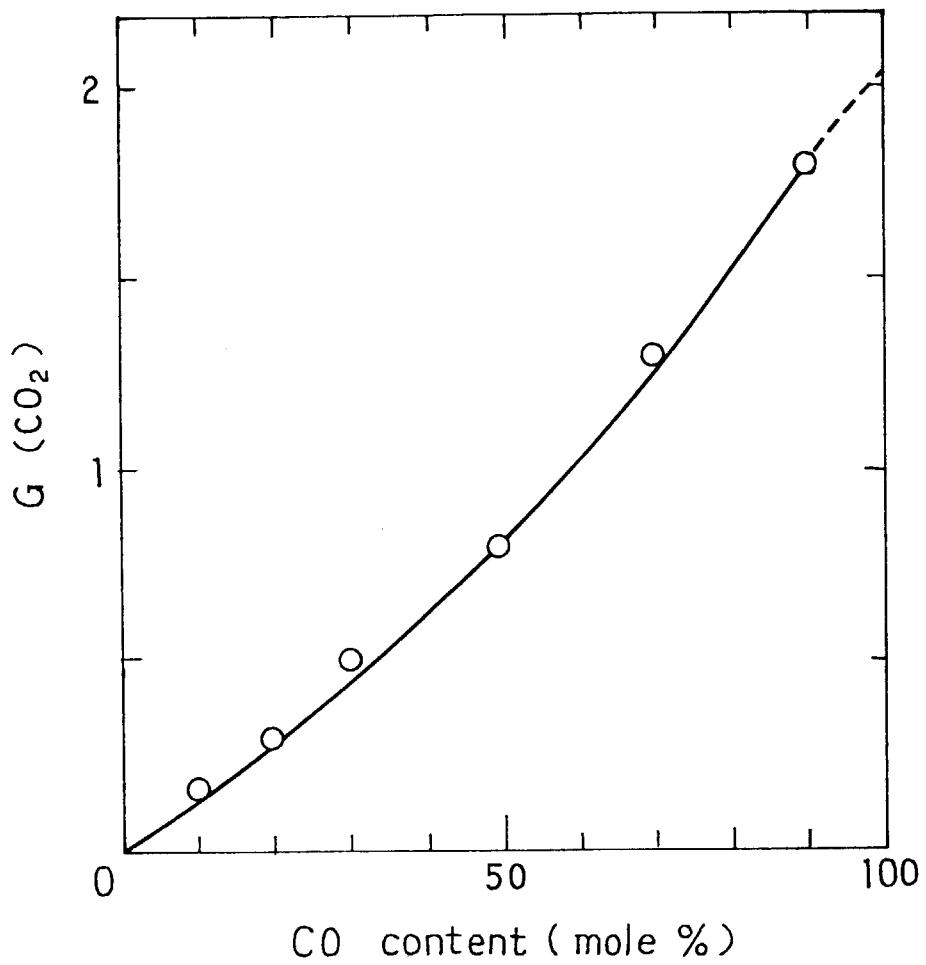

Fig. 7. G value of CO_2 as a function of CO content: Temperature, 120°C; Dose, 10 ∿ 13 Mrad; Residence time, 7 sec.

gives the $G(CO_2)$ value which agrees well with the value in the literature (2.0)[6] as shown in Fig. 7.

In the present study, it is revealed that by the irradiation of the gas mixture of methane and carbon monoxide, the acetic acid and propionic acid are produced via ionic intermediates with considerably high G values. The reactions producing the organic acids from the gas mixture of methane and carbon monoxide studied in the present report will be useful to produce organic acids containing carbon atoms more than 2 in a molecule from compounds having one carbon atom in a molecule.

(H. Arai, S. Nagai, and M. Hatada)

1) H. Arai, S. Nagai, K. Matsuda, and M. Hatada, JAERI-M 8569, 64 (1979).
2) K. Okazaki, S. Sato, and S. Ohno, Bull. Chem. Soc. Japan, 49, 174 (1976).
3) A. Seperhrad, R. M. Marshall, and H. Purnell, J. C. S. Faraday Trans., 1, 835 (1979).
4) K. Hiraoka and P. Kebarle, J. Chem. Phys., 63, 394 (1975).
5) G. G. Meisels, Abstracts, the 150th Meeting of A. C. S. Meeting, Sept. 1965, p. 17V.
6) A. R. Anderson, "Fundamental Processes in Radiation Chemistry", P. Ausloos, Ed., Interscience, N.Y., p.281 (1968).

9. The Effects of Dose and Dose Rate on the Radiation Chemical Reactions of Gas Mixture of Methane and Carbon Monoxide

In the previous report[1], it is revealed that the maximum G value of propionic acid was obtained at CO content of about 10 mole%. It is interesting to know the amounts of products as a function of dose and dose rate at this CO content.

The method and technique are the same as those described in the previous report. The irradiations were carried out with electron beams from the HDRA (0.6 MV, 0.2 ∿ 2 mA) at 120°C or

170°C. The dose was changed from 3.1 Mrad to 30.1 Mrad by changing the flow rate from 200 ml/min to 30 ml/min at 120°C and 1.14 Mrad/sec, and from 11.0 Mrad to 110 Mrad, and 200 ml/min to 20 ml/min at 170°C and 4.5 Mrad/sec.

In a series of experiments where dose rate was changed, the dose rates were from 0.454 Mrad/sec to 4.54 Mrad/sec at the beam current between 0.2 mA and 2 mA at 170°C. At ca. 120°C, the dose rates were 0.454 and 2.27 Mrad/sec at the beam currents of 0.2 mA and 1.0 mA, respectively.

All experimental results including the amounts of products and G values (the latter in parentheses) are listed in Table 1 through 4 together with experimental conditions. Table 1 shows the amounts of products and G values obtained at 120°C and 2.74 Mrad/sec, the residence time being changed. Table 2 shows the data obtained at 120°C at two different dose rates: 0.454 Mrad/sec and 2.74 Mrad/sec, while the dose were kept constant at 12.4 Mrad by changing the residence time. Table 3 shows the amounts of products and G values obtained at 170°C and 4.54 Mrad/sec, the residence time being changed. Table 4 shows the amounts of products and G values as a function of dose rate at 170°C, while the dose were kept constant at 11.0 Mrad.

The amounts of the main products listed in Table 1 are plotted as a function of dose in Fig. 1. The amount of ethane increases linearly with dose. The amounts of propionic acid, acetic acid, and acetaldehyde increase with increasing dose, but the amounts of products per unit dose become less as the dose increases. Similar dependence of the amounts of products on dose are obtained for the data obtained at 170°C at 4.5 Mrad/sec as shown in Figs. 2a and 2b. Again, the amounts of the oxygen containing products increase with increasing dose, but the increments per unit dose become less as the dose increases. The amount of ethane, on the other hand, increases linearly with dose (Fig. 2b).

In Fig. 3, the G values of the main products are plotted as a function of dose rate at 170°C on the basis of the data listed in Table 4. It is noted that G values of all hydrocarbon products increase with increasing dose rate, while those of the

Table 1. Electron Beam Irradiation of Gas Mixtures of Methane and Carbon Monoxide at 120°C
(Effect of Dose on the Product Yields)
Electron Acc. Voltage, 0.6 MV; Scanning Width, 30 cm

Exp. No. (19791119)	15:53	16:35	17:17	20:10
Beam Current (mA)	0.5	0.5	0.5	0.5
Flow-rate (ml/min) CH_4	180	90	45	27
Flow-rate (ml/min) CO	20	20	5	3.7
Irrad. Temp. (°C)	118	118	118	118
Yield (μmole/10ℓ reactant gas at 25°C, 1 atm), (G-value)				
H_2	130 (5.6)	250 (5.5)	470 (5.2)	810 (5.4)
C_2H_2	1.7 (0.077)	2.4 (0.053)	3.4 (0.037)	4.6 (0.031)
C_2H_4	4.7 (0.21)	11 (0.23)	13 (0.15)	15 (0.097)
C_2H_6	40.4 (1.79)	72.5 (1.60)	142 (1.57)	252 (1.67)
C_3H_6	0.35 (0.016)	0.56 (0.012)	0.84 (0.0092)	1.2 (0.008)
C_3H_8	7.64 (0.338)	15.1 (0.334)	32.4 (0.358)	61.6 (0.409)
$i\text{-}C_4H_{10}$	0.88 (0.039)	1.9 (0.043)	4.3 (0.048)	8.3 (0.055)
$1\text{-}C_4H_8$	0.065 (0.003)	0.069 (0.0015)	0.052 (0.0006)	0.16 (0.001)
$n\text{-}C_4H_{10}$	0.86 (0.038)	1.9 (0.042)	4.3 (0.048)	8.5 (0.057)
$neo\text{-}C_5H_{10}$	0.50 (0.022)	0.83 (0.018)	1.2 (0.013)	1.3 (0.008)
$i\text{-}C_5H_{10}$	0.52 (0.023)	0.97 (0.022)	2.5 (0.027)	5.1 (0.034)
$n\text{-}C_5H_{10}$	0.16 (0.007)	0.30 (0.007)	0.66 (0.007)	1.2 (0.008)
HCHO	7.0 (0.31)	10 (0.23)	19 (0.21)	23 (0.16)
CH_3OH	0.4 (0.02)	0.5 (0.01)	0.8 (0.008)	1.5 (0.009)
CH_3CHO	13 (0.56)	19 (0.42)	30 (0.33)	42 (0.28)
C_2H_5OH				
CH_3COCH_3	2.0 (0.089)	3.6 (0.079)	7.3 (0.080)	13 (0.089)
CH_3COOH	24 (1.1)	41 (0.91)	86 (0.95)	120 (0.80)
C_2H_5COOH	47 (2.1)	85 (1.9)	100 (1.1)	150 (1.0)
CO_2	8.1 (0.36)	14 (0.30)	29 (0.32)	58 (0.38)
H_2O	—	—	—	—
Absorbed Energy in Mrad	3.11	6.21	12.4	20.7
in eV/g	1.94×10^{20}	3.88×10^{20}	7.76×10^{20}	1.29×10^{21}
in eV/10ℓ gas	1.36×10^{21}	2.72×10^{21}	5.45×10^{21}	9.07×10^{21}
Residence Time (sec)	2.74	5.48	10.97	18.29
Irradiation Time before Sampling (min)	45	40	42	50

Table 2. Electron Beam Irradiation of Gas Mixtures of Methane and Carbon Monoxide at 120°C
(Effect of Dose Rate on the Product Yields)
Electron Acc. Voltage, 0.6 MV; Scanning Width, 30 cm

Exp. No. (19791119)	18:10		19:15	
Beam Current (mA)	1		0.2	
Flow-rate (ml/min) CH_4	90		18	
Flow-rate (ml/min) CO	10		2.0	
Irrad. Temp. (°C)	118		118	
Yield (μmole/10ℓ reactant gas at 25°C, 1 atm), (G-value)				
H_2	490	(5.1)	480	(5.3)
C_2H_2	5.0	(0.055)	3.5	(0.038)
C_2H_4	14	(0.15)	10	(0.11)
C_2H_6	156	(1.72)	143	(1.58)
C_3H_6	1.0	(0.012)	0.74	(0.0082)
C_3H_8	34.6	(0.383)	30.9	(0.342)
$i\text{-}C_4H_{10}$	4.8	(0.053)	3.8	(0.041)
$1\text{-}C_4H_8$	0.06	(0.0006)	0.02	(0.003)
$n\text{-}C_4H_{10}$	4.8	(0.053)	3.7	(0.041)
$neo\text{-}C_5H_{10}$	1.2	(0.013)	0.83	(0.0092)
$i\text{-}C_5H_{10}$	2.8	(0.031)	2.0	(0.022)
$n\text{-}C_5H_{10}$	0.69	(0.008)	0.57	(0.006)
HCHO	16	(0.18)	23	(0.25)
CH_3OH	0.4	(0.004)	3	(0.03)
CH_3CHO	28	(0.31)	37	(0.41)
C_2H_5OH				
CH_3COCH_3	6.5	(0.072)	9.0	(0.100)
CH_3COOH	87	(0.96)	110	(1.2)
C_2H_5COOH	110	(1.2)	120	(1.3)
CO_2	30	(0.33)	69	(0.77)
H_2O	—		—	
Absorbed Energy in Mrad	12.4		12.4	
in eV/g	7.76×10^{20}		7.76×10^{20}	
in eV/10ℓ gas	5.45×10^{21}		5.45×10^{21}	
Irradiation Time before Sampling (min)	50		55	

Table 3. Electron Beam Irradiation of Gas Mixtures of Methane and Carbon Monoxide at 170°C
(Effect of Dose on the Product Yields)
Electron Acc. Voltage, 0.6 MV; Scanning Width, 30 cm

Exp. No. (19791206)	15:00	15:58	16:50	17:43
Beam Current (mA)	2	2	2	2
Flow-rate (ml/min) CH_4	180	90	45	18
Flow-rate (ml/min) CO	20	10	5	2.0
Irrad. Temp. (°C)	167	167	167	167
Yield (mole/10 reactant gas at 25°C, 1 atm), (G-value)				
H_2	510 (6.3)	960 (6.0)	1900 (5.9)	4600 (5.7)
C_2H_2	3.7 (0.046)	4.8 (0.030)	6.0 (0.019)	8.2 (0.010)
C_2H_4	13 (0.16)	18 (0.11)	24 (0.075)	38 (0.047)
C_2H_6	156 (1.91)	288 (1.79)	490 (1.52)	1350 (1.68)
C_3H_6	1.1 (0.014)	1.6 (0.010)	2.2 (0.007)	3.6 (0.005)
C_3H_8	32.0 (0.391)	62.5 (0.389)	129 (0.401)	316 (0.392)
$i\text{-}C_4H_{10}$	4.5 (0.054)	9.8 (0.061)	21 (0.067)	51 (0.064)
$1\text{-}C_4H_8$	0.13 (0.002)	0.17 (0.001)	0.09 (0.0003)	0.17 (0.0003)
$n\text{-}C_4H_{10}$	4.4 (0.053)	9.5 (0.059)	21 (0.066)	56 (0.070)
$neo\text{-}C_5H_{10}$	1.2 (0.014)	1.8 (0.011)	3.5 (0.011)	14 (0.017)
$i\text{-}C_5H_{10}$	2.7 (0.033)	6.2 (0.038)	14 (0.045)	41 (0.050)
$n\text{-}C_5H_{10}$	0.84 (0.010)	1.5 (0.009)	2.7 (0.008)	5.9 (0.007)
HCHO	0	0	0	0
CH_3OH	trace	≈0	≈0	3 (0.004)
CH_3CHO	24 (0.29)	32 (0.20)	41 (0.13)	57 (0.071)
C_2H_5OH				
CH_3COCH_3	4.2 (0.051)	8.2 (0.052)	14 (0.043)	29 (0.036)
CH_3COCH	42 (0.51)	65 (0.41)	120 (0.36)	200 (0.24)
C_2H_5COOH	70 (0.85)	104 (0.65)	140 (0.45)	200 (0.25)
CO_2	16 (0.20)	17 (0.10)	32 (0.10)	75 (0.093)
H_2O	35 (0.43)	—	—	—
Absorbed Energy in Mrad	11.0	22.1	44.2	100
in eV/g	6.89×10^{20}	1.38×10^{21}	2.76×10^{21}	6.89×10^{21}
in eV/10ℓ gas	4.84×10^{21}	9.68×10^{21}	1.94×10^{22}	4.84×10^{21}
Residence Time (sec)	2.44	4.88	9.76	24.4
Irradiation Time before Sampling (min)	80	52	52	53

Table 4. Electron Beam Irradiation of Gas Mixtures of Methane and Carbon Monoxide at 170°C
(Effect of Dose Rate on the Product Yields)
Electron Acc. Voltage, 0.6 MV; Scanning Width, 30 cm

Exp. No. (19791129)	11:48	12:50	14:00	14:57
Beam Current (mA)	2	1	0.5	0.2
Flow-rate (ml/min) CH_4	180	90	45	18
Flow-rate (ml/min) CO	20	10	5	2.0
Irrad. Temp. (°C)	170	170	169	167
Yield (μmole/10ℓ reactant gas at 25°C, 1 atm), (G-value)				
H_2	570 (7.0)	530 (6.6)	510 (6.4)	510 (6.3)
C_2H_2	4.1 (0.050)	3.5 (0.044)	3.2 (0.040)	3.0 (0.037)
C_2H_4	14 (0.17)	11 (0.14)	9.5 (0.12)	9.7 (0.12)
C_2H_6	172 (2.11)	152 (1.90)	145 (1.81)	130 (1.16)
C_3H_6	1.1 (0.013)	0.88 (0.011)	0.74 (0.0092)	0.62 (0.0077)
C_3H_8	34.3 (0.422)	31.9 (0.399)	29.9 (0.373)	29.2 (0.362)
$i\text{-}C_4H_{10}$	4.9 (0.061)	4.7 (0.058)	4.6 (0.057)	4.2 (0.052)
$1\text{-}C_4H_8$	0.13 (0.002)	0.08 (0.001)	0.07 (0.0008)	0.04 (0.0005)
$n\text{-}C_4H_{10}$	4.8 (0.058)	4.3 (0.054)	4.1 (0.052)	3.6 (0.045)
$neo\text{-}C_5H_{10}$	1.4 (0.017)	1.4 (0.017)	1.5 (0.018)	1.5 (0.019)
$i\text{-}C_5H_{10}$	3.3 (0.040)	1.8 (0.035)	2.7 (0.034)	2.4 (0.029)
$n\text{-}C_5H_{10}$	0.47 (0.006)	0.61 (0.008)	0.67 (0.008)	0.62 (0.007)
HCHO	0	0	0	0
CH_3OH	0.6 (0.007)	0.4 (0.006)	0.7 (0.008)	1.1 (0.014)
CH_3CHO	27 (0.33)	27 (0.335)	28 (0.35)	31 (0.39)
C_2H_5OH				
CH_3COCH_3	2.8 (0.034)	3.7 (0.047)	4.2 (0.053)	4.4 (0.055)
CH_3COOH	70 (0.86)	70 (0.88)	96 (1.2)	99 (1.2)
C_2H_5COOH	100 (1.2)	130 (1.6)	83 (1.0)	110 (1.4)
CO_2	11 (0.13)	9.0 (0.11)	13 (0.16)	20 (0.24)
H_2O	—	—	—	—
Absorbed Energy in Mrad	11.0	11.0	11.0	11.0
in eV/g	6.85×10^{20}	6.85×10^{20}	6.85×10^{20}	6.85×10^{20}
in eV/10ℓ gas	4.81×10^{21}	4.81×10^{21}	4.81×10^{21}	4.81×10^{21}
Residence Time (sec)	2.44	4.88	9.76	24.4
Irradiation Time before Sampling (min)	60	60	45	57

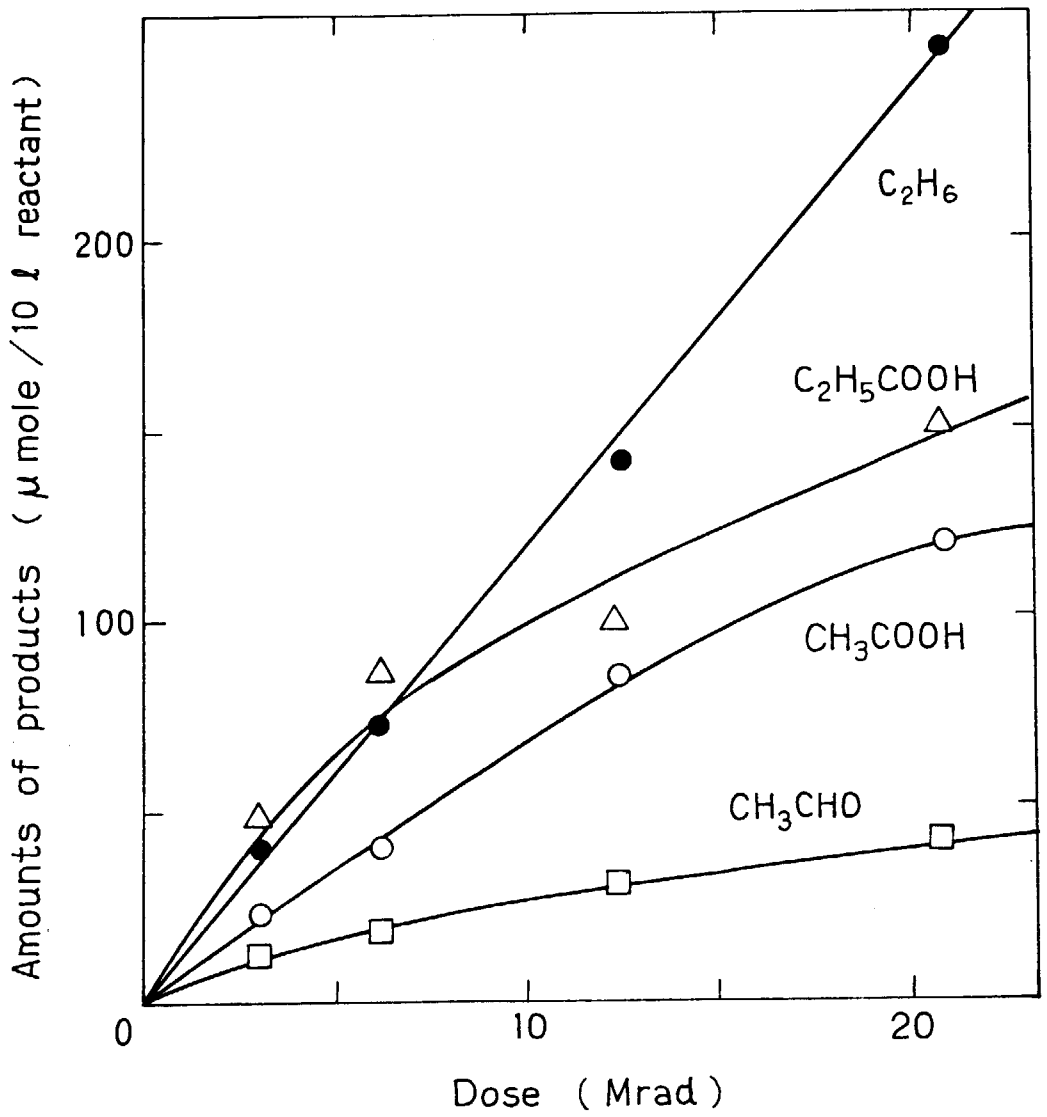

Fig. 1. Amounts of ethane, propionic acid, acetic acid, and acetaldehyde as a function of dose: Temperature, 118°C; Dose rate, 1.14 Mrad/sec; CO content, 90 mole%.

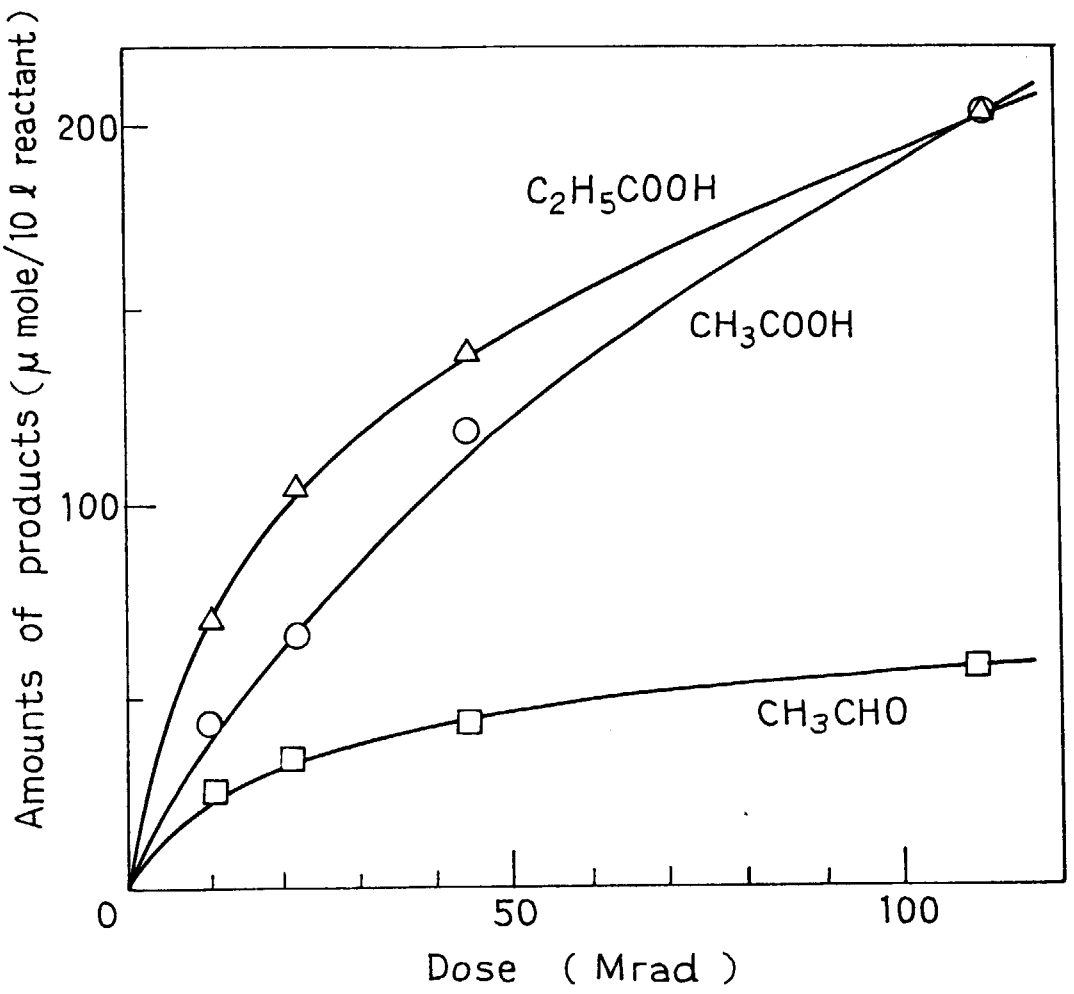

Fig. 2a. Amounts of the acetaldehyde, acetic acid and propionic acid as a function of dose: Temperature, 167°C; Dose rate, 2.27 Mrad/sec; CO content, 90 mole%.

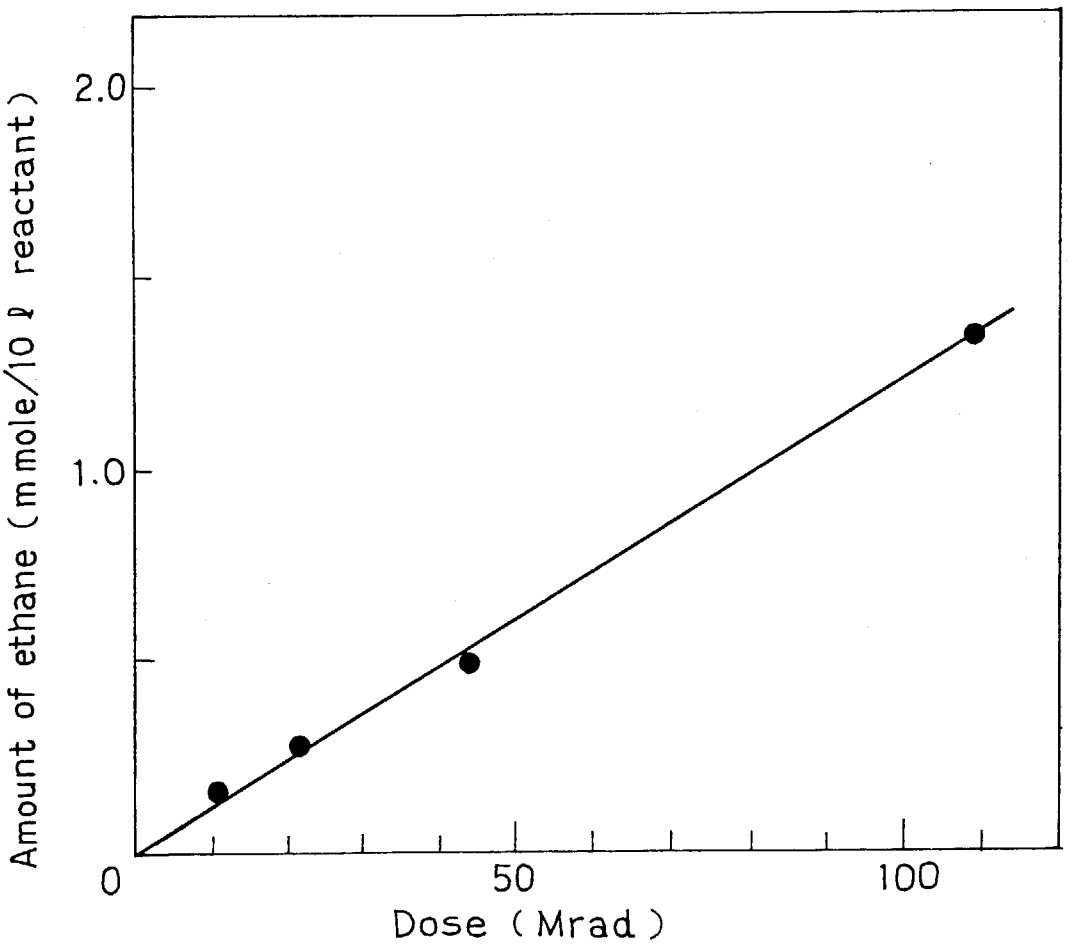

Fig. 2b. Amount of ethane as a function of dose: Temperature, 167°C; Dose rate, 2.27 Mrad/sec; CO content, 90 mole%.

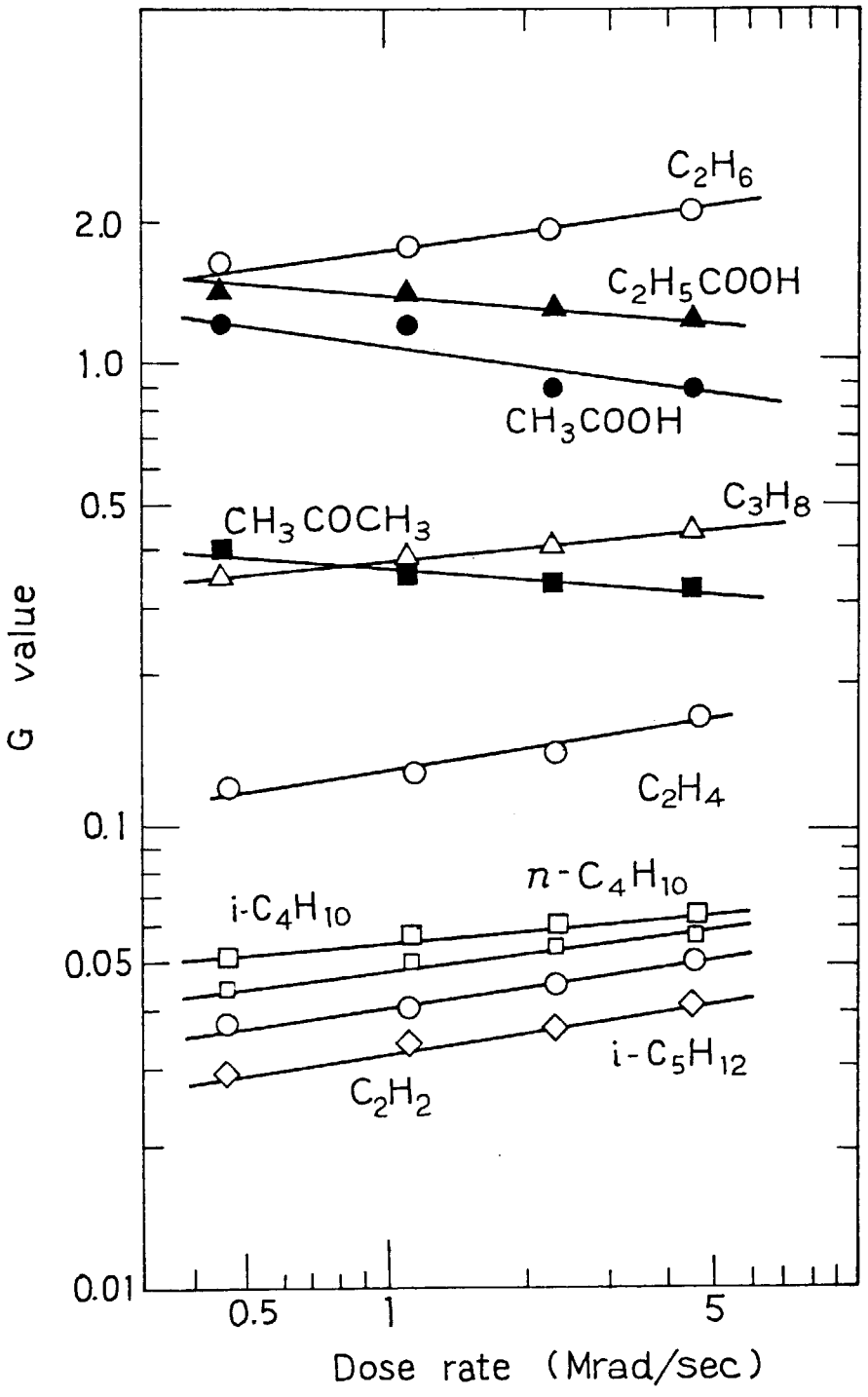

Fig. 3. G values of the main products as a function of dose rate: Dose, 11.0 Mrad; Temperature, 170°C; CO content, 90 mole%.

oxygen containing products such as propionic acid, acetic acid, and acetone decrease with increasing dose.

(H. Arai, S. Nagai, and M. Hatada)

1) H. Arai, S. Nagai, and M. Hatada, This report.

10. Spin Trapping of Radicals Produced by Irradiation of Methane-Carbon Monoxide Gas Mixture

As described in the preceding report[1], irradiation of CH_4-CO gas mixtures has been found to produce acetic acid and propionic acid in good yield. Although the formation of these acids has been accounted for by non-radical processes, that is, the Koch-Haaf reactions, it is of importance to obtain information concerning radicals produced for the understanding of the reactions occurred in this system. As reported already[2], the spin trapping technique has been successfully applied to the radiation chemistry of CO-H_2 to permit detection of H atoms and methyl radicals. We have now applied this technique to the CH_4-CO reaction.

Phenyl-N-tert-butylnitrone (PBN) and 2-methyl-2-nitroso-propane (t-BuNO) were used as spin trapping agents. Experimental methods and apparatus employed are almost the same as described in our previous report[2]. In brief, either PBN or t-BuNO powder dispersed on quartz wool was placed in the irradiation zone of the flow reactor and irradiated under 7 : 3 CH_4-CO gas stream at the total flow rate of 100 ml/min for 1 $\sim$ 3 min. A benzene trap was attached to the outlet of the reactor to collect the volatile spin adducts which flowed downstream with the reactant gas. After irradiation, the PBN or t-BuNO and products in the reactor were dissolved in benzene as soon as possible. The benzene solution as well as the solution in the benzene trap were inspected by ESR after outgassing. For comparison, experiments were also carried out on CH_4, CD_4 (99 atom % D, Merck Sharp & Dohme Canada Ltd.), and CD_4-CO mixture.

The products in the reactor after irradiation of PBN in

the 7 : 3 CH_4-CO flow for 2 min gave rise to a complex spectrum consisting at least of five components. Irradiation for longer period influenced the observed spectrum in such a way that nitroxide (I) produced by H atom addition to PBN, for instance, was no longer observed from the products in the reactor but instead it was observed from the solution of the benzene trap, possibly because of a temperature rise due to irradiation, which forced volatile nitroxides to flow outside the reactor. The nitroxides in the experiment on PBN irradiated in the CH_4-CO flow were identified by reference to the data obtained from experiments on PBN irradiated in a CH_4 flow together with those from the CO-H_2 experiment[2], and are shown below.

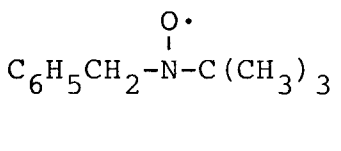

(I)

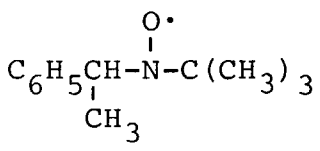

(II)

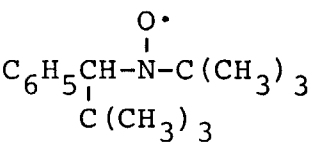

(III)

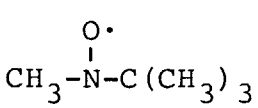

(IV)

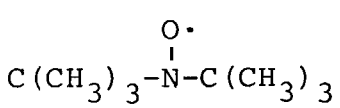

(V)

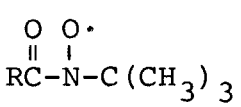

(VI)

R ≡ C_6H_5 + ?

As reported already[2], these nitroxides could be produced by irradiation of PBN either in a flow of He or CO-H_2 mixture. Therefore, it is not possible to determine whether the H atoms and methyl radicals trapped by PBN or t-BuNO which was produced by decomposition of PBN, as shown in the formation of nitroxides (I), (II), and (IV), are produced from the CH_4-CO mixture. In addition, the ESR spectrum of nitroxide (VI) is not dependent on the substituent R, either alkyl or phenyl[3], the definite structure of nitroxide (VI) may not be known.

The first of the above problems was studied by performing an experiment using CD_4 instead of CH_4. The ESR spectrum obtained from irradiated PBN under 7 : 3 CD_4-CO gas flow shows the presence of nitroxides produced by addition of not only D atom but also H atom to PBN. Therefore, it may be concluded

that the H atoms detected by irradiation of PBN in the CH_4-CO flow are produced from both PBN and CH_4-CO mixture.

Fig. 1 shows the ESR spectrum observed from the products in the reactor after irradiation of t-BuNO in the CH_4-CO flow. The spectrum consists of three-line spectrum due to nitroxide (V) accompanied by the satellite lines and another three-line spectrum shown by arrows. The latter spectrum is identical with the one of nitroxide (VI). Since nitroxide (VI) is not produced neither by decomposition of t-BuNO nor by irradiation of t-BuNO in the CH_4 flow as observed separately, the nitroxide detected here is attributed to nitroxide (VI) where R is an alkyl group, probably methyl group, produced from CH_4-CO mixture.

On the other hand, the solution of the benzene trap in this experiment gives an ESR spectrum which shows the presence of nitroxide produced by addition of ethyl radical to t-BuNO

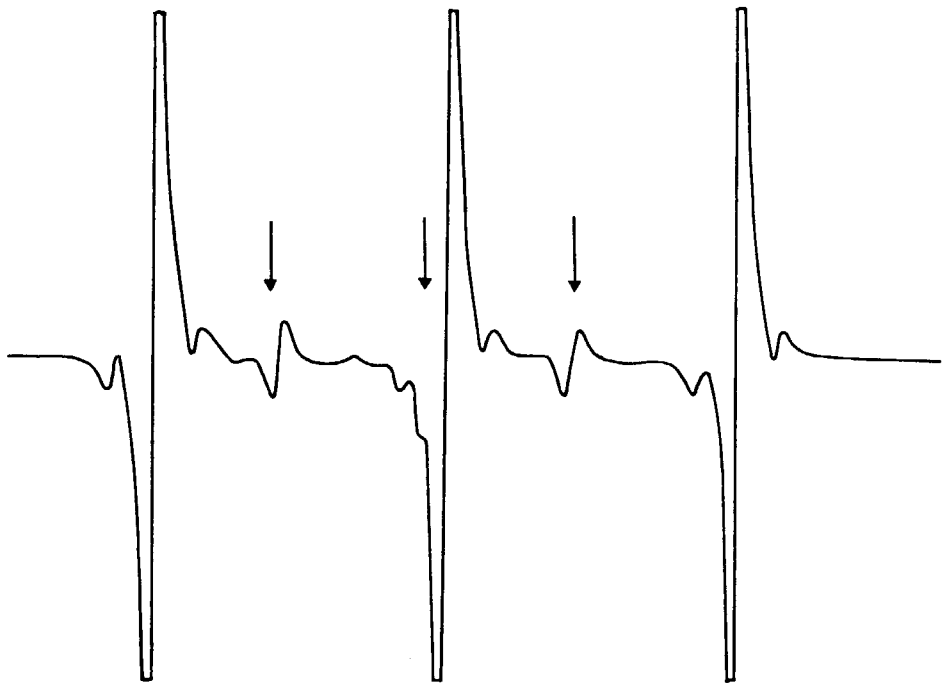

Fig. 1. ESR spectrum of products by irradiation of 7 : 3 CH_4-CO mixture in the presence of t-BuNO.

and nitroxide (IV) in addition to nitroxide (V). Evidence that methyl radicals trapped by t-BuNO as shown in the formation of nitroxide (IV) are produced from CH_4-CO mixture was obtained from the experiment on CD_4-CO using t-BuNO where the nitroxide produced by CD_3 addition to t-BuNO was observed from the solution of the benzene trap.

In summary, H atoms, methyl radicals, ethyl radicals, and acyl-type radicals, most likely acetyl radicals were confirmed to be produced by irradiation of CH_4-CO mixture by the spin trapping technique. (S. Nagai)

1) H. Arai, S. Nagai, and M. Hatada, This report.
2) S. Nagai, K. Matsuda, and M. Hatada, J. Phys. Chem., 82, 322 (1978).
3) E. G. Janzene and B. J. Blackburn, J. Amer. Chem., Soc., 91, 4481 (1969).

[2] Polymerization of Vinyl Monomers by High Dose Rate Electron Beams

1. Radiation-Induced Radical Polymerization of Styrene in Binary Mixture with n-Butylamine

General aspects of the radiation-induced polymerization of styrene in n-butylamine (BA) were reported in the last Annual Report[1]. The most prominent effect of BA is that it is an inhibitor for the cationic polymerization. The present report is concerned with radical polymerization of styrene in a binary mixture of styrene and BA.

Concerning the radical polymers it was reported that they consist of two parts: one is the main part and supposed to be produced by coupling of two growing chains (M·'s),

$$M\cdot + M\cdot' \longrightarrow M_m$$

and the other is produced by termination reaction with free radicals (S·) from the solvent molecules.

$$M\cdot + S\cdot \longrightarrow M_m\cdot S$$

Kinetic equations which were used for the radiation induced solution plymerization of styrene by radical mechanism in styrene-carbontetrachloride and styrene-ethylene dichloride are employed in the present case also[2]. In the derivation of the equations the two types of chain termination were not differentiated. In the present report also the total radical polymerization is to be discussed.

The rate of polymerization R is given by the following equation:

$$R = k_p[M](I/k_t)^{1/2}(\Phi_m[M] + \Phi_s[S])^{1/2} \qquad (1)$$

where k_p and k_t are the rate constants of polymerization and

termination: [M] and [S] concentrations of the monomer and solvent, and Φ_m and Φ_s are the rate constants of free radical production of the monomer and solvent, respectively; I is the dose rate.

The equation (1) shows that R is proportional to $I^{1/2}$, when the polymerization is carried out at a fixed composition of the polymerization mixture and only the reaction at lower conversion is concerned. As may be seen from Fig. 1, where the dependence of the rate of polymerization on the dose rate is shown for 80 and 20 vol% styrene in styrene-butylamine (BA), rates of polymerization are approximately proportional to the square root of the dose rate. It is rather astonishing that the experimental results agree with the theoretical equation, at least apparently, in such a wide range of dose rate as seven orders of magnitude.

Equation (1) was transformed to calculate the values of Φ_m

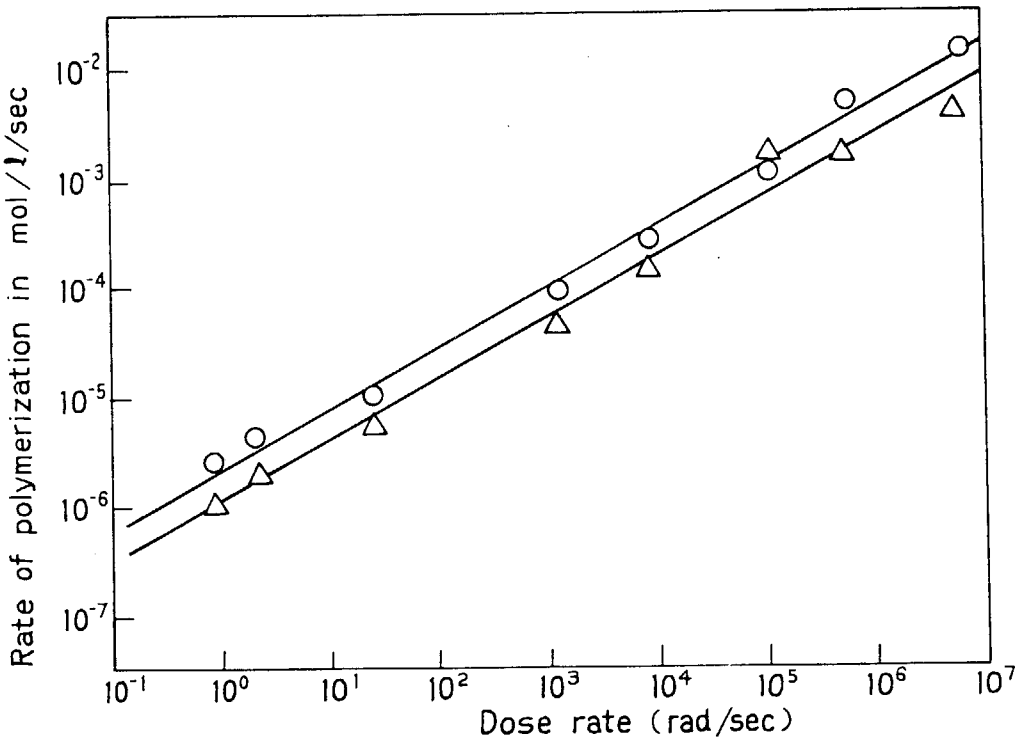

Fig. 1. Dose rate dependence of radical polymerization of styrene in styrene/BA: (○) 80 and (△) 20 vol% styrene.

and Φ_s from the experimental value of the rate of polymerization.

$$\left(\frac{R}{R_0}\right)^2\left(\frac{[M]_0}{[M]}\right)^3 = 1 + \frac{\Phi_s}{\Phi_m}\frac{[S]}{[M]} \qquad (2)$$

R_0 and $[M]_0$ are the polymerization-rate (mole/l/sec) and concentration (mole/l) of styrene in bulk, respectively. It is noteworthy that eq. (2) contains no more I, and therefore is independent of the dose rate.

Table 1 shows experimental values of R/R_0 of the equation (2); values at higher dose rates are omitted in the table, because the irradiation time is short and small errors are exaggerated due to employment of the multiple of the square by the cube of the raw experimental values.

Table 1. Experimental Values of R/R_0 at Various Dose Rates and Styrene Contents of the Mixture

Dose rate rad/sec	Volume % Styrene				
	100	80	60	40	20
7.5×10^{-1}	1	4.45	7.00	8.43	23.6
2.5	1	5.00	6.57	12.37	23.1
1.2×10^{3}	1	4.75	—	—	—
1.2×10^{4}	1	4.08	6.54	—	—
Average	1	4.56	6.70	10.4	23.4

It is seen from the table that the experimental values are essentially independent of the dose-rate. Average values of $(R/R_0)^2([M]_0/[M])^3$ are plotted against [S]/[M] in Fig. 2, a straight line is obtained as expected, and Φ_s/Φ_m is found from the inclination to be 5.8, which means that about six times more initiating radicals are formed from a molecule of BA than that of styrene.

From these agreement of the experimental results, it may

be said that the rate of radical polymerization can be explained simply: 1) initiating radical formation from monomer and solvent, 2) growing of radical chains by addition of monomer, 3) chain termination of radicals by coupling reaction.

An interesting reaction in the catalytic radical polymerization in solution is chain transfer to the solvent. Though chain transfer has no effect on the rate of polymerization, it is a dominant factor for the degree of polymerization. An equation to be used to check a role of chain transfer to solvent

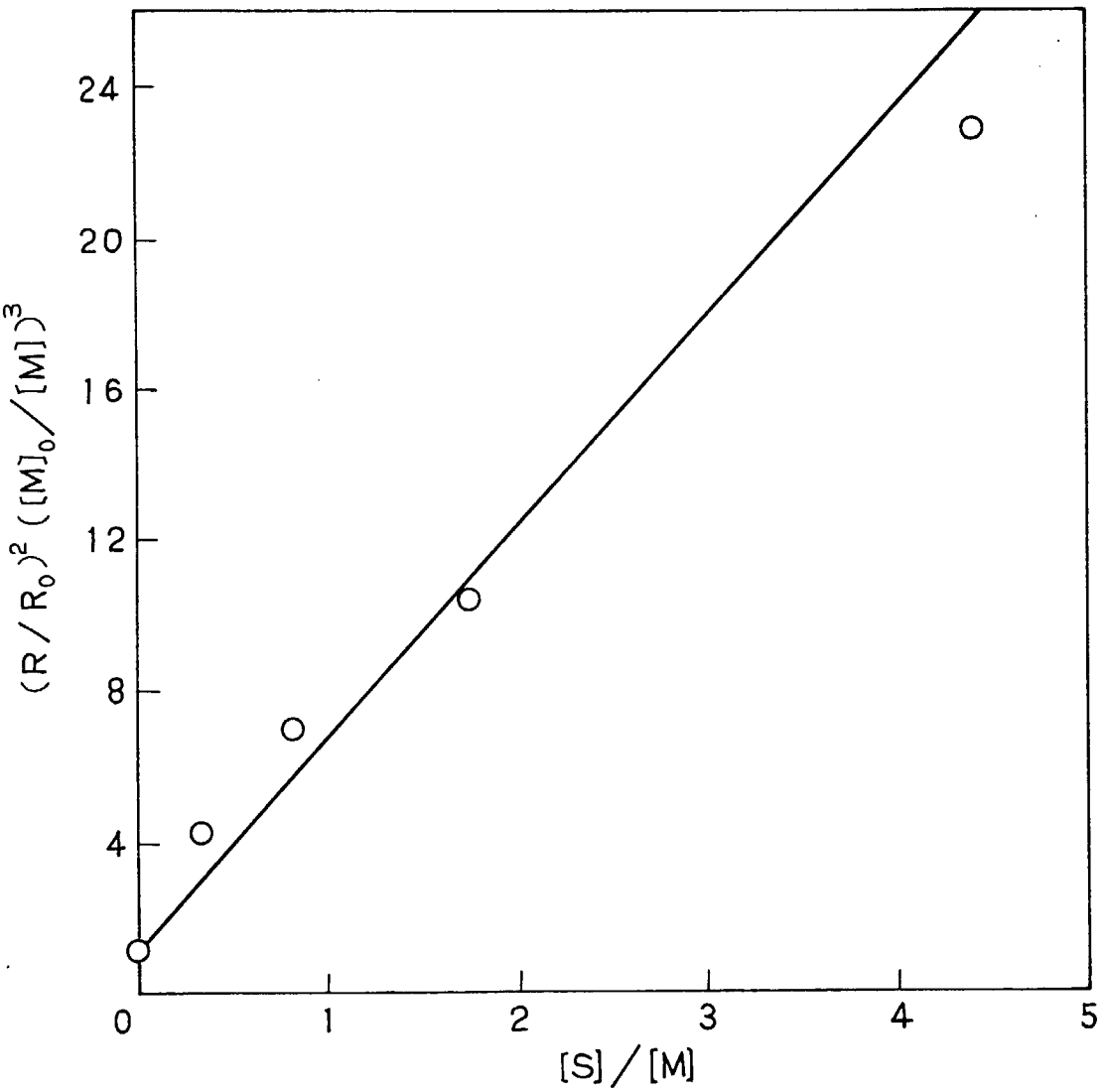

Fig. 2. Graphical representation of equation (2) to find the value of Φ_s/Φ_m.

is as follows:

$$\frac{P_0}{P} = \frac{k_{tr}}{k_p}\frac{[S]}{[M]}P_0 + \left(\frac{[M]_0}{[M]}\right)^{1/2}\left(1+\frac{\Phi_s}{\Phi_m}\frac{[S]}{[M]}\right)^{1/2} \qquad (3)$$

where P_0 and P are average degree of polymerization of styrene in bulk and in BA solution respectively and k_{tr} the chain transfer constant.

The first term in the right hand side of the equation (3) is attributed to the solvent transfer and the second term to the termination. We can calculate the second term and the left

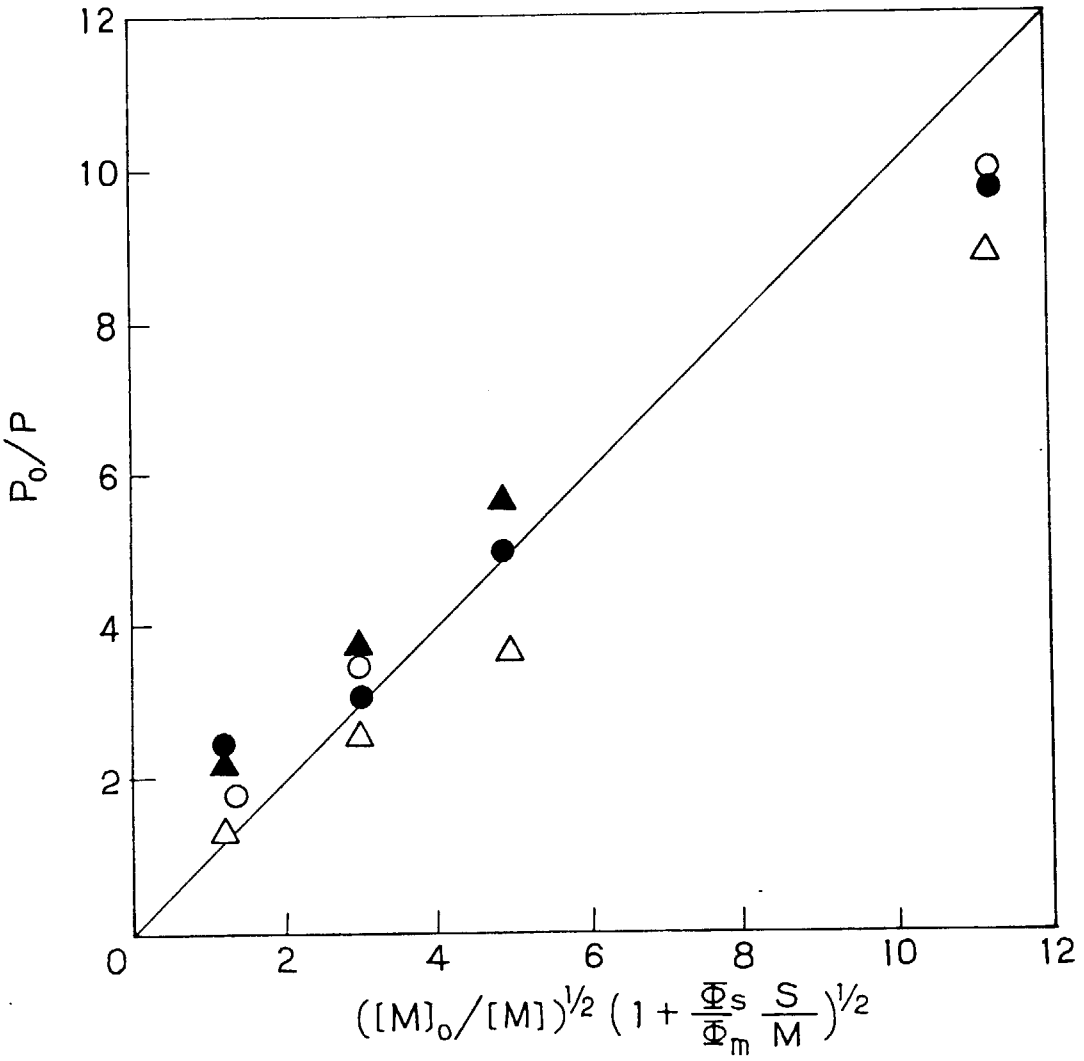

Fig. 3. Graphical representation of equation (3) to estimate the value of solvent transfer.

hand side of the equation; the difference of the two corresponds to the chain transfer. For the sake of getting a general idea of the largeness of the solvent transfer term, P_0/P were plotted, for the four series of experiments at different dose rates, against the second term of equation (3) in Fig. 3; the same scale was used for the ordinate and the abscissa. It is seen that a straight line which goes through the origin and has a slope of 45° may be drawn to represent the general tendency. It means nothing other than that the solvent transfer is negligibly small. There is no doubt that butylamine has the same transfer constant and the transfer takes place to the same extent as in the case of catalytic polymerization, however, the chain termination is overwhelming so that the former is masked by the latter. (J. Takezaki, T. Okada, and I. Sakurada)

1) J. Takezaki and T. Okada, JAERI-M 8569, 92 (1979).
2) I. Sakurada, J. Takezaki, and T. Okada, JAERI-M 8569, 72, 83 (1979).

2. Radiation-Induced Polymerization of Styrene in Binary Mixtures with Benzene

Binary mixtures with carbontetrachloride and ethylene dichloride have been studied and reported in the last annual report[1]. Benzene is a simple solvent or diluent for the polymerization of styrene and was studied three decades ago by A. Chapiro. Chapiro's experiments were carried out with a 0.4 Curies radium source, at a dose-rate of 0.023 rad/sec. The present series of experiments on the radiation polymerization of styrene in binary mixture with halogenated hydrocarbons are carried out mainly at higher dose-rates up to 10^7 rad/sec. Therefore it is of interest to know the aspects of polymerization of styrene in benzene at higher dose-rates.

Four mixtures containing 80, 60, 40 and 20 vol% styrene were irradiated at room temperature with electron beams from an accelerator at dose rates of 2.4×10 and 1.2×10^5 rad/sec.

The conversion was in most cases less than 10%. Molecular weight distribution curves as determined by GPC for the products obtained at the lower dose rate are shown in Fig. 1. The uppermost curve is for styrene in bulk; prominent and rather flat peaks correspond to radical polymer and oligomer, respectively. It is seen from the figure that the peak of the radical polymer is gradually shifted to the left as the styrene content decreases; this is the dilution effect.

GPC curves for the higher dose rate are shown in Fig. 2. Generally the curves are more complicated than those for the lower dose rate. It is due to the appearance of ionic and super polymers.

Four peaks are from left to right: I. oligomer, II. radical polymer, III. cationic polymer, IV. super polymer.

Under employment of kinetic equations obtained for the polymerization of styrene in solution, the radical polymerization of styrene in benzene is to be discussed.

The first interesting thing is the contribution of benzene in the initiating radical formation. The relative rates of free radical production of solvent and styrene i.e. Φ_s/Φ_m are calculated with the following equation.

$$\left(\frac{R}{R_0}\right)^2\left(\frac{[M]_0}{[M]}\right)^3 = 1 + \frac{\Phi_s}{\Phi_m}\frac{[S]}{[M]} \qquad (1)$$

Here R and R_0 are rates of polymerization (mole/l/sec) and [M] and $[M]_0$ are concentration (mole/l) of styrene in solution and in bulk, respectively, and [S] is concentration (mole/l) of the solvent molecule.

Experimental values of the rate of radical polymerization R and the ratio R/R_0 for the mixtures of various styrene content at the two different dose rates are shown in Table 1. The average values R/R_0 are used to find Φ_s/Φ_m graphically with equation (1). $(R/R_0)^2([M]_0/[M])^3$ is plotted against [S]/[M] in Fig. 3. The experimental points lie approximately on a straight line, whose slope shows that $\Phi_s/\Phi_m = 1.0$. Chapiro gives a value 0.95. It is rather astonishing that two measurements carried out at dose rates at least three orders of magnitude different

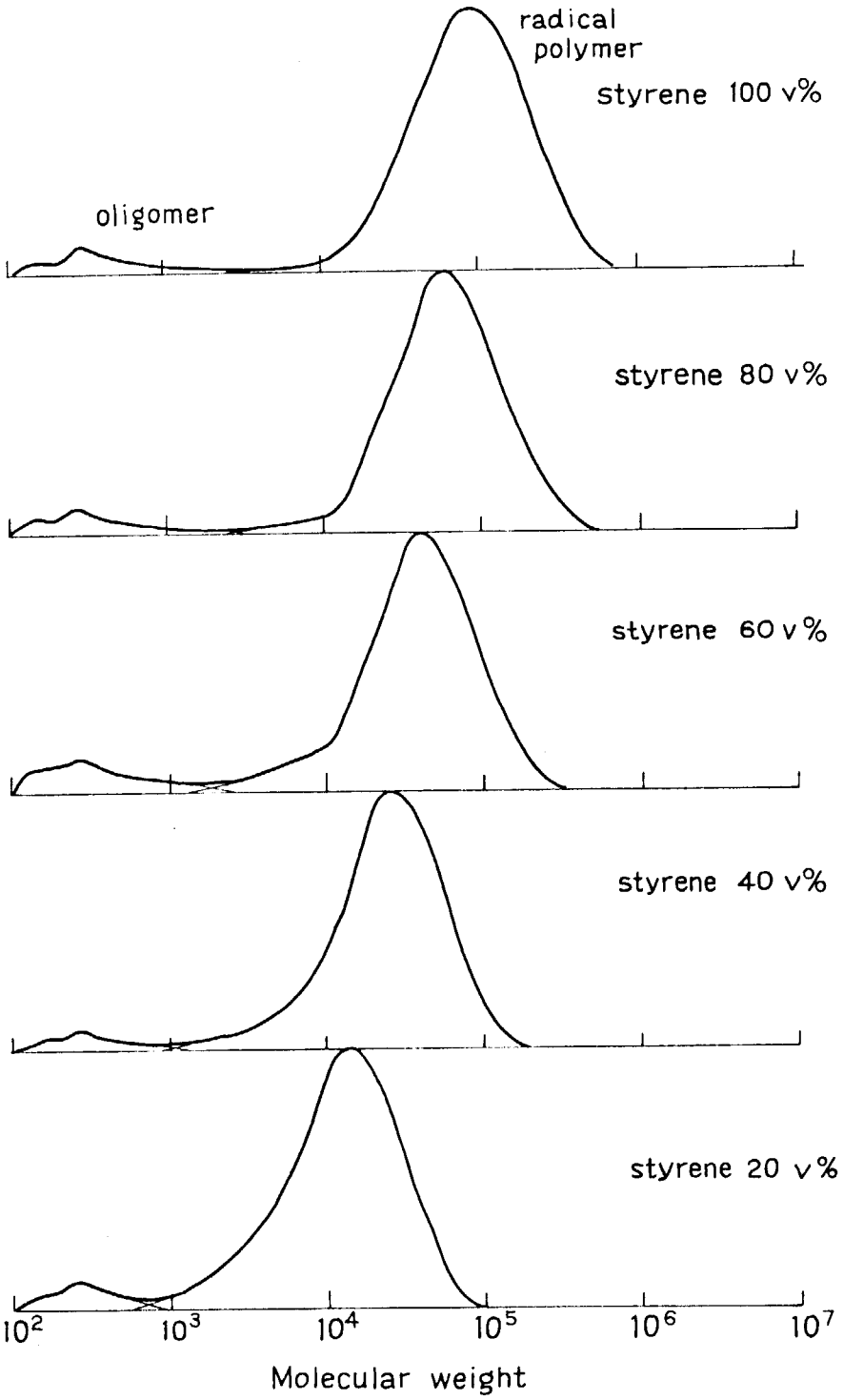

Fig. 1. Molecular weight distribution curves of polymerization product for styrene/benzene mixtures of various styrene contents at a dose rate of 2.4 x 10 rad/sec (dose 1.4 Mrads).

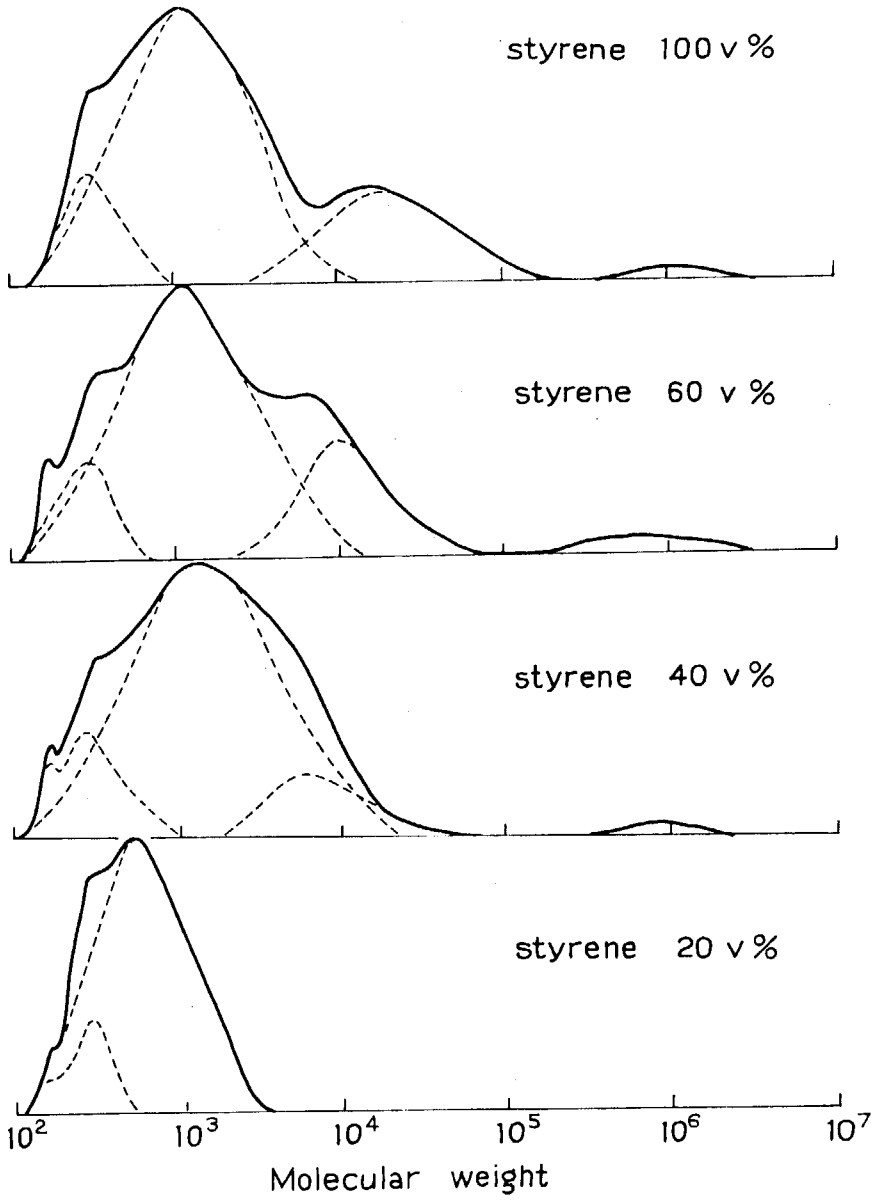

Fig. 2. Molecular weight distribution curves of polymerization product for styrene/benzene mixtures of various styrene contents at a dose rate of 1.2×10^5 rad/sec (dose 60 Mrads).

Table 1. Rate of Radical Polymerization R and the Ratio R/R_0 for the Binary Mixture of Styrene/Benzene

Conc. of styrene vol%	100	80	60	40	20
Dose rate 2.4×10 rad/sec					
$R \times 10^6$ mole/l/sec	8.30	6.59	4.43	2.69	1.06
R/R_0	1	0.794	0.533	0.324	0.193
Dose rate 1.2×10^5 rad/sec					
$R \times 10^3$ mole/l/sec	1.7	—	0.84	0.81	0.41
R/R_0	1	—	0.50	0.47	0.241

provide results which agree so closely with one another.

Next problem is the chain transfer to a solvent molecule. In the case of solution radical polymerization initiated by a chemical initiator, usually the transfer constant C, defined as k_{trs}/k_p i.e. (rate constant of chain transfer)/(rate constant of propagation) is calculated graphically from the experimental data. Unfortunately the same equation can not be applied for the radiation polymerization, and the following equivalent equation is proposed.

$$\frac{P_0}{P} = \frac{k_{trs}}{k_p}\frac{[S]}{[M]} P_0 + \left(\frac{[M]_0}{[M]}\right)^2 \frac{R}{R_0} \qquad (2)$$

The transfer constant k_{trs}/k_p is easily calculated with equation (2) and the results are shown in Table 2. The calculated average value of k_{trs}/k_p is 1.0×10^{-3}. In the case of catalytic polymerization values of 1.8×10^{-6} (at 65°C), 3.0×10^{-5} (at 100°C) and 8.1×10^{-5} (at 132°C) are reported. The present value is at least two orders of magnitude greater than

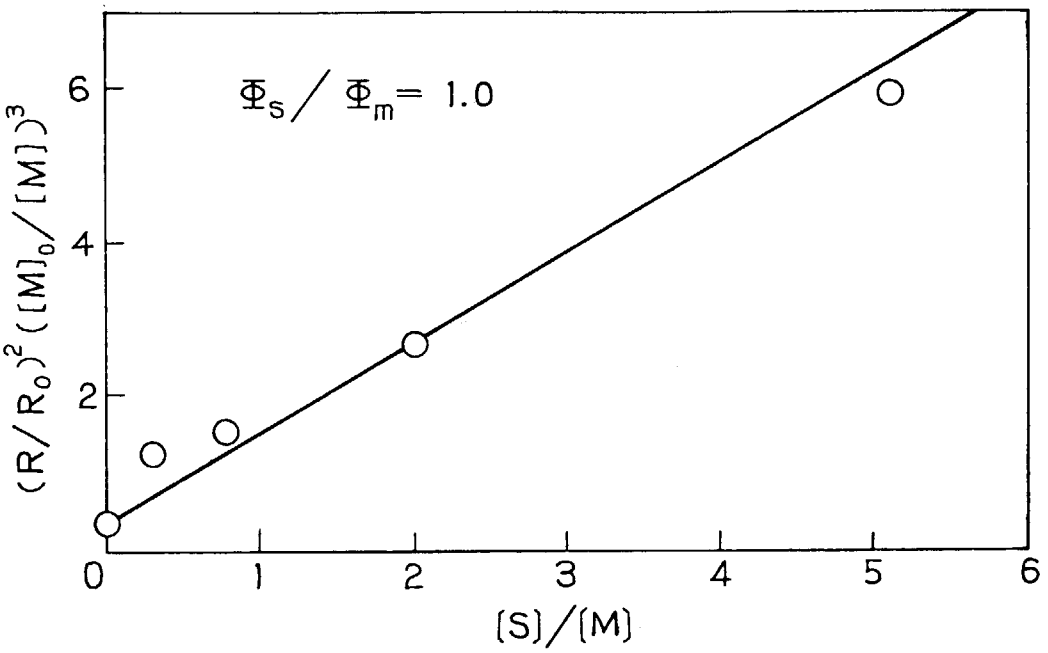

Fig. 3. Graphical representation of eq. (1) to find the value of Φ_s/Φ_m for styrene/benzene.

Table 2. Degree of Polymerization P, the Ratio P_0/P and the Calculated Values of Transfer Constant

Volume % styrene	100	80	60	40	20
Degree of polymerization P	893	605	384	241	115
Ratio P_0/P	1	1.476	2.325	3.705	7.765
Transfer const. $k_{trs}/k_p \times 10^3$	—	0.88	1.084	0.970	(0.62)
		Average = 1.0×10^{-3}			

* Polymerization carried out at a dose rate of 2.0 x 10 rad/sec

the others. Such a large difference cannot be due to the experimental error. The authors are engaged in the investigation to find if some reactions have been neglected.

(J. Takezaki, T. Okada, and I. Sakurada)

1) I. Sakurada, J. Takezaki, and T. Okada, JAERI-M 8569, 72, 83 (1979).
2) A. Chapiro, Radiation Chemistry of Polymeric Systems, Interscience, New York, 1962, p.251-255.

3. Radiation-Induced Bulk Polymerization of Vinyl Acetate

As a continuation of the radiation-induced polymerization of styrene[1], that of vinyl acetate was taken up. Bulk polymerization was carried out in a dose rate range from 1.8 rad/sec to 1.6 x 10^5 rad/sec at room temperature and essentially the same technics as in the case of styrene were used throughout the experiment.

Fig. 1 shows time conversion curves of bulk polymerization of vinyl acetate at three different dose rates. As is known they show at higher conversion self accelerating effect, which is attributed to the Trommsdorff effect in the radical polymerization. Vinyl acetate is a well known vinyl monomer which is liable to bring about polymer transfer in the polymerization.

GPC analysis of the polymerization products was carried out and the curves for the products obtained at various doses are shown in Fig. 2a and 2b. Elution counts and the molecular weights of polystyrene for the corresponding counts are also shown, because the relation between the molecular weight of polyvinyl acetate and the elution count has not yet been available.

It is seen from the figure that the products at higher dose rates through 8.0 x 10^3 rad/sec consist of three parts. According to the designation used in the case of polystyrene these three parts may be called from the left to the right as follows. I is oligomer, II (main peak) radical polymer and

III super polymer. Below 8.0 x 10^3 rad/sec the super polymer disappears. A similar phenomenon was observed in the case of styrene also.

The rate of total polymerization is plotted in Fig. 3 against the dose rate and compared with classical experimental results carried out by Goethals[2]. A straight line with a slope of 45° may be drawn as the dependence of the rate of polymerization on the dose rate. It is noteworthy that the classical experimental results at dose rates four orders of magnitude lower than the present ones lie approximately on the same straight line. The proportionality of the rate of polymerization R_p on the square root of the dose rate I is the consequence that the rate of initiating radical formation is directly proportional to the dose rate and the growing radicals are terminated only by mutual reaction either by coupling or by disproportionation. Theoretically R_p is expressed as follows.

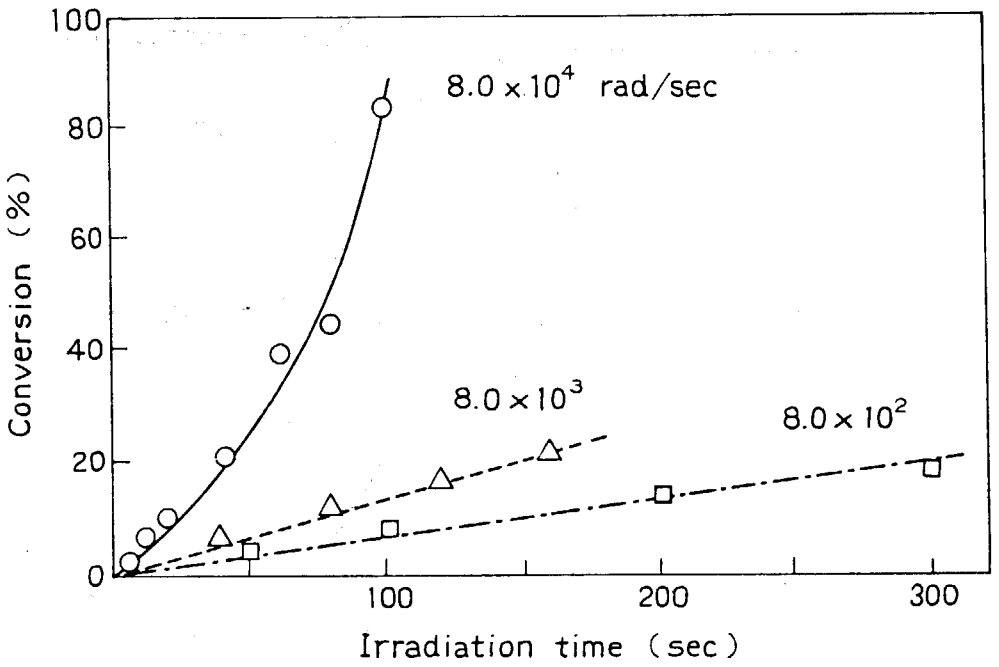

Fig. 1. Time-conversion curves of radiation induced polymerization of vinyl acetate at various dose rates.

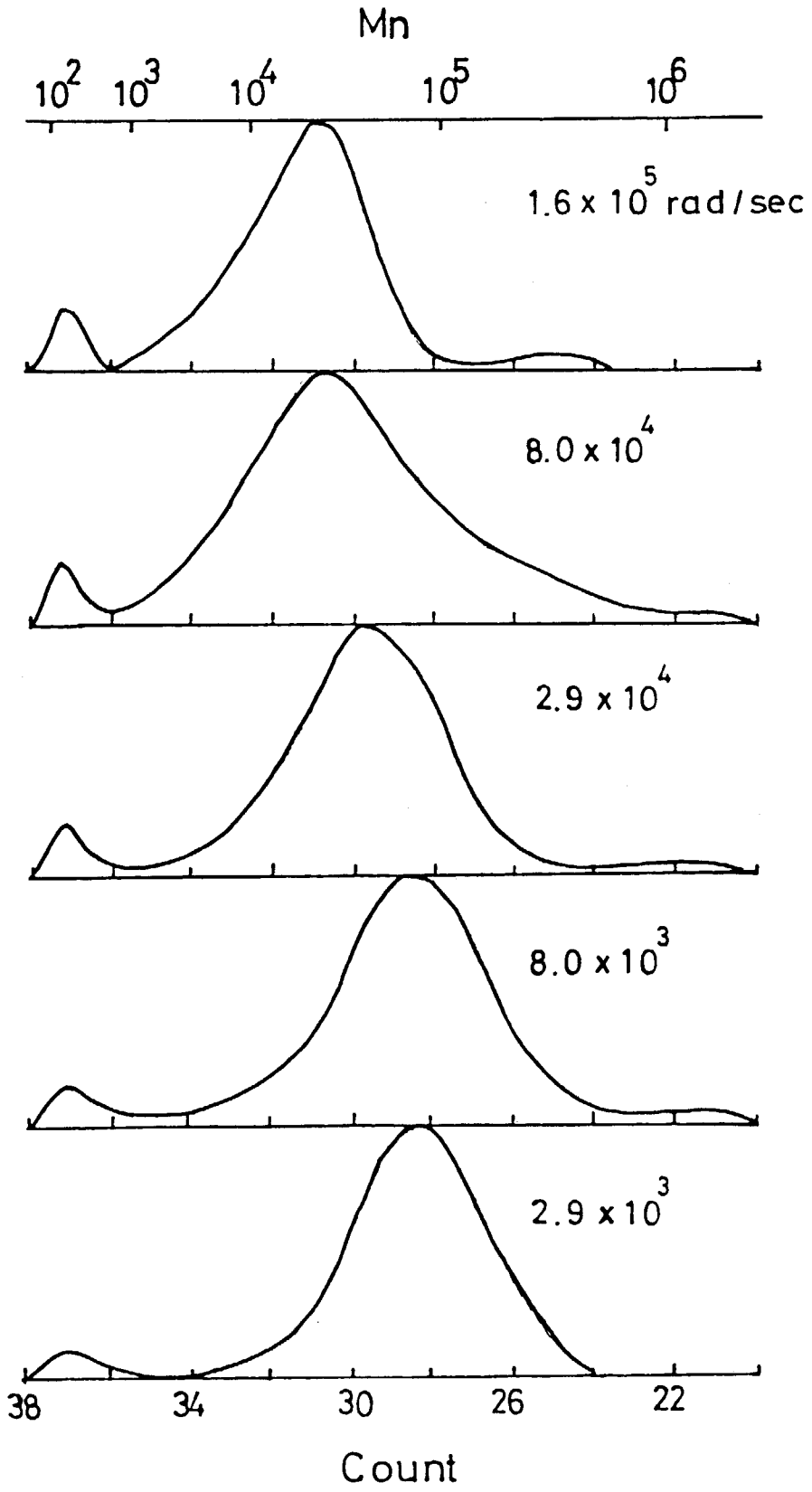

Fig. 2a. GPC curves of polymerization products at various dose rates: $1.6 \times 10^5 \sim 8.0 \times 10^3$ rad/sec.

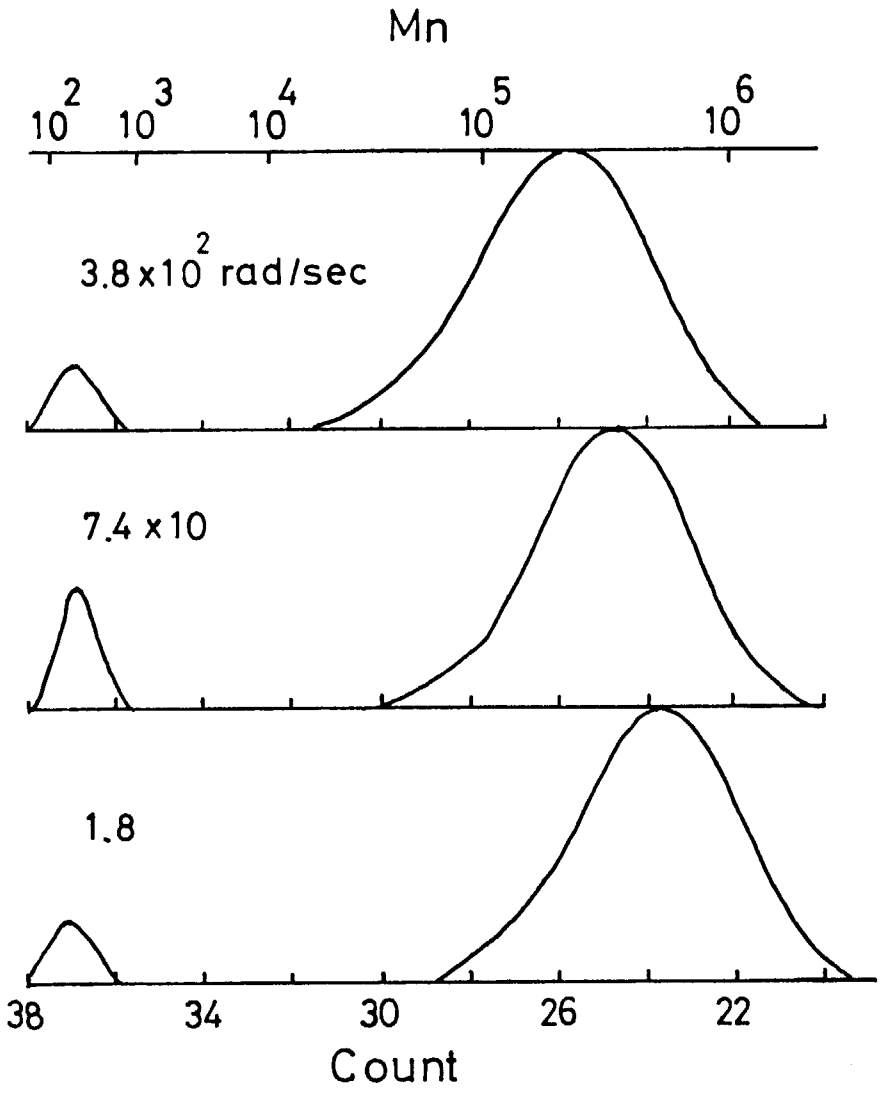

Fig. 2b. GPC curves of polymerization products at various dose rates: $2.9 \times 10^3 \sim 1.8$ rad/sec.

$$R_p = k_p \, k_t^{1/2} (\Phi I)^{1/2} [M]^{3/2} \qquad (1)$$

Here k_p and k_t are rate constants of polymerization, termination by coupling and termination by disproportionation, respectively. Φ is number of initiating radicals formed from the monomer in mole per irradiation of the unit dose, and [M] number of vinyl acetate molecules in mole/l i.e. 11.62.

Though precise determination of the average molecular weight of polyvinyl acetates from the GPC curves in Fig. 2 has not yet been carried out, apparent values read out from Fig. 2 are used tentatively.

For the discussion of the molecular weight or degree of polymerization it is necessary that not only termination but also transfer are taken into consideration. In the present case monomer transfer is likely to give influence on the degree of polymerization even at the initial stage of the polymerization. The following equation gives the relation between the

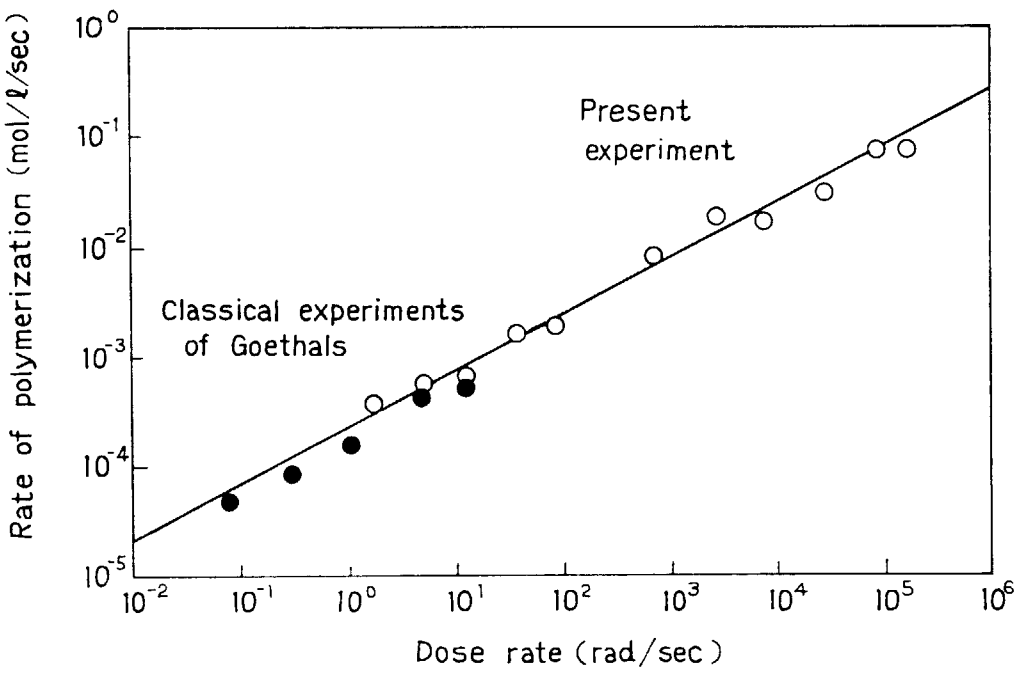

Fig. 3. Dose rate dependence of the rate of polymerization of vinyl acetate.

degree of polymerization and dose rate for the radical polymerization, where stable molecules are formed by both mutual termination and monomer transfer reactions.

$$\frac{1}{\bar{P}} = \frac{k_{tm}}{k_p} + \frac{k_t^{1/2}}{k_p} \Phi^{1/2} I^{1/2} [M]^{-1/2} \qquad (2)$$

Here $\bar{P}$ and k_{tm} are average degree of polymerization and rate constant of monomer transfer, respectively.

Dependence of $1/\bar{P}$ on $I^{1/2}$ is shown graphically in Fig. 4; as was expected the dependence may be plotted by a straight line, which does not pass through the origin but cuts the ordinate at a certain value corresponding to k_{tm}/k_p.

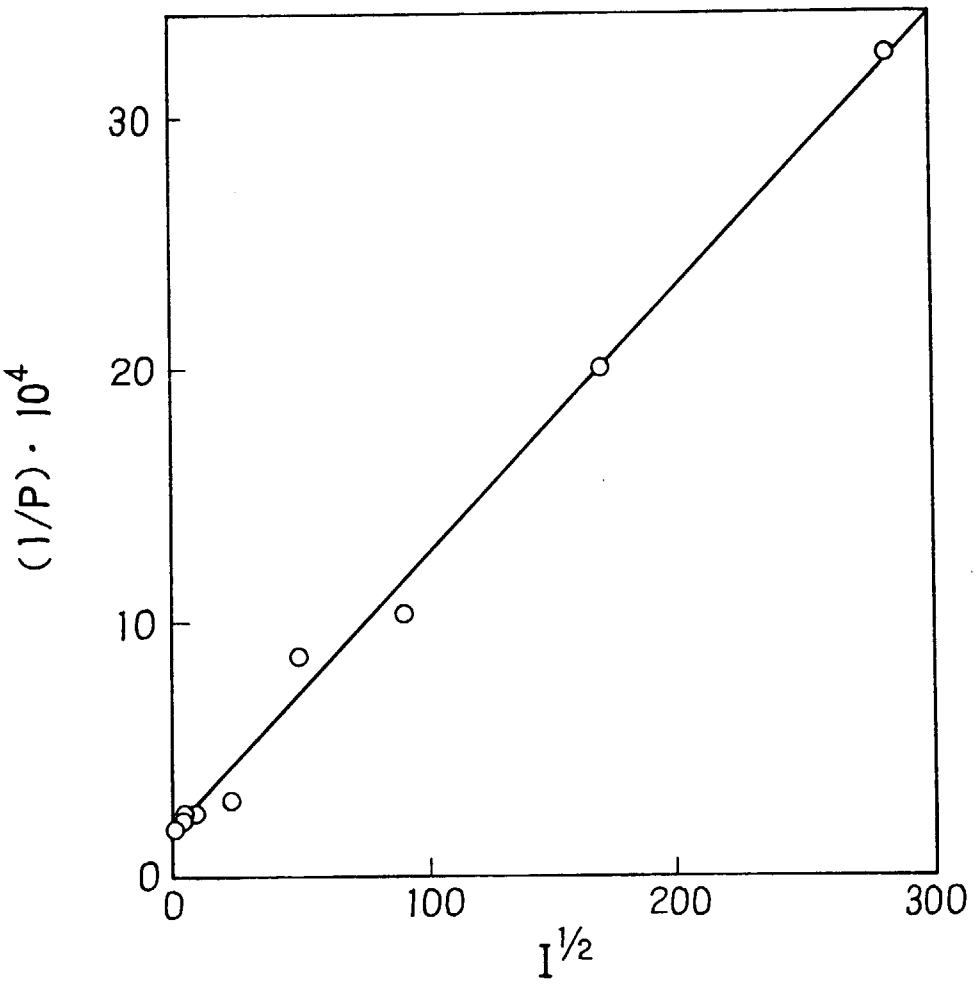

Fig. 4. Dependence of 1/P on the square root of the dose rate.

By combination of equation (1) and (2) it is formally possible to calculate the values of $k_t^{1/2}/k_p$, and Φ. The reliability of the values are, however, not sufficient because the molecular weights of the GPC curves in Fig. 2 are not yet standardized.

To find the rate of initiating radical formation from vinyl acetate by irradiation, the DPPH method was used to determine the G value of free radical formation. As may be seen from Fig. 5, rate of polymerization decreases with increasing amount of DPPH to vinyl acetate, and the polymerization is almost inhibited at about 2.5×10^{-2} mole/l of DPPH. The dose and dose rate of the experiments are given in the figure. Similar experiments with DPPH were carried out further at 8.0×10^{3} rad/sec and 8×10^{-2} rad/sec and led to the conclusion that in an average 7×10^{-9} mole/l/rad initiating radicals were formed by the irradiation; the G value for the formation of the

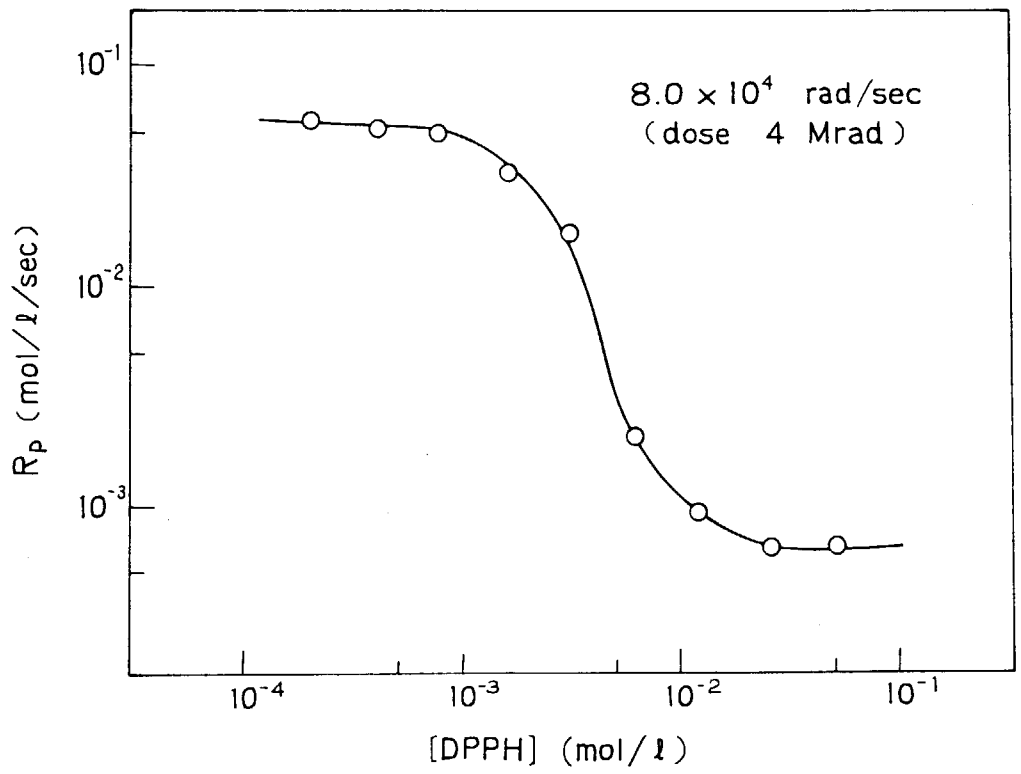

Fig. 5. Effect of added DPPH on the polymerization rate of vinyl acetate.

free radicals were calculated to be 7. Chapiro[2] reported G = 9 - 6 radicals per 100 eV, based on the experiments whose highest dose rate was less than 10^2 rad/sec. Both the values are in fair agreement with each other.

GPC curves of polymerization products of vinyl acetate obtained by irradiation at a dose rate of 8.0×10^4 rad/sec for 5 seconds in the absence and presence of DPPH are compared in Fig. 6. Polymer yields in the absence and presence of DPPH were 2.00 and 0.01%, respectively. It is seen from the GPC curves that the three peaks I, II and IV completely disappears by the addition of DPPH, and instead a new peak corresponding to a molecular weight of about 1000 appears. Fig. 6 suggests further that the fractions I and III also are formed by a radical mechanism as in the case of the fraction II.

In connection with the mechanism of polymerization it is of interest to know the dose rate dependence of the polymeriza-

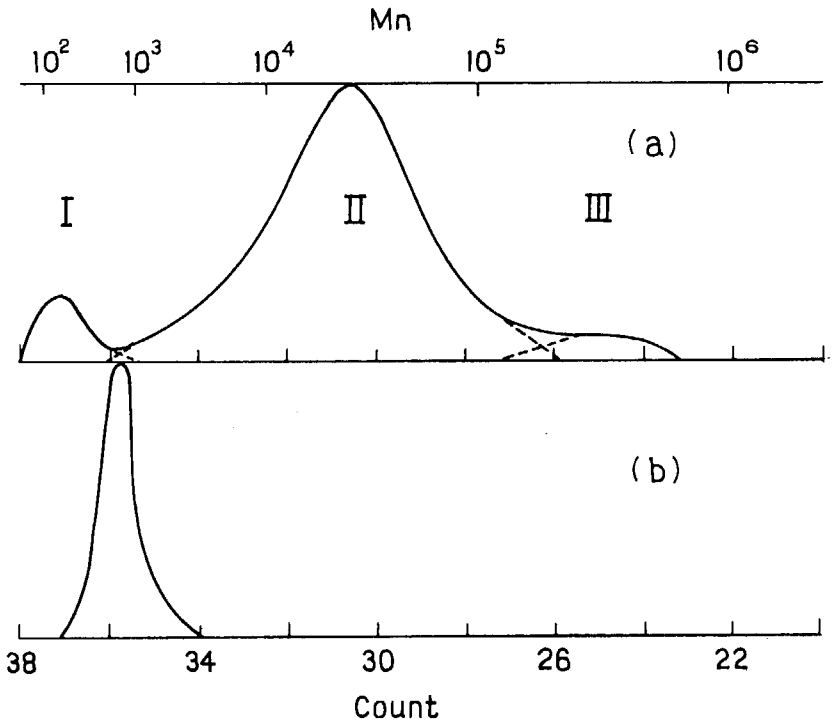

Fig. 6. GPC curves of polymerization product of vinyl acetate in the absence (a) and presence (b) of DPPH (2.5×10^{-2} mole/1). Dose rate 8.0×10^4 rad/sec, dose 0.4 Mrad.

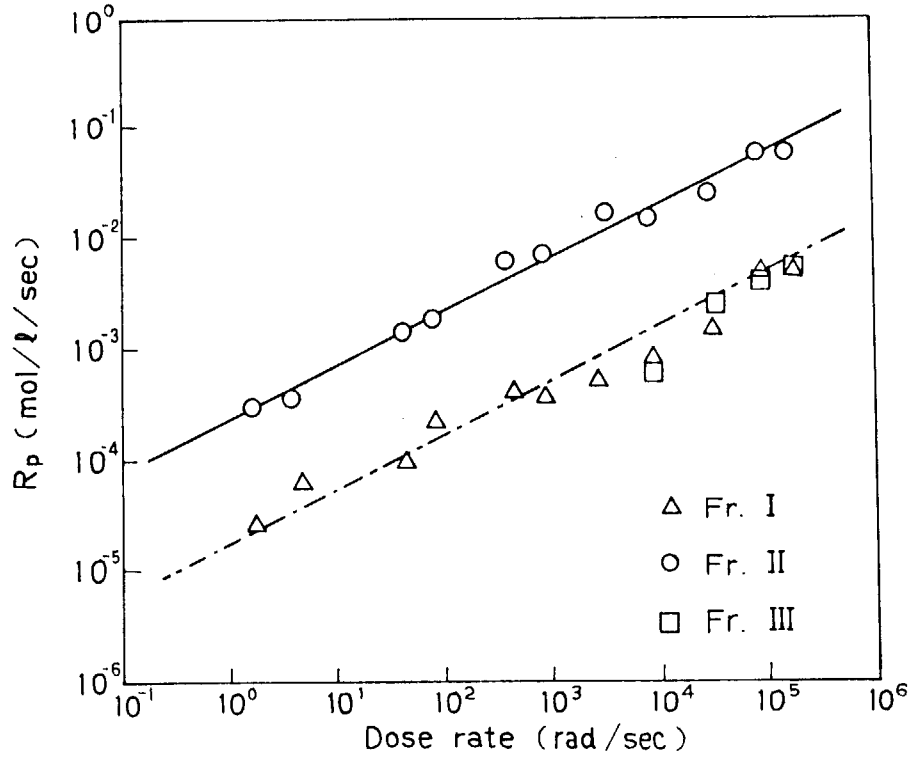

Fig. 7. Dependence of the rate of polymerization on the dose rate. Fr. I oligomer, Fr. II main radical polymer, Fr. III super polymer.

tion. A graphical representation of the dependences for the fractions I, II and III is shown in Fig. 7.

Fraction II is the main product of the present radiation induced polymerization of vinyl acetate and has been already described. It is noteworthy that the square root rule of the radical polymerization, which means that the polymerization rate is proportional to the square root of the dose rate, is applicable also to fraction I (oligomer) and III (super polymer). Apparently initiating radicals for fractions I and III are formed in proportion to the radiation dose and destroyed by the mutual reaction as in the case of the formation of the main radical polymer (II). To clarify the detailed mechanism of the three types of the radical polymerization is an interesting problem.

(J. Takezaki, T. Okada, and I. Sakurada)

1) J. Takezaki, T. Okada, and I. Sakurada, J. Appl. Polymer Sci., 21, 2683 (1977); 22, 3311 (1978).
2) A. Chapiro, Radiation Chemistry of Polymeric Systems, Interscience, New York, 1962, p.188-192.

[3] Radiation-Induced Polymerization of Dienes

1. Polymerization of Butadiene in n-Hexane Solution

In the last issue[1] of this report, it was described that in the bulk polymerization of butadiene by electron beams the reaction proceeded with single mechanism, i.e., cationic. To avoid gel formation in the polymerization at conversion above 10% in bulk system, solution polymerization was carried out.

First, polymerizations in several solvents were taken up to find an appropriate system. In halogen-containing solvents as methylene dichloride and carbon tetrachloride, though R_p and molecular weight (MW) of the products were higher than those in bulk system, gel formation took place at low conversion. In toluene and tetrahydrofuran, on the other hand, both R_p and MW were very low. n-Hexane was chosen as a solvent mainly because it does not form gel at low conversion and have moderate R_p.

n-Hexane was used after drying with calcium hydride. Butadiene was used as received. All the samples were sealed in metal cells[2] for electron beam irradiation after degassing. Irradiation was carried out at -10°C by 1.5 MeV electron beams from a Van de Graaff accelerator.

In Fig. 1, R_p and $\bar{M}_n$ of the product were plotted against mole fraction of butadiene, f, in n-hexane. With the addition of n-hexane to the bulk system, the R_p decreased by about 20% but it remained almost unchanged between 40 $\sim$ 95 mole% butadiene. $\bar{M}_n$ was tentatively evaluated from the molecular weight distribution (MWD) applying a MW-elution time relationship for polystyrene. The $\bar{M}_n$ decreased with decreasing monomer concentration though it scatters considerably.

The influences of dose rate on R_p and MWD were studied at the monomer fraction of 0.50. The R_p was proportional to the 1.0 power of the dose rate as shown in Fig. 2. The MWDs of the products at about 5% conversion were almost identical each other as shown in Fig. 3. Such a kinetic behavior, which is essentially the same as observed in the bulk system[1], indicates

cationic mechanism of the polymerization also in n-hexane solution.

In this sytem, the following reactions are considered.

Ion generation $\quad M \rightsquigarrow M^+$

Initiation $\quad M^+ + M \longrightarrow M_2^+$

Propagation $\quad M_n^+ + M \longrightarrow M_{n+1}^+$

Chain transfer to monomer $\quad M_n^+ + M \longrightarrow M_n + M^+$

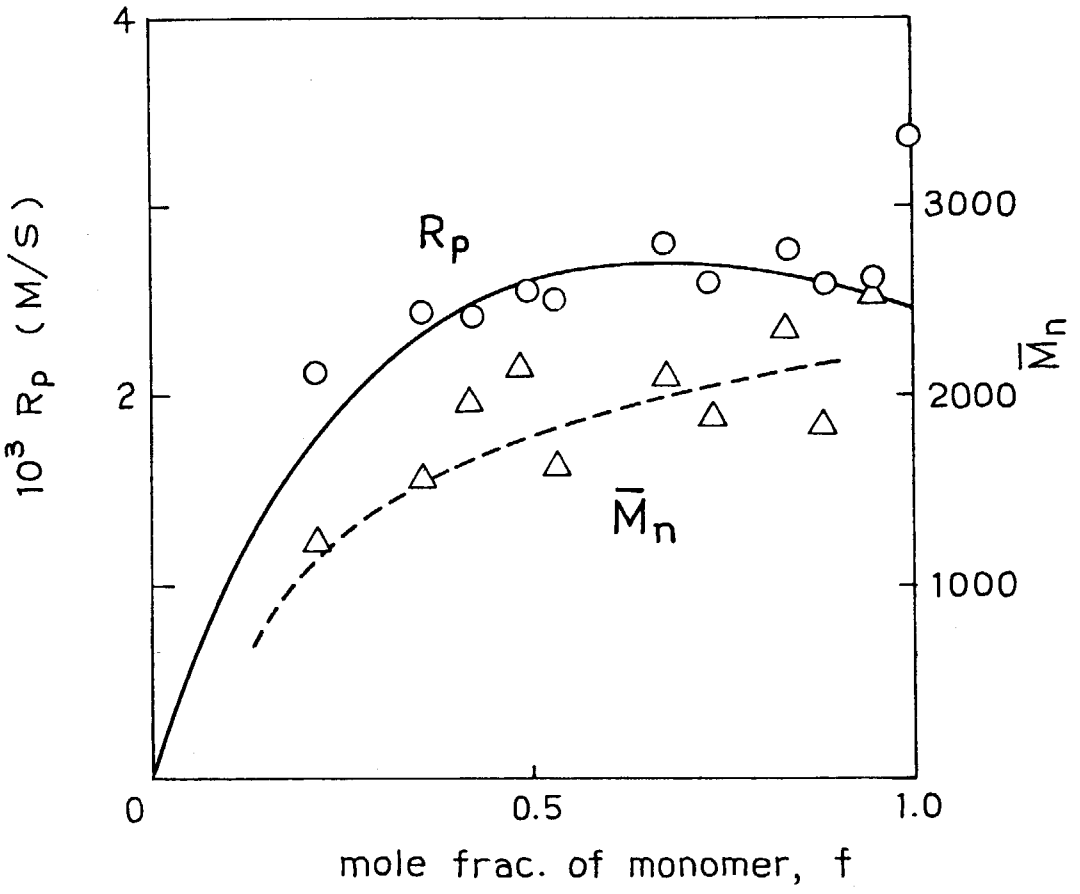

Fig. 1. R_p and $\bar{M}_n$ in the polymerization of butadiene in n-hexane solution at -10°C: Dose rate, 2.2 x 10^5 rad/sec.

Chain transfer to solvent $\quad M_n^+ + S \longrightarrow M_n + S^+$

Termination with water $\quad M_n^+ + X \longrightarrow M_n + X^+$

Then we get,

$$R_p = \frac{k_p[M]}{k_X[X]} \cdot \frac{10adG}{N} \cdot I \qquad (1)$$

Here, a, d, and N mean rad-eV·g conversion factor, density of the system and Avogadro number, respectively. To evaluate R_p from equation (1), we have to know G value for the initiation and water concentration in the binary system even when we may

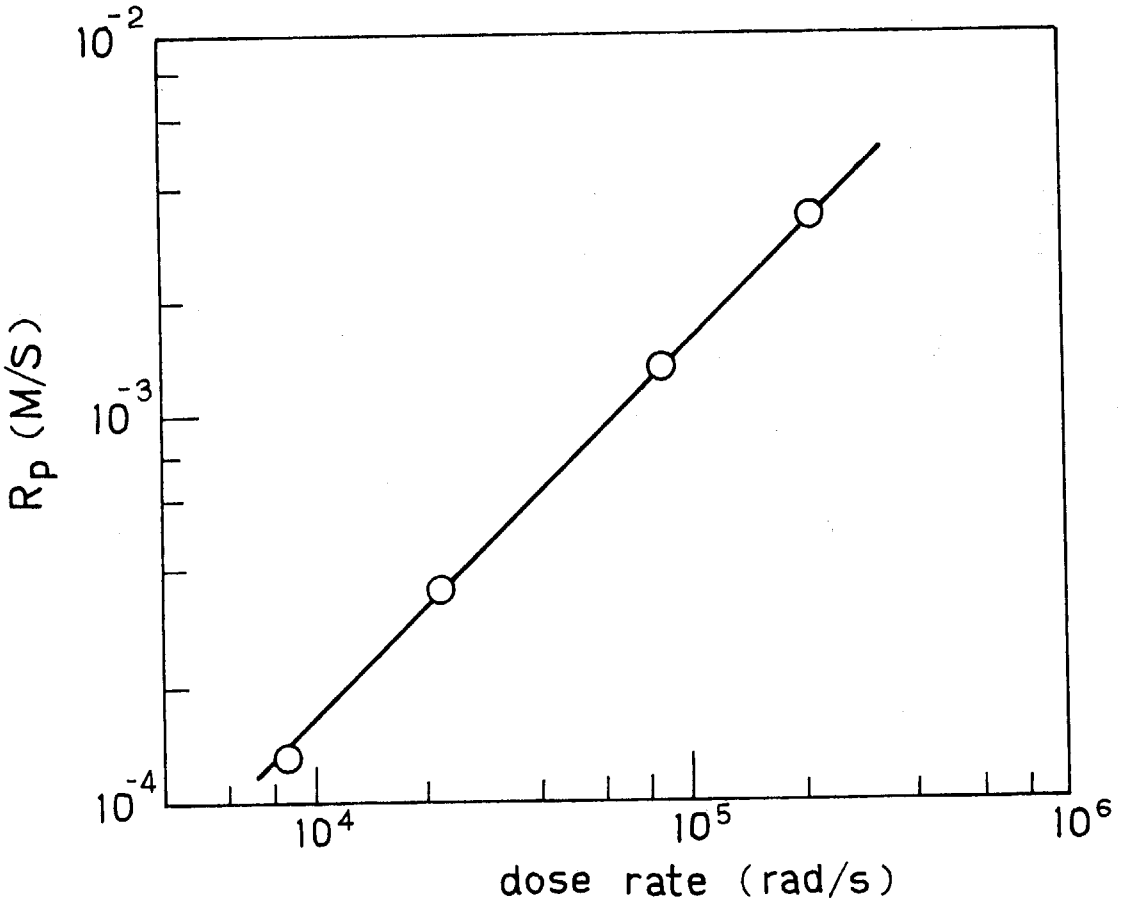

Fig. 2. Dose rate dependence of R_p at the monomer fraction of 0.50.

assume that other parameters are not changed with the value of f. A use of simple assumptions,

$$G = fG_M + (1-f)G_S \tag{2}$$

$$[M] = f[X]_M + (1-f)[X]_S \tag{3}$$

gives the following equation with three adjustable parameters, α, β, and γ.

$$R_p = \gamma \cdot \frac{f[f + (1-f)\alpha]}{f + (1-f)\beta} \tag{4}$$

$$\alpha = \frac{G_S}{G_M} \tag{5}$$

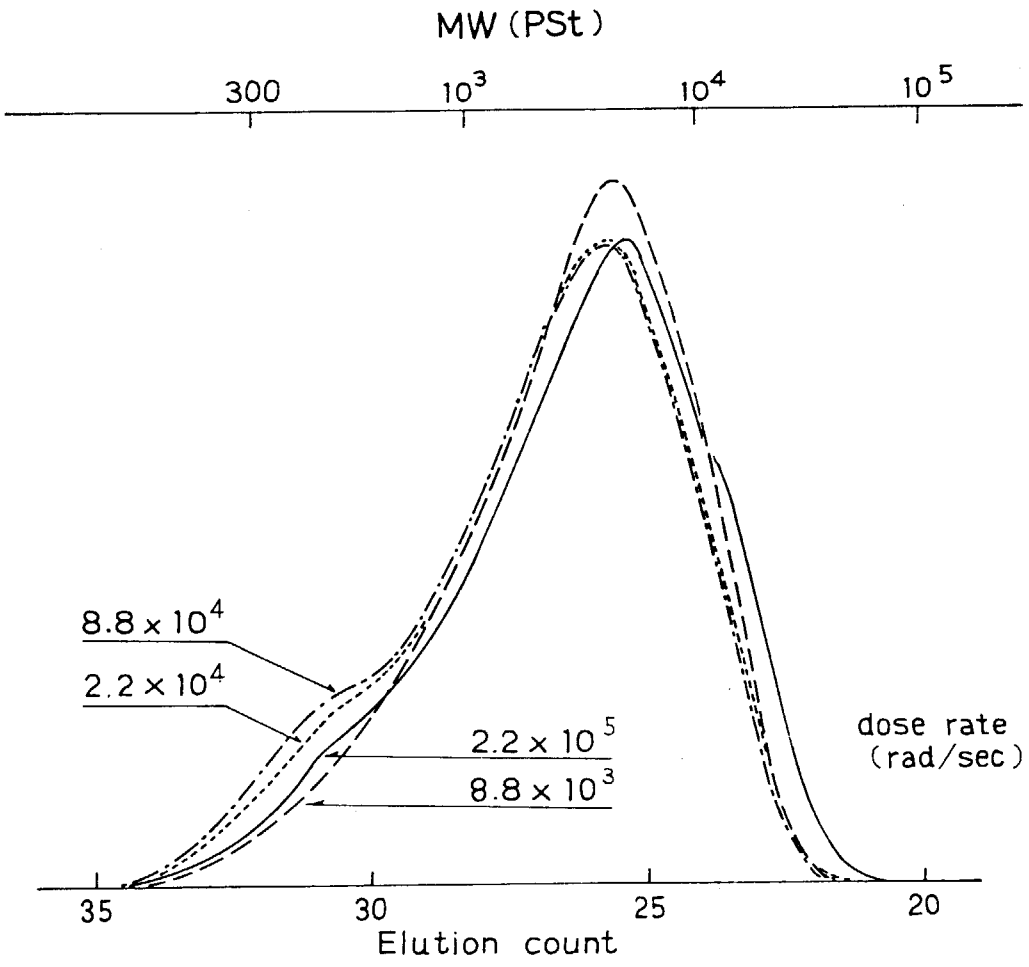

Fig. 3. MWDs of polybutadienes obtained at different dose rates.

$$\beta = \frac{[M]_S}{[X]_M} \tag{6}$$

$$\gamma = \frac{k_p[M]_0}{k_X[X]_M} \cdot \frac{10fdG_M}{N} \cdot I \tag{7}$$

The value α was evaluated to be approximately 2 on the basis of G(free ion) values in butadiene[3] and n-hexane[4]. The results of the calculation of equation (4) to give the best fit to the experimental values are shown with solid curve in Fig. 1. The obtained value of β was 0.3, which was close to the ratio of saturated water contents in n-hexane and butadiene, 4 mM/10 mM. The other parameter, γ means R_p at f = 1, i.e., R_p in bulk system. In Fig. 1, it is obvious that the observed value of R_p in bulk system does not agree well with the γ value. This is probably because of the change of dissociation-association equilibrium of water in butadiene by the addition of n-hexane to give an influence on the value of actual water concentration [X] in the system. (K. Hayashi and S. Okamura)

1) K. Hayashi and S. Okamura, JAERI-M, 8569, 105 (1979).
2) K. Hayashi, J. Polym. Sci. Polym. Chem. Ed., 18, 179 (1980).
3) J.-P. Dodelet, K. Shinsaka, U. Kortsch, and G. R. Freeman, J. Chem. Phys. 59, 2376 (1973).
4) A. Hummel, A. O. Allen and F. H. Watson, Jr., J. Chem. Phys., 44, 3431 (1966).

[4] Radiation-Induced Emulsion Polymerization

1. Emulsion Polymerization of Styrene in a Flow System

In our previous studies it was found that the characteristic features of the high dose rate polymerization are high rate of polymerization, predominance of cationic mechanism and liability to form oligomer. Emulsion polymerization in a flow system was attempted to know the reaction behavior of the polymerization at high dose rate in a practical system. In this study, styrene was used as a monomer of low solubility in water. It is well known that styrene shows an ideal kinetic behavior to obey case II of Smith-Ewart theory, where average number of radicals present in a particle can be approximated to be 0.5.

In Fig. 1, schematic illustration of the reaction system is given. The monomer was treated width cation-exchange resin to remove inhibitor. Sodium lauryl sulfate (SLS) was used as

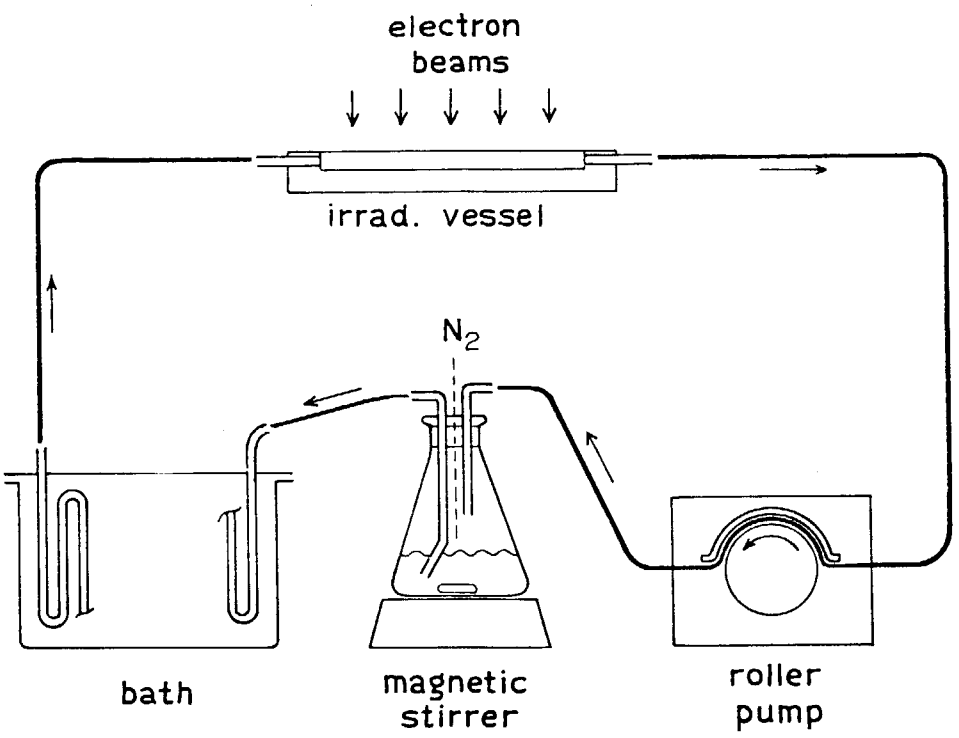

Fig. 1. A schematic diagram of the polymerization system.

an emulsifier. An emulsion of about 250 g was deaerated in a flask by passing nitrogen stream under stirring magnetically. By the use of roller-pump, the emulsion was circulated through an irradiation vessel after passing a heat exchanger to keep the sample temperature at 40°C. The inner size of the irradiation vessel was 10 mm width, 5 mm depth and 440 mm length. The electron beam of 1.5 MeV energy and of 300 mm scanning width penetrates 3 mm in the direction of the depth. The average dose rate in the vessel was 3.0×10^5 rad/sec for a space of 300 x 10 x 3 mm. The flow rate of the emulsion was 4.7 ∿ 5.0 ml/sec.

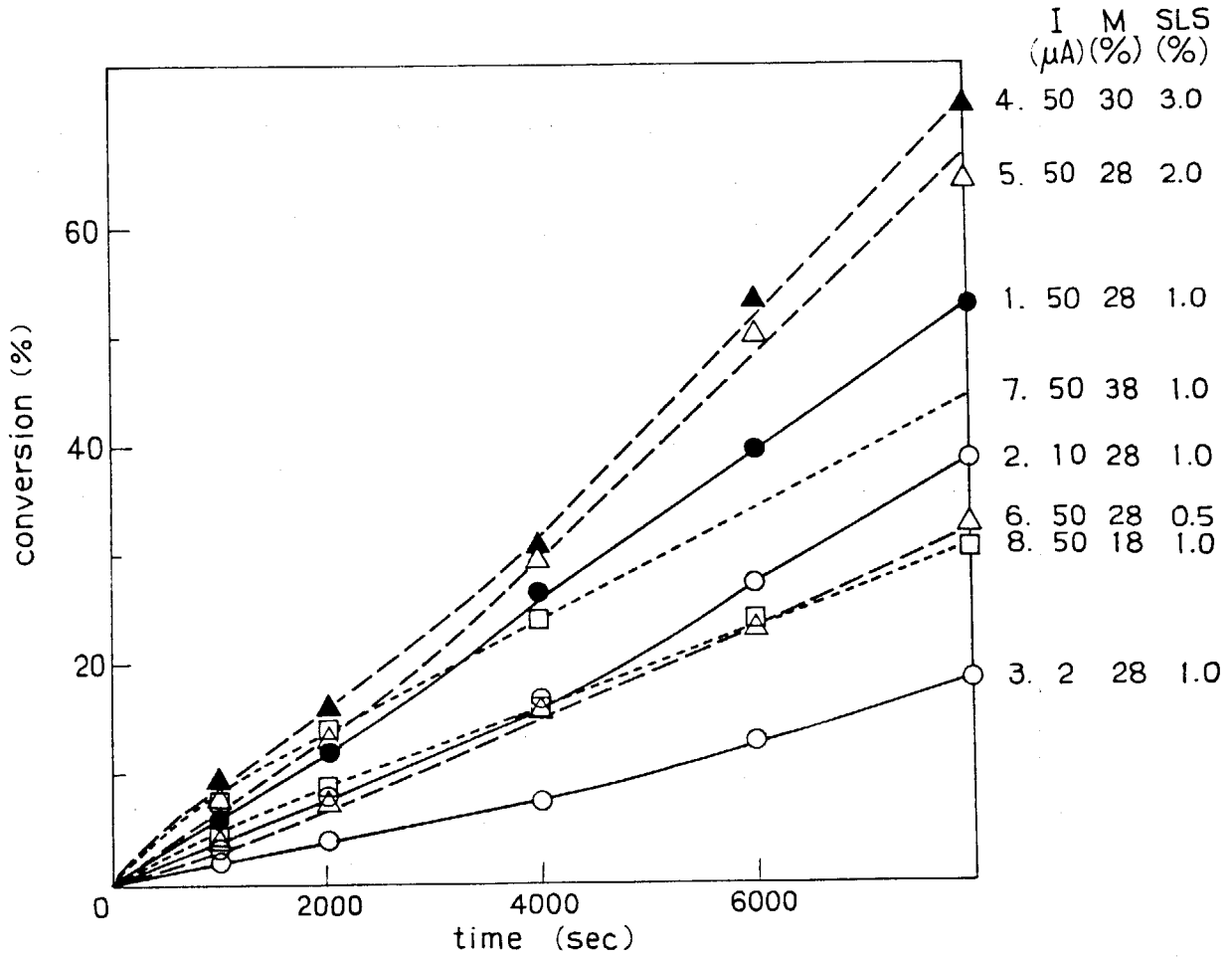

Fig. 2. Time-conversion relations in various styrene emulsions: I (μA), beam current of the irradiation; M, wt% of styrene in emulsion; S, wt% of SLS to the monomer.

All the results of polymerization where dose rate, monomer and emulsifier concentrations were changed are summarized in Fig. 2. In most cases, the polymer yield was proportional to irradiation time at low conversion up to 10 ∿ 20% and the rate slightly increases in the later part of the polymerization. From these results, it is found that the polymerization rate is considerably low in styrene. The molecular weight distributions (MWDs) of the products were broad ranging from 200 to 10^5 as shown in Fig. 3 and $\bar{M}_n$s were around 1000. It is notable that relatively low MW product was formed at the initial stage of the polymerization. All of the polymer emulsions obtained were stable on storing for several months.

From the results in Fig. 1, the following relation was obtained,

$$R_p \propto I^{0.33}[SLS]^{0.17}[M]^{1.8}$$

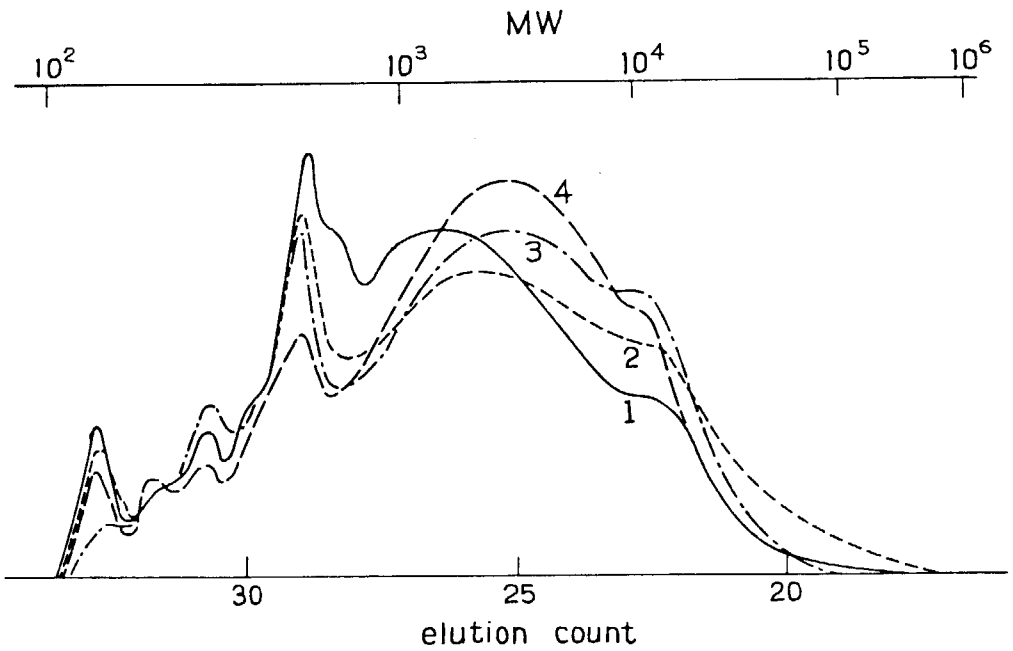

Fig. 3. MWDs of polystyrenes at various conversions:
I = 50 A; M = 28%; S = 1.0%.
Conversion: 1. 5.8%; 2. 12.7%; 3. 26.7%; 4. 52.8%.

which deviates from the consequence of Smith-Ewart theory, case II, i.e., $R_p \propto I^{0.4}[SLS]^{0.6}$. Such a deviation at high dose rate is also expected by a simple calculation. At the initiation rate of 10^{13} radicals/ml·sec which corresponds approximately to the rate of radical formation in ordinary catalytic system the particle diameter should be substantially lower than 9200A, which is easily met in most cases, to show the case II kinetics. At the initiation rate of 1.8×10^{17} radicals/ml·sec which corresponds to the rate of radical formation at our dose rate assuming G(radical) = 1, the critical diameter reduces to 1800A. This indicates that at high dose rate it is hard to keep the case II conditions.

One of the major difference in emulsion polymerization by radiation from that by catalytic initiation is radical formation by direct irradiation of the monomer in micells and droplets. In bulk polymerization of styrene[1], DP_n of the radical product at 1.8×10^5 rad/sec was reported to be 9.4. Therefore in our emulsion system, oligomer of DP_n less than 10 is expected. On the other hand, in our reaction condition, the emulsion was irradiated for 3 sec in a cycle time of 52 sec. During the unirradiated period, some complicated phenomena will take place as monomer feeding to micells, postpolymerization, coagulation of particles etc., which probably contribute to the polymer formation of $DP_n > 10$. (K. Hayashi and S. Okamura)

1) J. Takezaki, T. Okada, and I. Sakurada, J. Appl. Polym. Sci., 22, 3311 (1978).

2. Emulsion Polymerization of Vinyl Acetate in a Flow System

High dose rate polymerization of vinyl acetate in emulsion was carried out expecting high rate of polymerization. Another point of interest is a kinetic behavior of the polymerization of a monomer of substantial solubility in water.

The monomer was used as received. The experimental setup and conditions are almost the same as described in the preceding

article except otherwise noted. The reaction proceeds with much faster rate than in styrene as shown in Fig. 1. In all cases time-conversion relationship is sigmoidal and the reaction rate is gradually accelerated with time. The reaction conditions for curve (a) in Fig. 1 were 3.0×10^5 rad/sec, [SLS] = 1.5% to monomer and flow rate of 7.7 ml/sec. From curves (a), (b) and (c), the dose rate coefficient of R_p was found to be 0.6 when the slope at 30% conversion was taken as R_p. Only a slight increase in R_p was observed even when SLS concentration was doubled (curve (d)). As shown in curves (a) and (d), it is notable that the flow rate of the emulsion substantially influences the reaction rate.

MWDs of the products obtained in condition (a) in Fig. 1

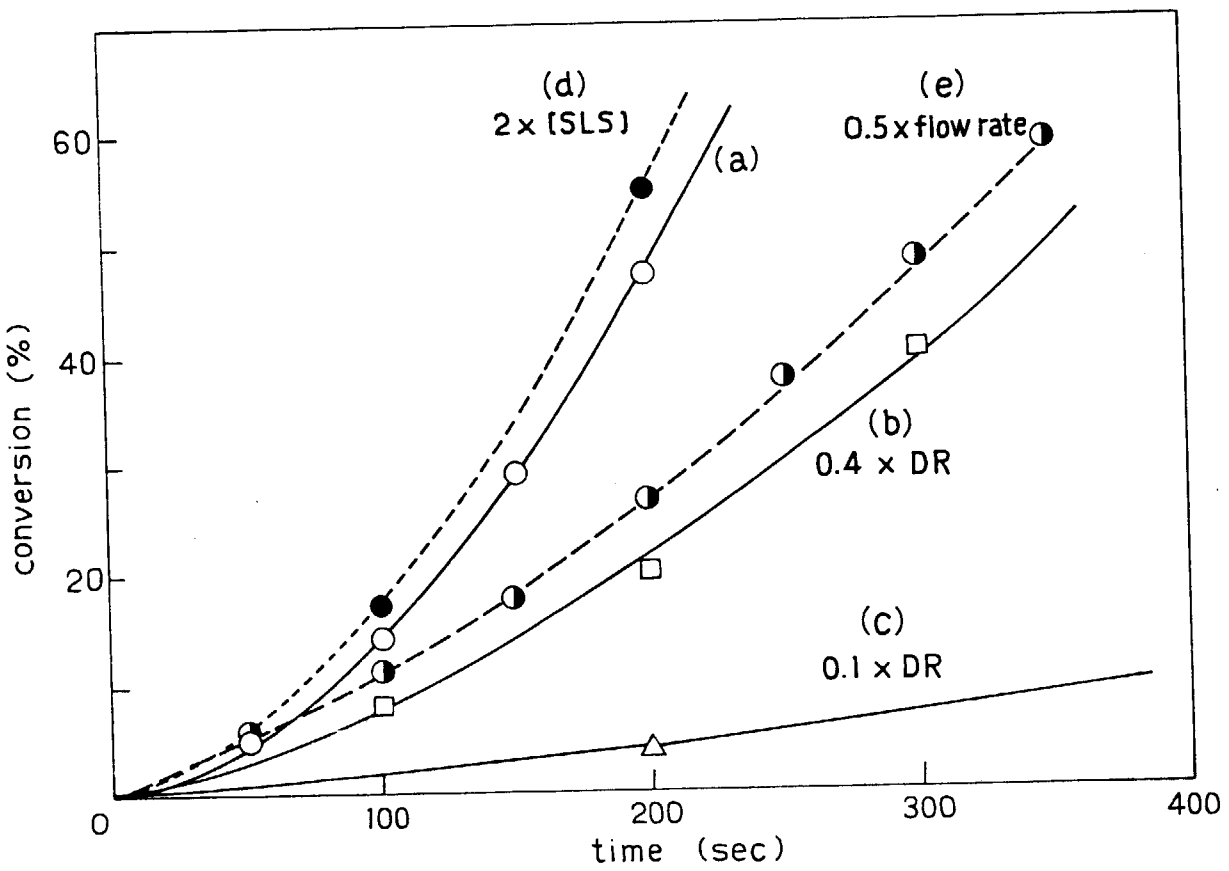

Fig. 1. Emulsion polymerization of 30 w/w% vinyl acetate in a flow system: Dose rate in reaction vessel, 3.0×10^5 rad/sec; Temperature, 40°C.

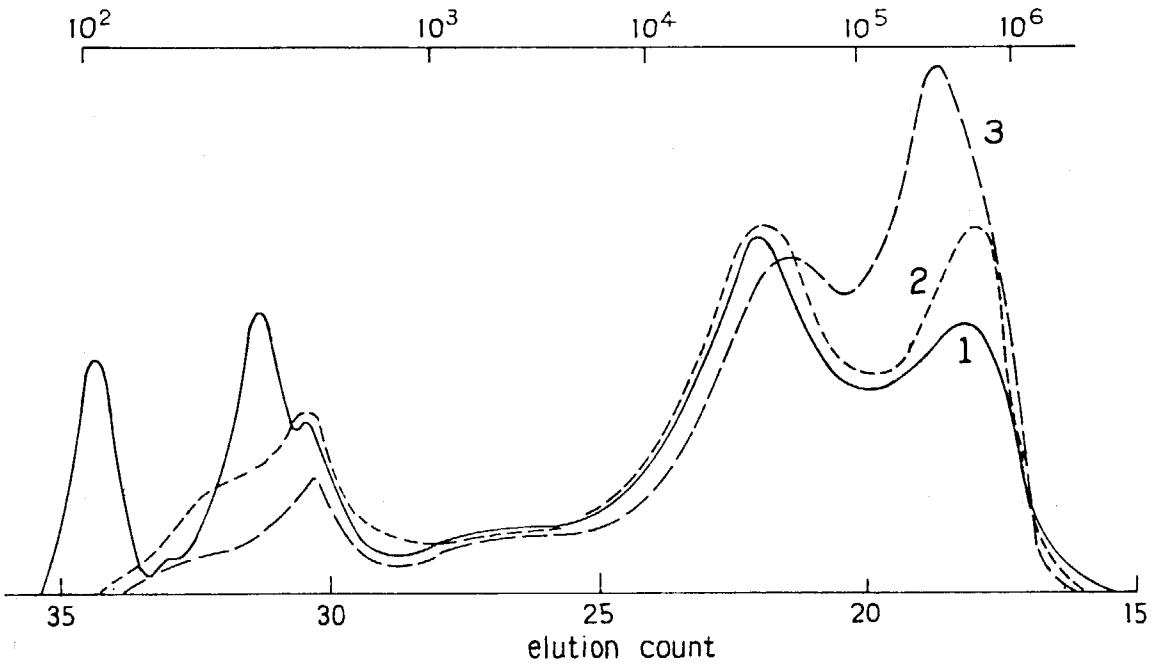

Fig. 2. MWDs of polyvinyl acetate in emulsion at 40°C: Irradiation time and conversion are; 1. 50 sec, 5.1%; 2. 100 sec, 14.1%; 3. 300 sec, 47.5%.

are shown in Fig. 2. They seem to be composed of three components whose peak MWs are 300 ∿ 500 (Peak I), $3 \sim 4 \times 10^4$ (peak II) and $3 \sim 5 \times 10^5$ (peak III). Fraction of peak I decreases with increasing conversion while peak III increases with conversion. In bulk polymerization of vinyl acetate at approximately the same dose rate[1], the polymer of peak MW = 2×10^5 was obtained. This suggests that peak II of the emulsion polymerization is attributed to the polymerization in micells. Peak III is probable due to a crosslinked polymer. Peak I is attributed supposingly to polymerization in the water phase.

(K. Hayashi and S. Okamura)

1) J. Takezaki, T. Okada, and I. Sakurada, unpublished results.

[5] Modification of Polymers

1. Radiation-Induced Grafting of Acrylic Acid onto Polyethylene Filaments

Radiation-induced grafting of acrylic acid onto high density polyethylene filament was carried out in order to raise the softening temperature, and impert flame retardance and hydrophilic properties.

Sample used was commercial high density polyethylene filament. Mutual γ-irradiation method was employed for the grafting in mixtures of acrylic acid, ethylene dichloride and water to which a small amount of ferrous ammonium sulfate was added.

As shown in the last annual report, inspite that the rate of grafting was very low at room temperature large graft percent was easily obtained when the grafting was performed at elevated temperature. Through grafting of acrylic acid and its conversion to calcium salt, thermal stability and hydrophilicity of polyethylene were improved.

In the present report further experiments on the thermal stability and flame retardance of acrylic acid graft polyethylene and its various salts are mainly described.

To estimate thermal stability, heat shrinkage of the sample was measured. The heat shrinkage of acrylic acid graft polyethylene filaments are given in Fig. 1 against temperature along with that of the starting polyethylene. The polyethylene filament begins to shrink at 70°C, reaches maximum shrinkage of 50% at 130°C and breakes at 137°C. By the grafting of acrylic acid the maximum shrinkage becomes smaller and breaking temperature higher. The filament of 50% graft gives a maximum shrinkage of 40% and retains the filament form even above 300°C. The 70% graft filament shrinks only less than 20% at temperature below 180°C.

Though the thermal stability of polyethylene filament is improved solely by grafting of acrylic acid, for further improvement the conversion of acrylic acid graft polyethylene

to various salts was tried. Fig. 2 and 3 give the heat shrinkage curves of Li, Na, K, Mg, Ca, Zn, Ba and Al salts of 34% acrylic acid graft polyethylene filament. All these metallic salts show shrinkage of less than 15% and retain the filament form even above 300°C. No appreciable difference was found among the heat shrinkage curves of monovalent, divalent and trivalent metallic salts in a temperature range up to 300°C.

The flammability test was carried out by the wire netting basket method, using fine filament of ca. 15d., which were kindly spun by Dr. K. Nakamae of Kobe University. Table 1 shows the results of the flammability test of acrylic acid graft polyethylene. The starting polyethylene flamed up instantaneously when it was brought into contact with the flame of a microburner and continued to burn for 27 sec after the removal from the flame until the sample in a basket was burned out. The melt drip formed during the burning was 62% of the original weight. Of course the sample is not self-extinguishing. In

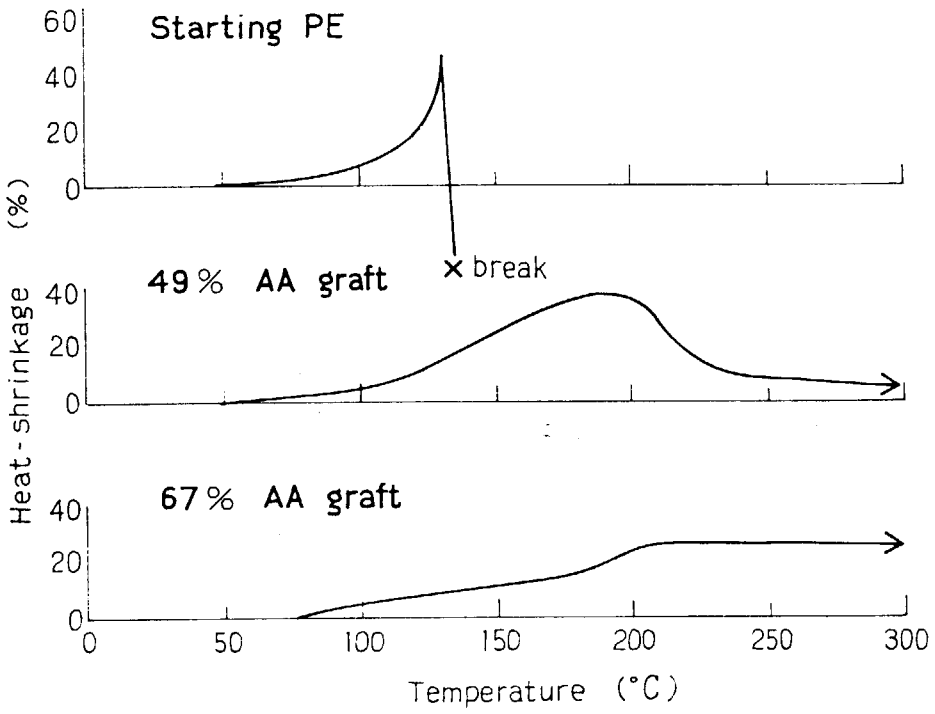

Fig. 1. Heat shrinkage of acrylic acid graft polyethylene filament.

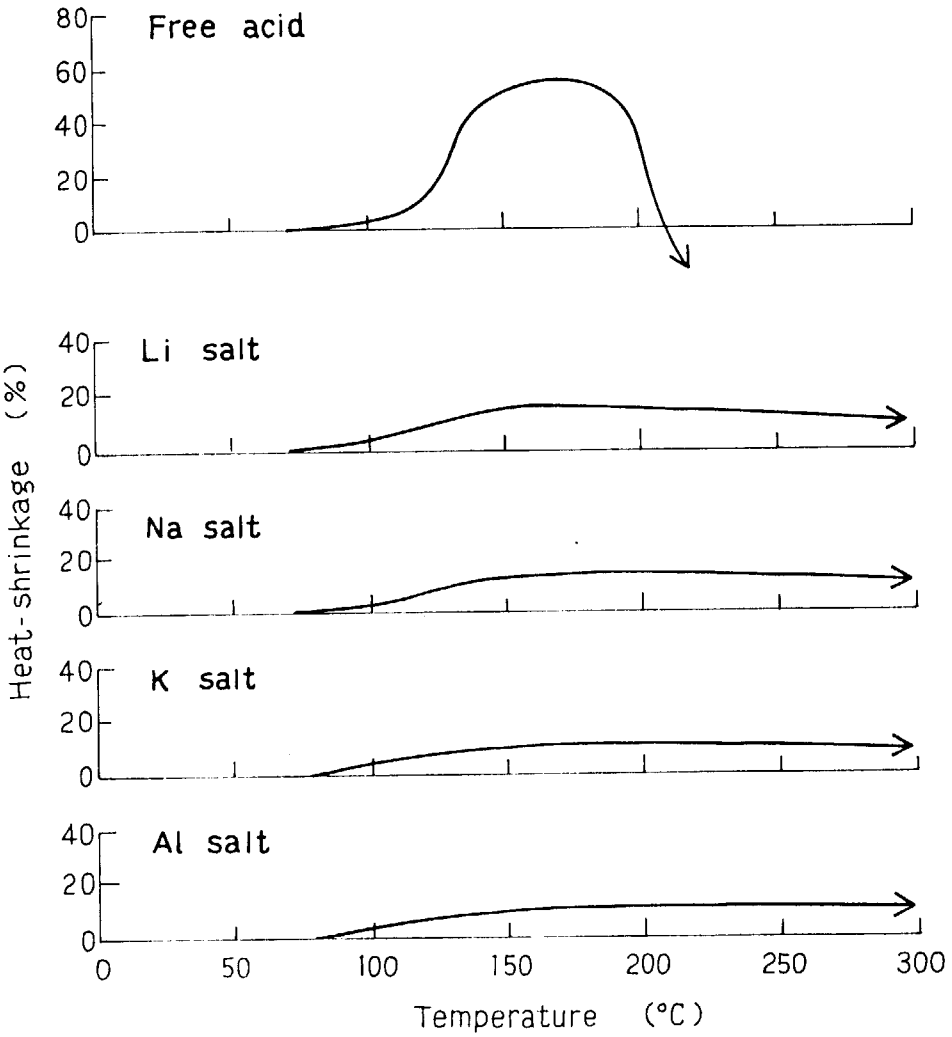

Fig. 2. Heat shrinkage of metallic salts of acrylic acid graft polyethylene filaments. (G = 33.5%)

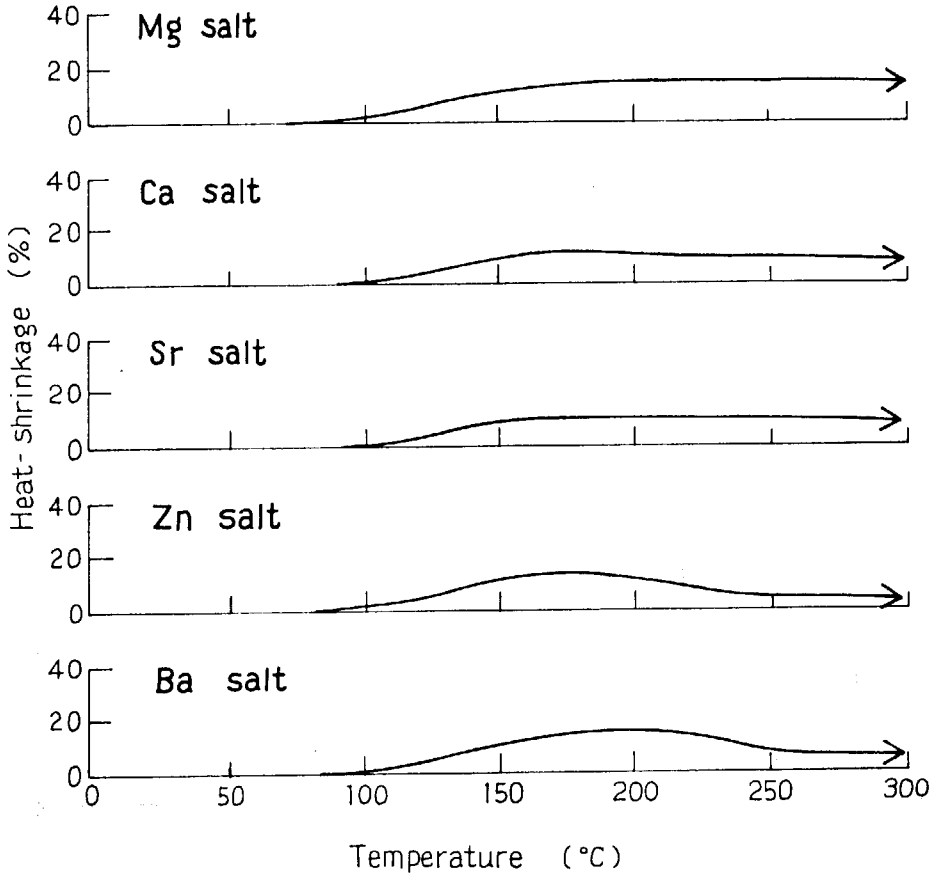

Fig. 3. Heat shrinkage of metallic salts of acrylic acid graft polyethylene filaments. (G = 33.5%)

the case of graft polyethylene, the time of after-flame was longer than that of the starting polyethylene when graft percent was low. This, however, does not mean that polyethylene became easy to burn but that the polyethylene became difficult to flow out due to the grafting and retained in the basket for a longer time. So the time of after-flame became shorter when graft percent became higher. Residue in a basket was a few percent for the graft filament with less than 80% graft. When graft percent is higher than 90%, the residue increased remarkably because the sample became self-extinguishing. Melt drip decreased with increasing graft percent.

Table 2 shows the result of flammability test for various salts of about 30% acrylic acid graft polyethylene. In the case of Na salt, the amount of melt drip was fairly low compared with

Table 1. Flame Retardance of Acrylic Acid Graft Polyethylene Filament (Wire netting basket method)

Graft %	After flame sec	Residue %	Melt drip %	Flame retardance*
0	27.1	0	62.0	N.S.E.
14.2	39.4	0	38.3	N.S.E.
30.1	52.6	2.3	21.1	N.S.E.
42.4	47.4	2.1	19.6	N.S.E.
68.8	24.4	2.0	24.7	N.S.E.
80.3	29.6	3.0	17.9	N.S.E.
94.7	11.2	68.6	0	S.E.
102.1	10.6	79.0	0	S.E.

* N.S.E.: not self-extinguishing, S.E.: self-extinguishing

Table 2. Flame Retardance of Metallic Salt of Acrylic Acid Graft Polyethylene Filament (Wire netting basket method)

Type of metal	Graft %	After flame sec	Residue %	Melt drip %	Flame retardance*	Remark
Starting PE	0	27.1	0	62.0	N.S.E.	
Acid form	30.1	52.6	2.3	21.1	N.S.E.	
Na	33.0	51.8	19.8	2.2	N.S.E.	
Mg	31.2	0	44.5	0	S.E.	Glow and smoke
Ca	33.1	4.0	55.6	0	S.E.	Glow and smoke
Zn	30.5	0	80.5	0	S.E.	Smoke
Sr	34.0	0	54.1	0	S.E.	Glow and smoke
Ba	34.0	0	58.2	0	S.E.	Smoke
Al	31.9	0	82.3	0	S.E.	Slight smoke

* N.S.E.: not self-extinguishing, S.E.: self-extinguishing

the starting polyethylene, but it was not self-extinguishing. Li and K salts show almost the same behavior as that of Na salt. In the cases of Mg, Ca, Zn, Sr, Ba and Al salts, no melt drip was formed and they were self-extinguishing. Thus divalent or trivalent metallic salts of about 30% acrylic acid graft polyethylene are not only thermally stable but also flame-retardant.

(K. Kaji, T. Okada, and I. Sakurada)

2. Adsorptive Activity of Acrylic Acid Grafted PVC Powder to Various Metal Ions

In the course of our study on the graft polymerization of acrylic acid (AA) onto PVC powder, we obtained a graft polymer having good adsorptive activity such as rate of adsorption and equilibrium adsorption to various metal ions by grafting of the monomer to surface of PVC powder which has an appropriate molecular weight and swelling property to the monomer. It was also revealed that the adsorption to metal ions are closely related to the distribution of the graft chain in the PVC powder.

As a continuation from the previous paper[1], studies have been carried out on the adsorptive activity to metal ions of the graft polymers obtained under different reaction conditions. In addition to the monomer mixture system containing monomer, water and ethylene dichloride (EDC), which were studied in the previous paper, we used acetone and toluene are also used as solvent, which are considered to affect the microstructure of the graft polymer. Chain transfer agent was further added to the mixture, if necessary, in order to adjust grafted chain length.

Selectivity of adsorbability was investigated under employment of cupric, alkali metal, and alkaline earth metal ions at low concentration using an atomic absorption spectrophotometer.

Figs. 1A ∿ 1C show the rate of graft polymerization in three different systems: (A) AA/water/acetone, (B) AA/toluene, and (C) AA/water/EDC/lauryl mercaptane.

The rate of grafting with larger amount of acetone was higher than the other as shown in Fig. 1A. On the other hand, the rate of grafting with larger toluene content is greater than the other, the effect of toluene content on the rate of grafting was very small when the fraction of toluene was above 0.5 (Fig. 1B). It was difficult to separate homopolymer from grafting product, because gelation of the AA homopolymer occurred when the grafting was carried out at 70% AA content solution.

Fig. 1C shows the rate of graft polymerization in AA/water/EDC system with lauryl mercaptane (10% of AA) as a chain transfer agent. The rate of grafting was markedly increased by the addition of lauryl mercaptane.

In Figs. 2A ∿ 2C, the amounts of adsorption of cupric ion by the graft polymer are plotted against adsorption time. The

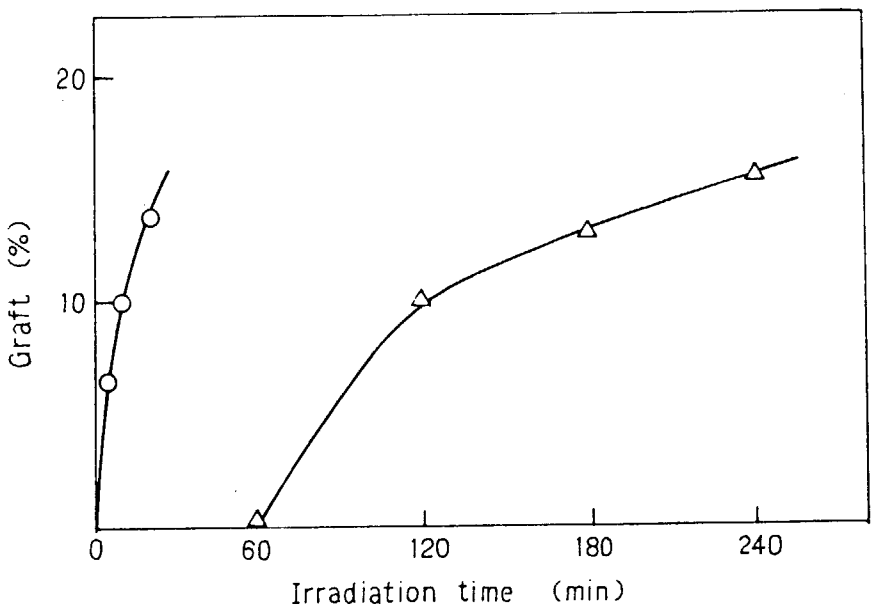

Fig. 1A. Grafting of acrylic acid onto PVC powder in two different monomer mixtures: Composition of the mixture of AA, H_2O, and acetone, (○) 50 : 5 : 45 and (△) 50 : 15 : 35 by volume; Dose rate, 6.0 x 10^4 r/h; Concentration of Mohr's salt, 0.4%.

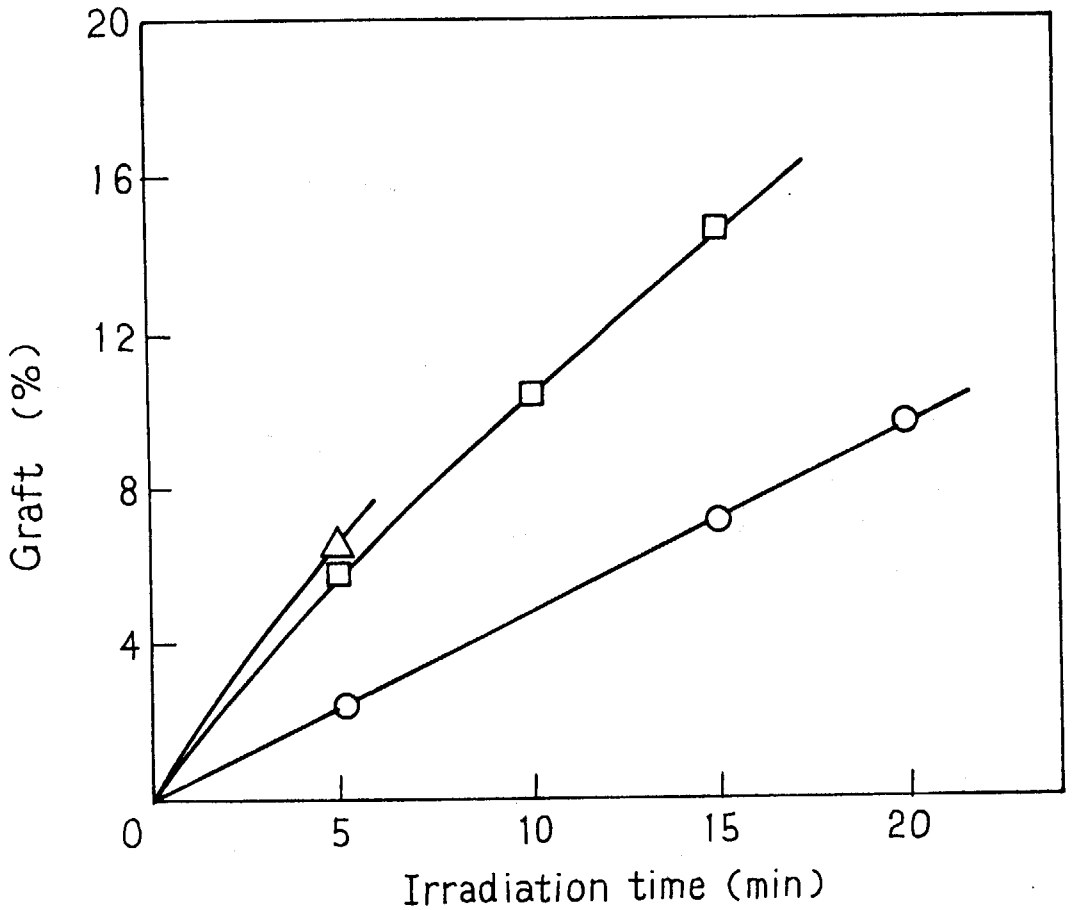

Fig. 1B. Grafting of acrylic acid onto PVC powder in three different monomer mixtures: Composition of AA and toluene, (Δ) 70 : 30, (□) 50 : 50, and (○) 30 : 70; Dose rate, 6.0 x 10^4 r/h.

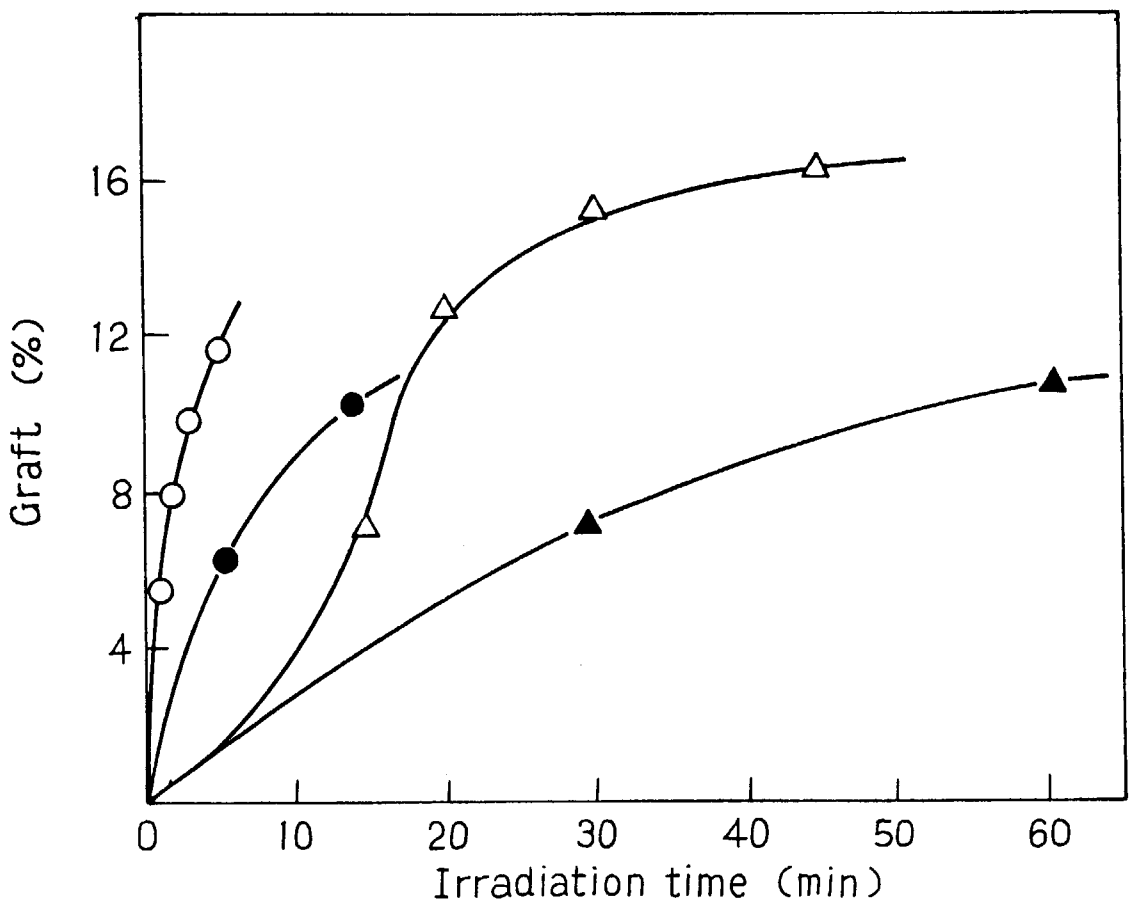

Fig. 1C. Grafting of acrylic acid onto PVC powder in two different monomer mixtures: Dose rate, 6.0 x 10^4 r/h; Concentration of lauryl mercaptane, 10%; Composition of AA, H_2O and EDC by volume, (○) 50 : 15 : 35, (△) 50 : 40 : 10, (○) the same as (●) but without lauryl mercaptane (chain transfer agent), (▲) the same as (△) but without lauryl mercaptane.

adsorption (%) is defined as mole-percent of carboxylic groups combined with metal ions to total carboxylic groups in the polymer, and therefore, the adsorption is 100% if all carboxylic groups in the polymer are occupied by cupric ions. Higher equilibrium adsorption was attained in the case of the graft polymer obtained in the solution containing less acetone than that obtained in the acetone rich solution (45% acetone) (Fig. 2A). Similar tendency was observed in the system containing toluene as shown in Fig. 2B, where the equilibrium adsorption was 70% in the case of the graft polymer obtained in the mixture (AA/toluene = 70/30) while it was only 20% in the case of the mixture (AA/toluene = 50/50).

The adsorptive activity of graft polymer obtained in AA/water/EDC solution in the presence of lauryl mercaptane is shown in Fig. 2C together with that obtained in the absence of

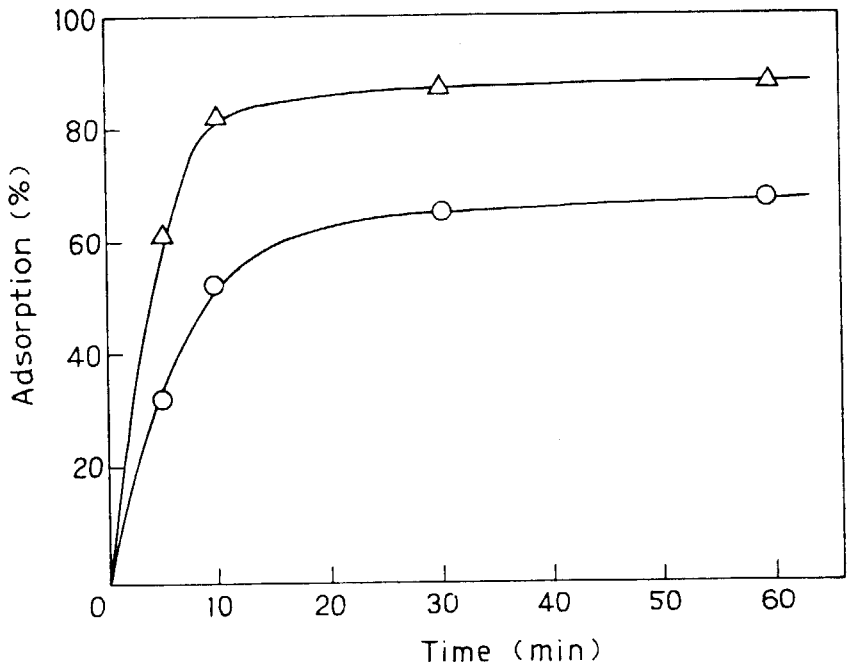

Fig. 2A. Adsorption of cupric ion by the graft polymer: Degree of grafting, (○) 13.9%, (△) 15.6%; The composition of the monomer mixtures are the same as those in Fig. 1A.

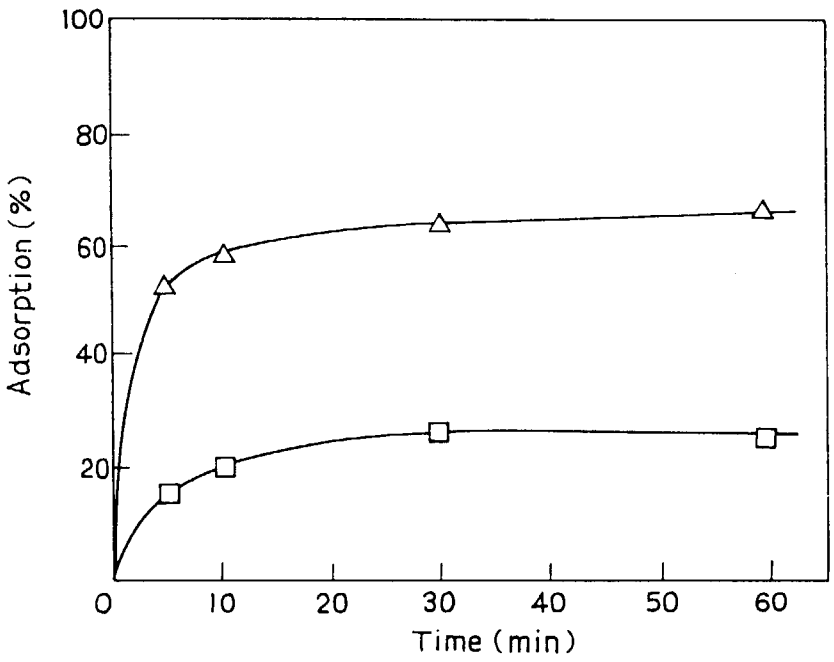

Fig. 2B. Adsorption of cupric ion by the graft polymer: Degree of grafting, (Δ) 6.3%, (□) 6.0%; The compositions of the monomer mixtures are the same as those in Fig. 1B.

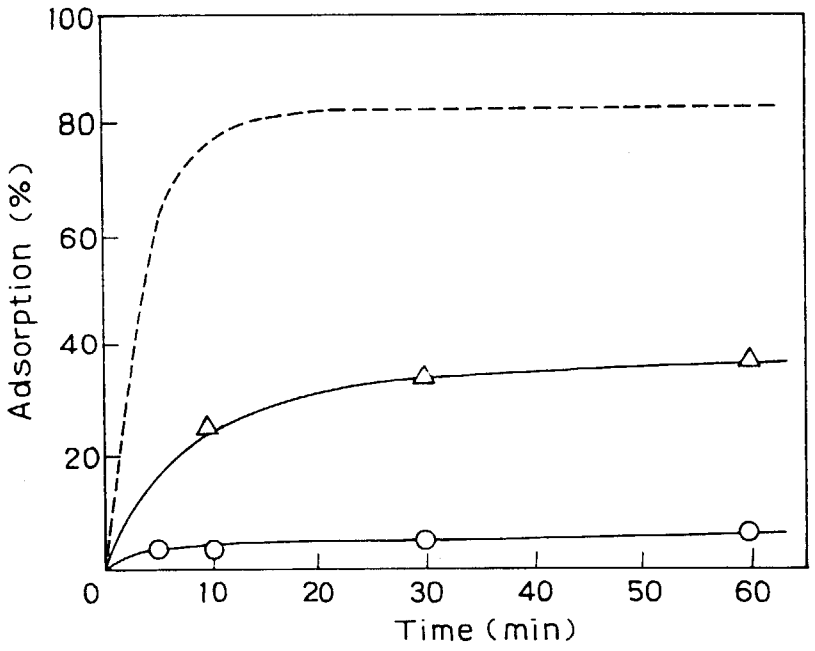

Fig. 2C. Adsorption of cupric ion by the graft polymer: Degree of grafting, (○) 11.7%, (△) 16.0%; Compositions of the monomer mixture from which the polymer was obtained are the same as shown in Fig. 1C, (---) the same as (△) but without lauryl mercaptane.

lauryl mercaptane and reported in the previous paper for the graft polymer. It is noticed that the equilibrium adsorption decreased to the value which is only one-third of that obtained for graft polymer prepared without lauryl mercaptane.

The adsorptive activity of alkali metal ions is shown in Fig. 3 for the graft polymers which was obtained in the AA/water/EDC system (40/54/6); the graft copolymer showed excellent adsorption to cupric ion[1]. The results obtained for the graft polymer indicate that the adsorption to alkali metal ions is in the order of decreasing atomic number as known for conventional ionic exchange resins, and no selectivity to particular metal ion was observed.

Similar adsorption of alkaline earth metal ions was found in the case of the graft polymers obtained in AA/acetone/water

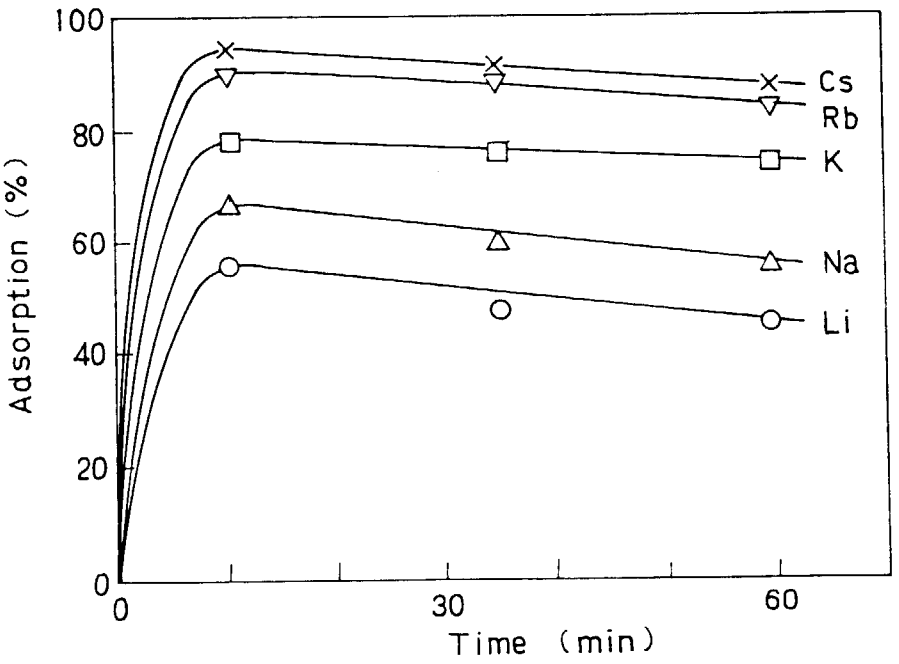

Fig. 3. Adsorption of alkali metal ions by the graft polymer: The polymer was obtained from the monomer mixture containing AA/H_2O/EDC = 40/54/6; Degree of grafting, 17.2%; Concentration of alkali metal ions, 4.3 x 10^{-5} mole/l.

and AA/toluene mixtures. However, further investigations are necessary to elucidate the relation between microstructure and adsorptive activity of graft polymers. (Y. Kusama and T. Yagi)

1) Y. Kusama and T. Yagi, JAERI-M 8569, 117 (1979).

[6] Studies on Radiation Dosimetry

1. On the Reaction of the CTA Film Dosimeter with NO_2

In a previous report[1], we have described the species responsible for the in situ coloration which proceeds during irradiation of the CTA film dosimeter. The species for the post coloration, on the other hand, has not been identified although it has been suggested that the species would be certain products formed by a reaction involving NO_2 produced by irradiation of air. The present report describes the results obtained by experiments on the reaction products between NO_2 and the CTA film dosimeter.

The CTA film dosimeter employed was supplied by Fuji Photo Film Co. Additive-free CTA films prepared by evaporation of CTA solution, and cellulose films (Tokyo Cellophane Co.) were also studied for comparison. Reactions of these films induced by NO_2 were investigated using ultraviolet (UV), ESR, and infrared spectrometers.

When the CTA film dosimeter was exposed to 19 Torr NO_2, the UV spectrum showed an increase in OD(280), optical density at 280 nm which is the wavelength used for the dosimetry, together with appearance of a new spectrum, designated as spectrum X hereafter, composed of several lines around 350 nm. Fig. 1 shows the UV spectrum observed immediately after exposition of the film to NO_2. The fine structure noted above 400 nm is due to NO_2 in gas phase. The OD(280) and OD(354) where 354 nm corresponds to the wavelength of the maximum in spectrum X were found to increase gradually with time of exposition to NO_2, the increment in OD(280) being about twice that in OD(354). Similar changes in the OD(280) and OD(354) were also observed for additive-free CTA films and cellulose films, so that they would result from reaction of NO_2 not with triphenyl phosphate contained in the CTA film dosimeter but with CTA or cellulose molecules.

The band separations in spectrum X are from $910 \sim 1070$ cm^{-1}

which agree with the N=O stretching frequency in an excited state[2]. This fact together with the wavelength of the bands, 350 nm, suggest that spectrum X may arise from either NO_2^-, HNO_2, or alkyl nitrites. Of these, NO_2^- may be excluded as a species for spectrum X since the UV spectrum is known to be quite complex in the crystal[3] and a structure-less single band in aqueous solution[4]. On the other hand, the six wavelengths of the bands in spectrum X agree well with those of the UV spectra of HNO_2 and ethyl nitrite, as shown in Table 1. Therefore, spectrum X may be attributed to either HNO_2 or alkyl nitrite, RNO_2.

It is expected that the molar extinction coefficient at 280 nm would be much smaller than that at 354 nm in the UV spectra of HNO_2 and RNO_2 as for NO_2^-.[4] Therefore, if these molecules

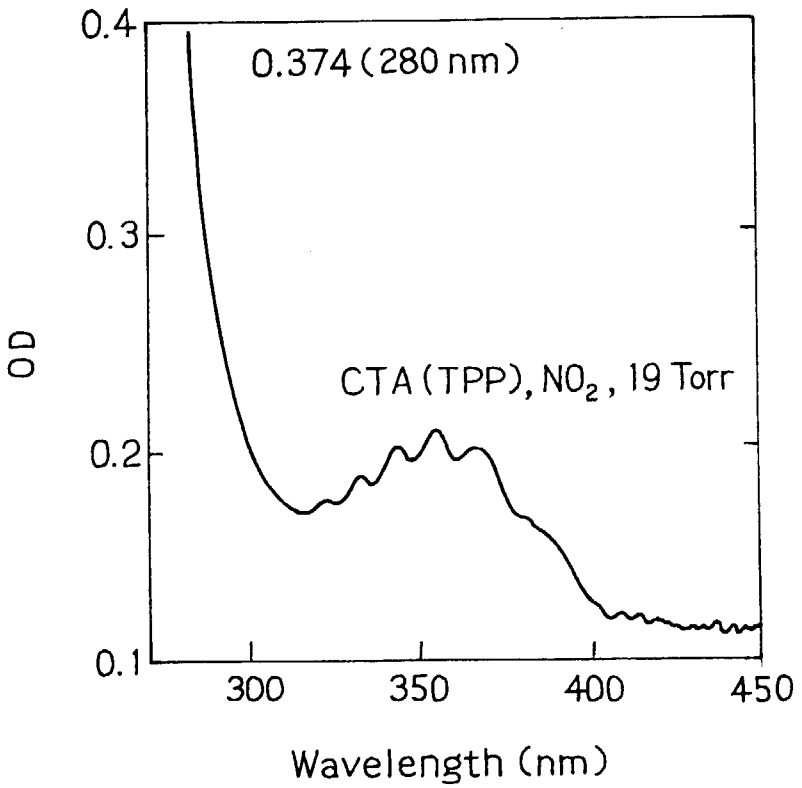

Fig. 1. Ultraviolet spectrum of the CTA film dosimeter immediately after contact with 19 Torr NO_2.

Table 1. Comparison of Wavelengths in nm of Bands between Spectrum X and the UV Spectra of Nitrous Acid and Ethyl Nitrite

NO_2—CTA film dosimeter	$HONO$[2]	C_2H_5ONO[5]
∿320	321	321
331	331	332
341	342	343
354	354	355
366	368	369
∿380	384	∿385

would be responsible for the increase in OD(280) for the CTA film dosimeter exposed to NO_2, the increment in OD(280) should be smaller than that in OD(354), contrary to our result. Accordingly, the increase in OD(280) may be due to species other than HNO_2 or RNO_2 which gives rise to spectrum X.

The infrared spectrum of additive-free CTA films after exposition to NO_2 shows the presence of characteristic absorptions due to N=O and N-O groups which correspond to spectrum X in the UV spectrum. On the other hand, cellulose films exposed to NO_2 give an infrared spectrum which reveals absorptions due to C=O and N=O groups. The formation of C=O groups suggests that NO_2 induces scission of the glucose rings or oxidation of the OH groups in the cellulose molecules. It seems likely that C=O groups would be similarly produced in additive-free CTA films and the CTA film dosimeter, by taking into account the above result of the UV study which shows that these films undergo identical changes to cellulose films by exposition to NO_2. The formation of the C=O groups may result in the increase in OD(280), as, in fact, it has already been shown that C=O groups are identified as the species responsible for the stable component of the in situ coloration.

From these results, it may be concluded that NO_2 reacts with the CTA film dosimeter to produce HNO_2 or alkyl nitrite, and C=O groups, and that the latter is responsible for the increase in OD(280). (K. Matsuda and S. Nagai)

1) K. Matsuda and S. Nagai, JAERI-M 8471 (1979).
2) G. W. King and D. Moule, Can. J. Chem., 40, 2057 (1962).
3) J. W. Sidman, J. Amer. Chem. Soc., 79, 2669 (1957).
4) S. J. Strickler and M. Kasha, J. Amer. Chem. Soc., 85, 2399 (1963).
5) P. Tarte, J. Chem. Phys., 20, 1570 (1952).

2. Energy Transfer in the Binary Mixture of Argon and Ethane as Studied by Optical Emission Spectra

In the previous annual report[1], it was reported that the minimum W value appeared at about 4% ethane content in the ionization current measurements of gas mixtures containing argon and ethane irradiated with electron beams (0.6 MV, 10 μA) from the HDRA in the gas pressure range between 1 and 7 atm. The decrease of W values of argon by addition of ethane has been explained by energy transfer from excited argon to ethane resulting ionization. This year, studies have been carried out in order to elucidate the energy transfer process from optical emission from the gas mixture induced by electron irradiation.

For the recording of the optical emission spectra under electron irradiation of the gas, the apparatus schematically drawn in Fig. 1 was used. The reaction chamber is of 1.5 ℓ volume made of brass having irradiation window (17 μm thickness aluminium) through which the electron beam penetrated in the vessel and quartz window through which the optical emission was introduced to a grating spectrometer (Shimadzu Model GF-16R). The grating of the spectrometer was oscillated automatically to allow display of the emission spectrum on recorder at a scanning rate of 300 nm/min. The wavelength of the emission was calibrated with emission of mercury arc. All optical emission

measurements were carried out at 1 atm. using electron beam of 5 μA and 1.0 MeV from a Van de Graaff accelerator.

Typical optical emission spectra from the gas mixture of different ethane concentrations are shown in Fig. 2. Main feature of the spectrum from pure argon (a) consists of broad peak due to argon excimer (210 nm)[2], peaks due to OH (306.4 nm), and N_2 (337.1, 357.7 nm), the peaks of the latter two being from H_2O and N_2 contained in argon in extremely small quantities (less than 5 ppm) as impurities which were difficult to remove by ordinary purification procedures. The large intensities of the emissions due to the impurities regardless of their minor abundance may be explained by effective energy transfer from Ar^* or Ar_2^* to these impurities.

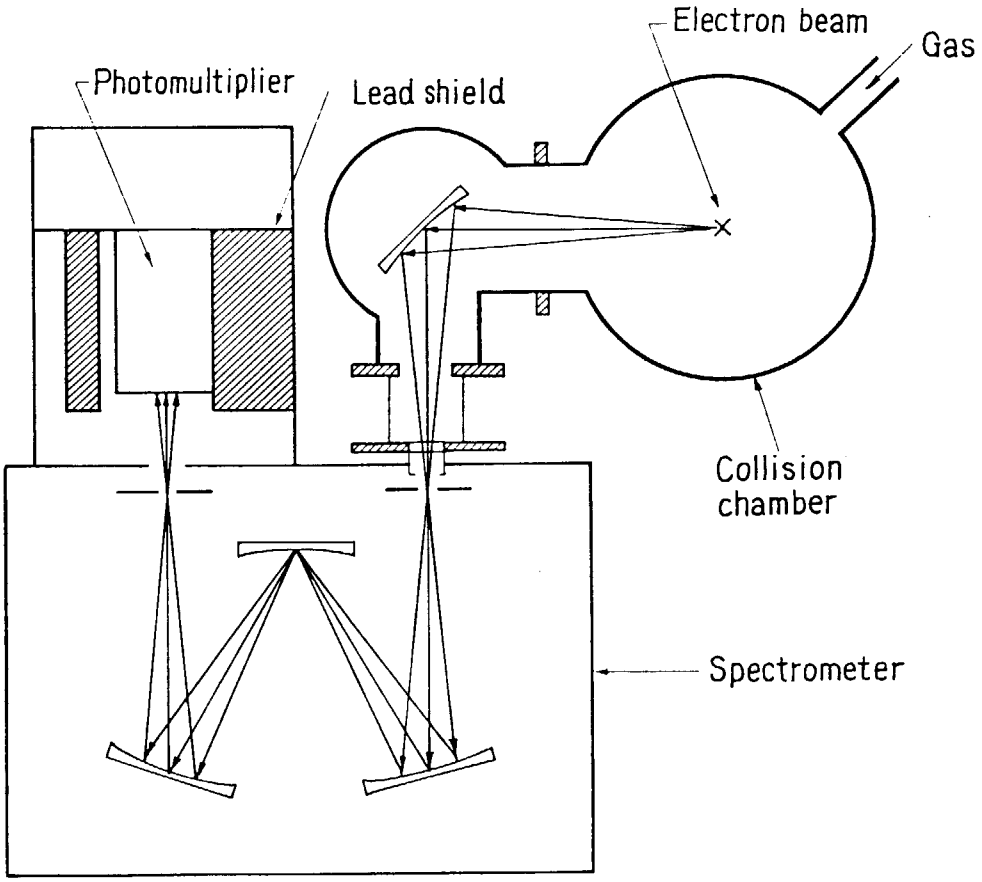

Fig. 1. Optical system and reaction vessel.

When the concentration of ethane increases the intensity of emission from Ar_2^* decreases and simultaneously the emissions due to the impurities decreases. This means that ethane may quench Ar_2^* and possibly Ar* which is a precursor of Ar_2^*, as shown in the following reaction scheme:

$$Ar \longrightarrow\!\!\!\!\!\!\sim\!\!\!\!\!\!\sim\!\!\!\!\!\!\sim\!\!\!\!\!\!\sim\!\!\!\!\!\!\sim\!\!\!\!\!\!\rightarrow Ar^*$$

$$Ar^* + Ar \xrightarrow{k_1} Ar_2^*(1) \xrightarrow{k_5} Ar_2^*(2) + h\nu$$

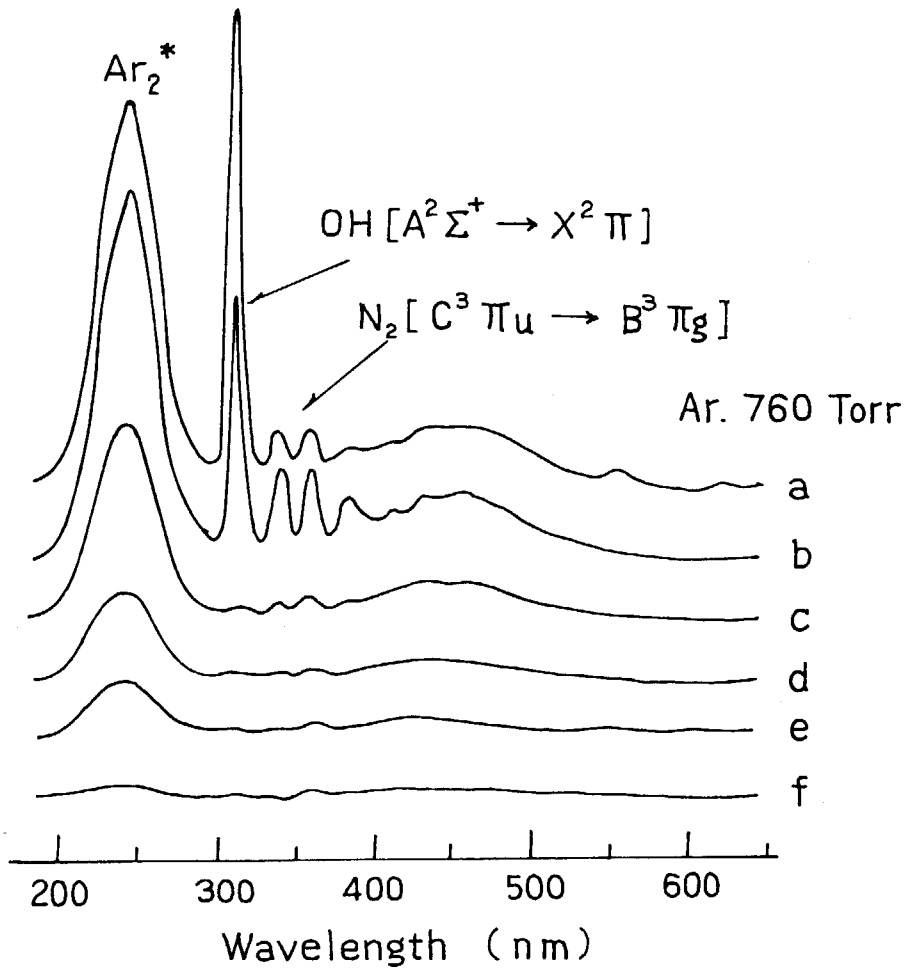

Fig. 2. Spectra of optical emission during irradiation of Ar (760 Torr): Ethane pressure, (a) 0, (b) 5, (c) 6, (d) 8, (e) 10, and (f) 14 Torr.

$$Ar^* + X \xrightarrow{k_2} Ar + X^+ + e$$

$$Ar_2^* + X \xrightarrow{k_2'} 2Ar + X^*$$

$$Ar^* + Y \xrightarrow{k_3} Ar + Y^*$$

where X and Y denote ethane and an impurity, respectively. Assuming steady state condition for [Ar*] and [Ar_2*], the concentration of Ar_2*, [Ar_2*] can be expressed by the following equation:

$$\left\{\frac{1}{[Ar_2^*]} - A\right\} \frac{1}{[X]} = B + C\,[X]$$

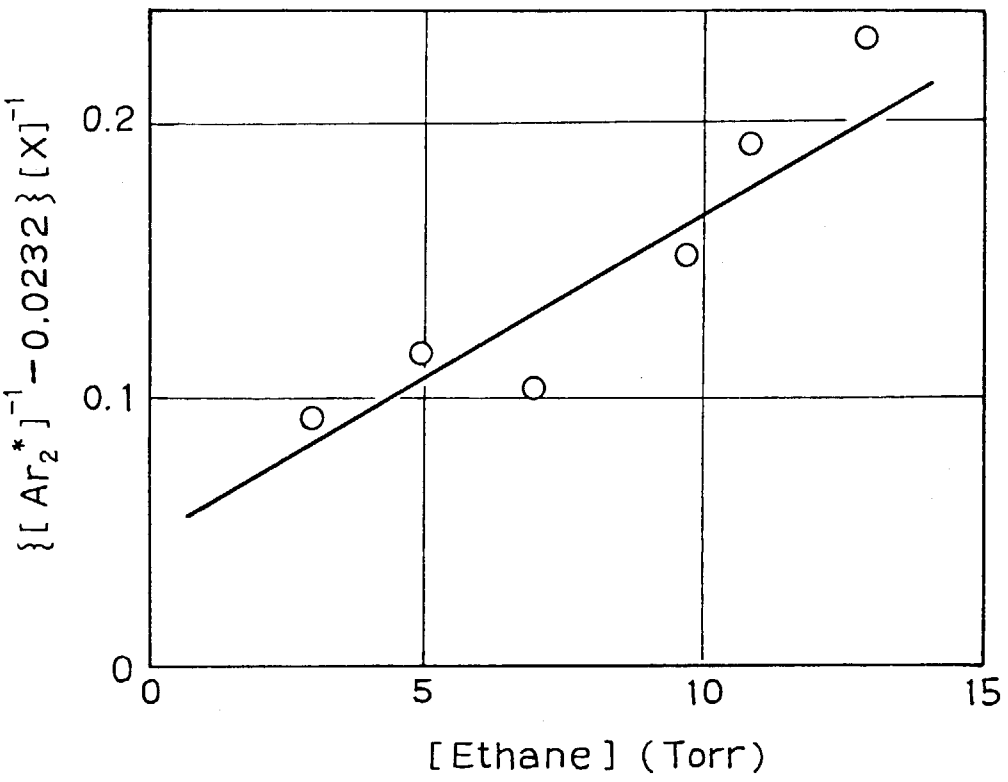

Fig. 3. Plot of $\{[Ar_2^*]^{-1} - A\}[X]^{-1}$ as a function of ethane concentration.

where

$$A = \frac{k_5\{k_1[Ar] + k_3[Y]\}}{k_1[Ar]^2 GI}$$

$$B = \frac{k_5k_2 + k_2'k_3[Y] + k_2'k_1[Ar]}{k_1[Ar]^2 GI}$$

$$C = \frac{k_2'k_2}{k_1[Ar]^2 GI}$$

and k_i is the rate constant. The plot of $\{[Ar_2^*]^{-1} - A\}[X]^{-1}$ vs. [X] are shown in Fig. 3, where the parameter A (= 0.0232) was determined so that the square of the deviation from the linear line becomes as small as possible.

Linear plots in Fig. 3 qualitatively indicate the presence of energy transfer from Ar* and Ar_2^* to ethane as proposed, and this is approved by an energy level diagram of Ar* and Ar_2^* which indicates both excited levels lie above the ionization and excitation levels of ethane. The lack of knowledge on rate constants makes it difficult to go further discussions on our terms containing rate constants. (K. Matsuda)

1) K. Matsuda and T. Takagaki, JAERI-M 8569, 129 (1979).
2) G. S. Hurst and T. E. Bortner, Phys. Rev. 178, 4 (1969).

III. LIST OF PUBLICATIONS

[1] Paper Presentations

1. S. Nagai, H. Arai, and M. Hatada, "Radiation Effects on $CO-H_2$ Gas Mixture in the Presence of Silica Gel", Radiat. Phys. Chem., 16, 175 (1980).

2. K. Matsuda and S. Nagai, "Coloration Mechanism of the CTA Film Dosimeter", JAERI-M 8471 (1979).

3. K. Hayashi, "Radiation-Induced Polymerization at High Dose Rate. I. Isobutyl Vinyl Ether in Bulk", J. Polym. Sci., Polym. Chem. Ed., 18, 179 (1980)

4. K. Hayashi and N. Kotani, "Radiation-Induced Polymerization at High Dose Rate. II. α-Methylstyrene in Bulk", J. Polym. Sci., Polym. Chem. Ed., 18, 191 (1980).

* * * * *

5*. H. Arai, S. Nagai, K. Matsuda, and M. Hatada, "Preparation of Acetic Acid and Propionic Acid from Gas Mixture Containing CH_4 and CO or CH_4 and CO_2", Japan Kokai, 54-19702.

6*. H. Arai, S. Nagai, K. Matsuda, and M. Hatada, "Preparation of Formic Acid and Acetic Acid from Gas Mixture Containing Hydrogen and Carbon Monoxide", Japan Kokai, 54-54393.

7*. K. Hayashi and S. Okamura, "Preparation of Butadiene-vinylchloride Copolymer", Japan Kokai, 54-134758.

8*. I. Sakurada, T. Okada, and K. Kaji, "Preparation of Synthetic Fiber of Excellent Thermal Stability from Polyethylene Filament by Radiation", Japan Kokai, 54-13639.

9*. I. Sakurada, T. Okada, and K. Kaji, "Self-Extinguishing Polyethylene Filament", Japan Kokai, 55-5656.

* * * * *

10. Y. Oshima, N. Tamura, and R. Tanaka, "Dosimetry and Irradiation Facilities", Nuclear Engineering, 25, (No. 6) 79, (No. 7) 107 (1979).

11. Y. Oshima, N. Tamura, and W. Kawakami, "Irradiation Technology", Nuclear Engineering, 25, (No. 8) 75, (No. 9) 71 (1979).

12. Y. Oshima, "Radiation Chemistry and C_1 Chemistry", Kagaku-Keizai, 27, (No. 2) 17 (1980).

13. Y. Oshima and S. Machi, "Application of Radiation Chemistry to Chemical Industry -- Present Status and Future Scope", Nuclear Engineering, 26, (No. 1) 17 (1980).

14. Y. Ikada, "Medical Polymers in the Present and the Future", Rubber and Plastics, 31, 2 (1979).

15. Y. Ikada, "Polymer and Medicine", Kobunshi Kako (Polymer Applications), 28, 437 (1979).

16. Y. Ikada, "Polymer Surface", Kagaku (Chemistry), 34, 861 (1979).

* Patent application

[2] Oral Presentations

1. S. Sugimoto, M. Nishii, and T. Sugiura, "Radiation Chemical Reaction of Mixture of Carbon Monoxide and Hydrogen", The 6th International Conference on Radiation Research, May 14, 1979.

2. S. Nagai, H. Arai, and M. Hatada, "Hydrocarbon Synthesis from Carbon Monoxide and Hydrogen by Radiation", The 6th International Conference on Radiation Research, May 14, 1979.

3. M. Hatada and M. Nishii, "Radiation Chemical Reactions of Lipid Monolayers at Gas-Water Interface Induced by Electron Beam Irradiation", The 6th International Conference on Radiation Research, May 18, 1979.

4. S. Nagai, H. Arai, and M. Hatada, "Radiation Effects on $CO-H_2$ Gas Mixture in the Presence of Silica Gel", The 22nd Discussion Meeting on Radiation Chemistry, Oct. 13, 1979.

5. S. Sugimoto and M. Nishii, "Radiation Effects on the Reaction of Mixtures of Carbon Monoxide and Hydrogen (IX) Irradiation of Circulating Gas", The 22nd Discussion Meeting on Radiation Chemistry, Oct. 13, 1979.

6. S. Nagai, H. Arai, and M. Hatada, "Spin Trapping Studies of Radicals Produced by Electron Beam Irradiation of CH_4-CO Gas Mixture", The 18th ESR Symposium, Oct. 17, 1979.

7. H. Arai, S. Nagai, K. Matsuda, and M. Hatada, "Formation of Organic Acids from Gas Mixtures of CH_4 and CO, and CH_4 and CO_2 by Electron Beam Irradiation", The 22nd Discussion Meeting on Radiation Chemistry, Oct. 13, 1979.

8. H. Arai, S. Nagai, K. Matsuda, and M. Hatada, "Formation of Organic Acids from Gas Mixture Containing CH_4 and CO_2 by Electron Beam Irradiation", Discussion Meeting on Carbon Dioxide Resources, Nov. 2, 1979.

9. K. Matsuda and S. Nagai, "Coloration Mechanism of CTA film Dosimeter", The 16th Annual Meeting on Radioisotopes in the Physical Sciences and Industry, Jun. 26, 1979.

10. K. Hayashi and S. Okamura, "Polymerization of Dienes at High Dose Rate", The 6th International Conference on Radiation Research, May 17, 1979.

11. K. Hayashi, Y. Tanaka, and S. Okamura, "Oligomerization of Butadiene by Electron Beam Irradiation", The 28th Annual Meeting of the Polymer Society, Japan, May 27, 1979.

12. K. Hayashi, Y. Tanaka, and S. Okamura, "Polymerization of Butadiene Induced by Electron Beam Irradiation", The 22nd

Discussion Meeting on Radiation Chemistry, Oct. 14, 1979.

13. K. Hayashi, Y.Tanaka, and S. Okamura, "Oligomerization of Butadiene Induced by Electron Beam Irradiation", The 28th Discussion Meeting of the Polymer Society, Nov. 2, 1979.

14. K. Kaji, T. Okada, and I. Sakurada, "Radiation Induced Grafting of Acrylic Acid onto Polyethylene Filaments", Annual Meeting of the Society of Fiber Science and Technology, Jun. 28, 1979.

15. Y. Kusama, T. Yagi, K. Hayashi, and S. Okamura, "Adsorption of Metal Ions to Polyvinylchloride Grafted with Acrylic Acid by γ-Ray Irradiation", The 22nd Discussion Meeting on Radiation Chemistry, Oct. 14, 1979.

IV. LIST OF SCIENTISTS

(Mar. 31, 1980)

[1] Staff Members

Yunosuke OSHIMA	Dr., radiation physicist, Head
Ichiro SAKURADA	Professor emeritus, Kyoto University, Ex-head
Seizo OKAMURA	Professor emeritus, Kyoto University
Motoyoshi HATADA	Dr., physical chemist
Kanae HAYASHI	Dr., polymer chemist
Shun'ichi SUGIMOTO	Physical chemist
Koji MATSUDA	Radiation physicist
Jun'ichi TAKEZAKI	Physical chemist
Yasuo KUSAMA*	Polymer chemist
Masanobu NISHII	Dr., polymer chemist
Siro NAGAI	Dr., physical chemist
Hidehiko ARAI	Physical chemist
Torao TAKAGAKI	Radiation physicist
Kanako KAJI	Polymer chemist
Toshiaki YAGI	Engineering chemist

[2] Advisors

Isamu NITTA	Professor emeritus, Osaka University, Advisor
Shun'ichi OHNISHI	Professor, Kyoto University, Advisor
Yoshito IKADA	Assoc. Professor, Kyoto University, Advisor

*) Present address:
Radiation Engineering Section, Pilot Scale Research Station, Takasaki Radiation Chemistry Research Establishment.